TECHNISCHE UNIVERSITÄT WIEN
Vienna University of Technology

MASTERARBEIT

Numerical simulations of the crack behavior of brittle cellular materials

ausgeführt zum Zwecke der Erlangung des akademischen Grades
eines Diplom-Ingenieurs unter der Leitung von
Assoc. Prof. Dr. Dipl.-Ing. Heinz E. Pettermann
Institut für Leichtbau und Struktur-Biomechanik (E317)
eingereicht an der
Technischen Universität Wien
Fakultät für Maschinenwesen und Betriebswissenschaften
von

Andrés Bellés Meseguer
1127628
a.belles-meseguer@primeaero.at

Wien, im Februar 2015

Acknowledgements

I want to sincerely thank Dr. Heinz E. Petterman for patiently guiding me trough this thesis and sharing his knowledge with me. Those thoughts and discussions about the matching of fracture mechanics theories and cellular materials have been the basis of this thesis as well as of my understanding in the topic. I also do not forget his tutoring in several courses, with special mention to the interesting Project Work in XFEM.

I wish to express my gratitude to the Institute of Lightweight Design and Structural Biomechanics, for the good work is made through all its courses and all the knowledge I have learned there. Special mention for Professor F. G. Rammerstorfer for his admirable classes. Particularly the explanations in Finite Elements topics give in my opinion a very valuable education for future engineers.

And thank you Batirtze, for being as you are and for supporting me all this time.

I would like to dedicate this thesis to the memory of Dr. Hans Peter Rossmanith, who not only was an excellent Professor in Fracture Mechanics, but lectured his lessons with extraordinary passion and enthusiasm.

Abstract

Nowadays cellular materials are widely used in the industry because of their good qualities such as low density, high energy absorption, and thermal resistance. New production methods as additive manufacturing will allow cellular structures being easily implemented in future designs. Therefore understanding their mechanics is crucial for an efficient use. However, the behavior in presence of cracks is not yet entirely understood. In this thesis a step forward in the comprehension of crack behavior in cellular materials is made, concretely for the case of short cracks in relation to the cell size.

A finite element model is created for several two- and three-dimensional open cellular structures in order to study the effect of cracks, focusing in quasi-isotropic behavior and ideal grid arrangement. In a first step, fracture constants such as fracture toughness are calculated using Linear Elastic Fracture Mechanics principles. From those results scaled formulas are determined according to structure, lattice wall length, and solid material properties. The evaluated criteria are compared with similar analysis found in literature.

In a second step the case of short cracks is presented. In order to evaluate the limits of Linear Elastic Fracture Mechanics the finite element model is parametrized and results are obtained in relation of the different variables. The derived approach of Finite Fracture Mechanics is also used to compare fracture variables of short cracks.

An important consideration is the adoption of two different fracture criteria. On one hand the classical strength criterion comparing local stress with material strength is used. On the other hand, a second stability criterion is adopted considering that local buckling causes the breaking of cell walls. That stability approach has been early used in the literature with cellular structures, flaws, and defects, but not together with fracture mechanics problems. Another thought is the consideration of an "anti" mode I in the crack evolution, related to the existence of anti-cracks. This is possible since in cellular structures this compressible deformation is no longer avoided by contact between crack faces.

In a last point, crack development on honeycombs is compared with that on solid continuous materials. Cell walls fulfilling the fracture criterion are consecu-

tively discarded, repeating the analysis, and evaluating the crack growing direction.

Kurzfassung

Verwendung von zellulären Materialien ist heutzutage in der Industrie sehr verbreitet. Grund dafür sind ihre hervorragenden Eigenschaften wie zum Beispiel geringe Dichte, hohe Energieaufnahme und Wärmewiderstand. Neue Produktionsmethoden wie generative Fertigungsverfahren stehen zur Verfügung und ermöglichen, dass zelluläre Strukturen eine einfachere Implementation in zukünftige Designs haben werden. Deswegen ist das Verstehen ihrer Mechanik entscheidend für eine effiziente Verwendung. Allerdings ist das Bruchverhalten noch nicht vollkommen verstanden. In dieser Masterarbeit wird ein Schritt voran gemacht zum Verstehen der Bruchmechanik in zellulären Materialen gemacht, insbesondere für den Fall von kurzen Rissen im Vergleich zur Zellgröße.

Ein Finite Elemente Modell für mehrere zwei- und dreidimensional offene zelluläre Strukturen wird mit dem Zweck erzeugt, den Effekt von Rissen zu analysieren, fokussiert auf quasi-isotropes Verhalten und ideale Gitteranordnung. Erstens werden bruchmechanischen Konstanten wie Bruchzähigkeit festgestellt, indem Prinzipien der Linear Elastischen Bruchmechanik verwendet werden. Aus diesen Ergebnissen werden Skalierungformeln bestimmt, die von Struktur, Zellwandlänge und Grundwerkstoff abhängig sind. Die ausgewerteten Kriterien werden mit ähnlichen Studien aus der Literatur verglichen.

Zweitens wird der Fall von kurzen Rissen dargestellt. Um die Grenzen der Bruchmechanik zu ermitteln wird das Finite Elemente Modell parametrisiert, damit die Ergebnisse in Abhängigkeit von verschiedenen Größe bezogen werden können. Eine abgeleitete Methode aus der Finiten Bruchmechanik wird auch mit den Parametern bei kurzen Rissen verglichen.

Eine wichtige Überlegung ist der Einsatz von zwei verschiedenen Bruchkriterien. Einerseits wird das klassische Festigkeitskriterium verwendet, bei dem die lokale Spannung mit der Werkstofffestigkeit verglichen wird. Andererseits findet hier ein Stabilitätskriterium Einsatz, damit das Beulen von Zellwänden als Versagen berücksichtigt wird. Dieses Stabilitätskriterium wurde früher bei anderen Forschern zum Einsatz gebracht, jedoch nur für Fehler und Defekte in zellulären Strukturen und nicht im Zusammenhang mit der Bruchmechanik. Eine andere Überlegung ist die Betrachtung von einem "Anti" Mode I für die Rissentwicklung,

in Bezug auf das Vorliegen von Anti-Rissen. Im Gegensatz zu kontinuierlichen Materialien, bei denen die Deformation bei Druck durch Kontakt zwischen den Rissflächen gehindert wird, existieren in zellulären Strukturen Hohlräume, die eine Verformung ermöglichen.

Als letztes wird die Rissentwicklung bei Wabenstrukturen untersucht und die Unterschiede zu kontinuierlichen Materialien festgestellt. Zellwände, die die Bruchkriterien erfüllen, werden in Folge vernachlässigt und die Analyse wird mehrmals wiederholt, um die Richtung des Risswachstums zu evaluieren.

Nomenclature

A	Macroscopic fracture surface
E^*	Young's modulus of cellular material
E_s	Young's modulus of solid wall material
$\overline{E}$	Relative Young's modulus
$\mathcal{E}$	Internal energy
$\dot{\mathcal{E}}$	Internal energy rate
G^*	Shear modulus of cellular material
$\mathcal{G}$	Energy release rate
$\mathcal{G}_c$	Critical energy release rate or fracture energy
K_i	Stress intensity factor of mode i
K_{Ci}	Fracture toughness of mode i
$\mathcal{K}$	Kinetic energy
$\dot{\mathcal{K}}$	Kinetic energy rate
L	Finite Fracture Mechanics material length constant
$\mathcal{P}$	Power of external forces
$\mathcal{Q}$	Non-mechanical energy transport rate
$\mathcal{U}$	Strain energy
$\dot{\mathcal{U}}$	Strain energy rate
W	Crack growth work per unit thickness
a	Half crack length
Δa	Crack growth length
l	Cell wall length
t	Cell wall thickness
$\mathbf{t}$	Traction force per area
$\dot{\mathbf{u}}$	Velocity
Γ	Effective fracture energy
Π	Total potential
Π^{ext}	External forces potential
Π^{int}	Strain energy

γ	Fracture surface energy density
ν^*	Poisson's ratio of cellular material
ν_s	Poisson's ratio of solid wall material
ρ^*	Cellular material density
ρ_s	Solid wall density
$\overline{\rho}$	Relative density
σ_0	Trial stress in simulations
σ_{el}^B	Uni-axial buckling stress
σ_{fs}	Solid material ultimate strength
σ_f	Fracture stress
σ_{in}	Inherent strength
σ_{ult}^*	Cellular material ultimate strength

Contents

Chapter 1

Introduction

Back then in 1665, Robert Hooke was the first one to use the word cell in order to describe the structure of cork, defining a cell as a walled compartment. Cellular materials can be thought of as "composites" made up of solid and space: the solid forms a set of connected struts or plates connected at their ends or edges, to give an open structure through which fluids can flow, or one in which the cells have faces and form closed spaces. They are present in many biological and engineering structures. When the cellular structures have a two-dimensional morphology they are usually called honeycombs, whereas with a three-dimensional topology they are named foams.

1.1 Cellular materials

The use of cellular materials has been growing because of the advantage of their properties, such as low density, high energy absorption, excellent insulation, thermal resistance, cost effectiveness, among others. That makes this kind of materials an attractive solution for many problems.

Cellular solids appear in engineering applications as well as in the nature. We can find as nature examples wood, trabecular bone, coral, and many other growing organisms. Lattice structures manufactured by man are synthetic polymer foams, core materials in sandwich construction, ceramics, etc. They are widely used in cushioning and packaging. Besides, they are well suitable for lightweight structures or energy-absorption applications. Figure 1.1 shows some examples of their uses.

1.2 Mechanical properties of cellular materials

In the last decades, cellular materials are being adopted for the most modern and demanding purposes. Thus, a good understanding of their behavior is required.

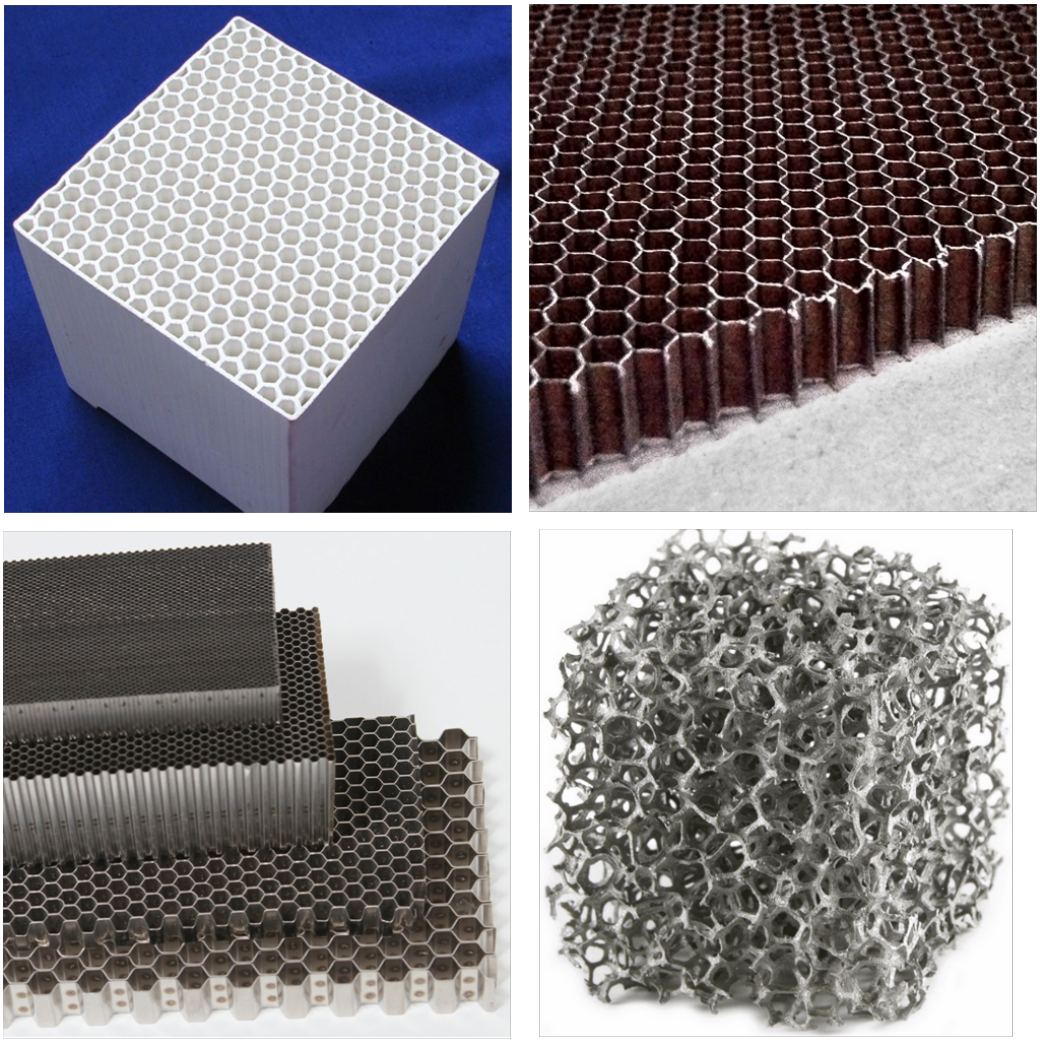

Figure 1.1: Examples of cellular materials used in engineering [Images adapted from, left to right, up to down, www.kfceramic.com, www.beessun.com, www.easycomposites.co.uk and www.raumprobe.de].

Thermal, electrical, and acoustic properties, among others, are desired to be known for some applications. However, mechanical properties are of central importance in almost all the cases. Numerous analytical, numerical, and experimental work can be found in the literature predicting their mechanical behavior. Gibson and Ashby [7] performed an excellent work in the field, gathering in their book the basis for further development. For describing cellular materials, their characteristics can be basically separated in two divisions:

- Cellular structure attributes: cell shape, size, topology...
- Solid cell wall material properties: Young's modulus, fracture strength...

Processing has its limitations, although they have been constantly overcome in the last years, giving the designer possibilities of choosing appropriate and desired cell architectures. Honeycombs and foams can be made out of metals, plastics,

ceramics, glasses, and even composites. The mechanical properties of the solid wall as Young's modulus, E_s, fracture strength, σ_{fs}, determine the nature of the material response. Brittle or plastic behavior, for instance, are obviously responses that depend directly on the solid cell wall material.

On the other hand, direct statements can be made regarding only the cellular structure, independently of the solid cell wall material. Relative density, stiffness, strength, may be defined as dependent on the cell type, shape, size, node connectivity, or regularity, as function of the cell wall properties. Buckling behavior can be likewise determined. When the failure is treated with Fracture Mechanics methods, this also occurs deriving fracture parameters, as the fracture toughness.

1.3 Scope of the work

Large research has been made figuring out different properties such as stiffness and strength on regular and irregular structures and also with multiple materials. In the case of fracture and failure behavior, studies have been made adopting fracture mechanics approaches, specially for honeycombs, but not a complete understanding has been achieved. The continuum assumptions have limitations when dealing with cellular structure materials, as the flaws and defects do not appear as sharp cracks. Literature about three-dimensional foams fracture is rather scarce. In [21] is pointed out that there exists an urgent need for the study of crack propagation behavior and fracture toughness of foams.

The objective of this work is analyzing and quantifying the failure of low-density cellular structures, concretely made of brittle materials, in the case of containing defects in form of "cracks". An embedded model based on the finite element method is used for this purpose. The studies are made in particular for regular topologies with elastic-brittle behavior. The selected topologies in two dimensions are triangular and hexagonal honeycombs, whereas in three dimensions the tetrakaidecahedral open-cell foam is used. The three of them are simple cases of many possible structures and share quasi-isotropic elastic properties.

Fracture Mechanics theories are applied for the analysis, considering a crack as the lack of some walls in line. First of all, the continuum hypothesis is verified and also the existence of a constant fracture toughness dependent on the cellular structures. In this case the crack is considered large when compared with the wall lengths.

In second place, short cracks are analyzed. Therefore, the consideration of small crack tip region is not longer valid. Finite fracture mechanics approaches have been taken to overcome this difficulty. Besides, the previous statement of constant fracture toughness has been called into question for small defects.

The last aim of this project is observing how a crack grows inside a cellular structure, in order to predict its evolution pathway and see the differences with a solid material.

Since cellular materials can collapse in compression, an anti-crack mode is presumed during the analysis. This is in contrast with solid materials, in which this deformation mode is avoided as contact between opposite crack faces arises. Further considerations are two possible failure criteria: strength failure due to a maximum tensile stress, and stability failure because of the elastic buckling of cell walls.

In summary, the questions posed in the thesis would be:

- *Fracture toughness predictions in dependence on the cellular structure.*
- *Is the fracture toughness constant and independent of the crack size?*
- *Does Finite Fracture Mechanics give a better approximation in the case of short cracks?*
- *Is the growth of cracks in cellular structures similar to continuum solids?*
- *Consideration of an anti-crack deformation mode.*
- *Predictions with two failure criteria: maximal strength and elastic buckling.*

Chapter 2

Mechanics of brittle cellular structures

In this chapter the mechanics of brittle honeycombs and foams are reviewed, describing the different mechanisms that appear either in compression or in tension. The mechanics of failure have been left for the next section.

Mechanical properties can be calculated with analytical methods based on classical beam theory. These approximations are derived and gathered in [7]. Here only expressions for regular and ideal structures are summarized, an assumption that in case of real cellular solids is sometimes far from truth.

Figure 2.1 illustrates various cellular topologies, such as triangular, hexagonal square or kagome as two-dimensional, and tetrakaidecahedral, simple cubic or Gibson-Ashby as three-dimensional. Their characteristics, such as cell size, connectivity, or regularity, have influence on the behavior. From them, the principal parameter is the relative density (the fraction of space occupied by the solid). Many other properties depend greatly on it.

2.1 Deformation mechanisms

Despite their different spatial dimension, brittle honeycombs and foam cellular structures share similar behavior and deformation mechanisms, in compression as well in and tension. Examples of stress-strain curves with both loadings can be seen in figure 2.2.

When cellular structures are loaded in compression they first deform linearly with classical elastic constants. After this phase, the deformation follows a plateau of roughly constant stress which corresponds to a brittle crushing, as long as material is brittle and plastic deformation can be neglected. A last densification step occurs in almost collapsed cells when opposite walls touch and the solid compresses

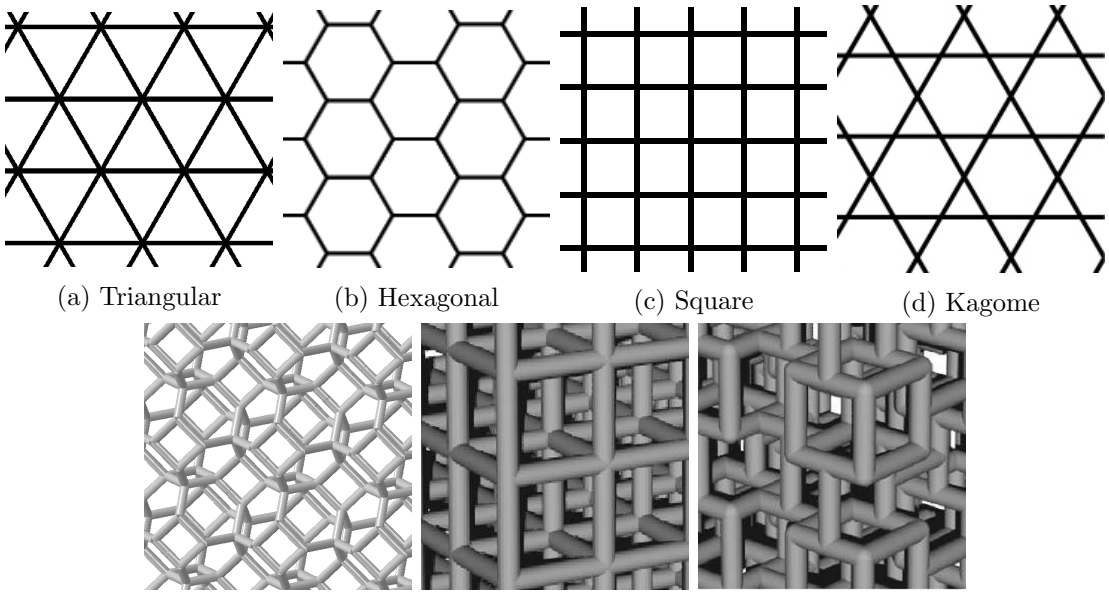

(a) Triangular (b) Hexagonal (c) Square (d) Kagome

(e) Tetrakaidecahedral (f) Simple cubic (g) Gibson Ashby

Figure 2.1: Some 2D (a, b, c, d) and 3D (e, f, g) cellular structures. Images (f) and (g) extracted from [12].

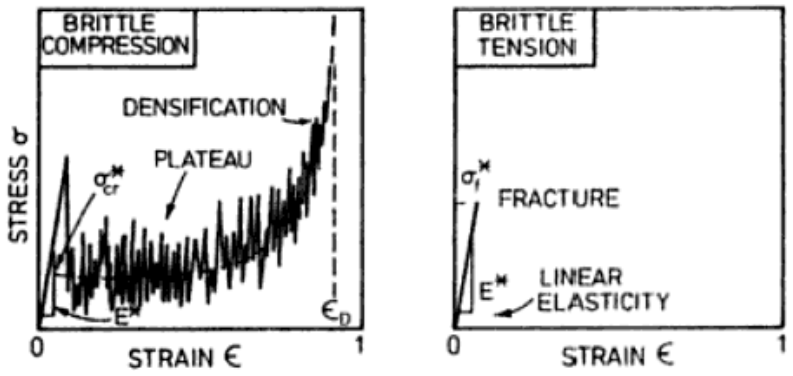

Figure 2.2: Compressive and tensile stress-strain curves for honeycombs, [7]

itself, increasing the stress abruptly. However, when describing tensile deformations, brittle cellular solids fail straight forward after the elastic deformation at a stress which is usually lower than the true crushing stress. The failure at this stress is controlled by the largest defect (a crack, a notch, or a cluster of damaged cells), which causes the breaking of struts and the consequently development of the fracture.

2.2 Relative density

The relative density, $\overline{\rho}$, is the most important structural parameter and is defined by the ratio of the density of the foam, ρ^*, to the density of the solid of which it is made, ρ_s. Its range extends from relative densities of 0.3 to much lower values

as 0.003. Relative density is also pictured as the porosity, defined as $(1 - \overline{\rho})$, referring to the fraction of pore space in the cellular material. When the relative density exceeds an approximated value of 0.3 the material is not longer considered a low density foam. Its properties differ considerably and it shows a behavior more similar to a "solid with holes".

Geometrical laws can be written in order to calculate the relative density. In the case of 2D honeycombs, the relative density is proportional to the correlation thickness, t, - length,l, of the struts according to

$$\overline{\rho} = \frac{\rho^*}{\rho_s} = A\frac{t}{l}. \tag{2.1}$$

The coefficient A is determined by the structure topology. In these estimations the overlapping at the beam ends are neglected, but this is considered a good approximation for slenderness ratio $t/l < 1/4$. A triangular architecture has a coefficient $A = 2\sqrt{3}$ and for a hexagonal one $A = 2/\sqrt{3}$. Both coefficient examples are considered for regular structures, meaning that all lattice members have the same length and constant angle between them.

The relative density of three-dimensional foams with negligible vertex volume is scaled with the square of the slenderness ratio as

$$\overline{\rho} = \frac{\rho^*}{\rho_s} = A'\left(\frac{d}{l}\right)^2, \tag{2.2}$$

where d refers to a "thickness" parameter of the struts. As example, for regular open-cell tetrakaidecahedral arrangement, $A' = 3/(2\sqrt{2}) = 1.06$ if the beam section is a square, d referring to the square side length. If the section is circular $A' = 3\pi/(8\sqrt{2}) = 0.833$, and d stands for the diameter of the section. Those relations can be found in [21] and [7].

2.3 Bending and stretching dominated architectures

Cellular solids can deform either by the bending or stretching of the cell walls. As discussed in [5], an open-cell foam can be considered a connected set of pin-jointed struts in order to analyze its behavior. Figure 2.3 shows two different frames. The frame (a) is a mechanism, which has one degree of freedom. It will collapse when a load is applied because the struts rotate around the joints. On the other hand the set (b) is a structure. The struts will support axial loads in a loaded case. Their deformation is stretching-dominated.

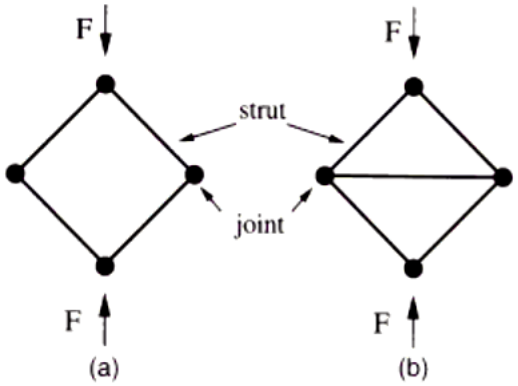

Figure 2.3: Node connectivity sketch from [5]. (a) A mechanism; (b) a structure.

Imaging the assemblages of figure 2.3 with their joints rigid, preventing free rotation of the struts, the deformation in the second case would be similar, stretching-dominated. But in the first set, an applied load induces bending moments at the frozen joints and these cause the struts to bend. Thus, it is a bending-dominated case. The behavior lies in the number of joints and bars connected. A note must be given in this differentiation, since for some structures the deformation mechanism depends also on the load type [14], as for example in a square structure.

In [5] the authors conclude with a condition that determines if the structure is bending or stretching dominated, depending on the node connectivity. For two-dimensional topologies the minimum node connectivity is 6 for beeing stretching-dominated. For three-dimension foams it is 12. Analyzing the structures used in the present work gives:

- Triangular (2D): node connectivity = 6 (≥ 6) $\Rightarrow$ *stretching dominated.*
- Hexagonal (2D): node connectivity = 3 (< 6) $\Rightarrow$ *bending dominated.*
- Tetrakaidecahedral (3D): node connectivity = 4 (< 12) $\Rightarrow$ *bending dominated.*

The strength and stiffness of a stretching-dominated cellular solid are much greater than those of a bending dominated with the same relative density. That makes the stretching dominated materials attractive for lightweight structural applications. Nevertheless, in compression bending dominated structures show a more attractive behavior for energy-absorvers, since this application needs a stress-strain response with a long, flat plateau. The stretching dominated materials show a softening post-yield response due the buckling of the struts.

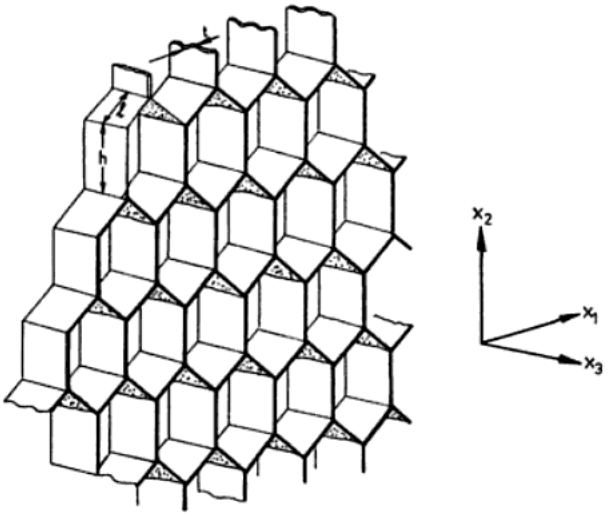

Figure 2.4: Honeycomb with hexagonal cells. In-plane deformation: plane x_1-x_2. Out-of-plane deformation: direction x_3.

2.4 Elastic deformation in honeycombs

In the case of honeycombs, it is to distinguish between in-plane and out-of-plane deformations, depending on the orientation of the cell. "In-plane" is referring to directions on the plane x_1-x_2, while "out-of-plane" are those along the x_3 direction, following the coordinates system of figure 2.4.

The elastic response of a honeycomb loaded in-plane can be approximated using simple beam theory. The approximations are good for small ratios of thickness over wall length ($t/l < 1/4$). The Young's modulus scales with the square of the relative density for bending dominated structures, e.g. the case of hexagonal cells, and is directly proportional to the relative density for stretching dominated structures, as triangular cells (see anterior point of node-connectivity dependency). The general power law for the relative density, $\overline{E}$, can be written

$$\overline{E} = \frac{E^*}{E_s} = B\overline{\rho}^b, \tag{2.3}$$

as presented in [16]. E^* represents the Young's modulus of the lattice, E_s the Young's modulus of the solid material, and B and b are characteristic parameters dependent on the cellular structure. Despite the non-continuum solid nature of the lattice, some structures show a quasi isotropic response to deformations, while other are strongly anisotropic. Figure 2.5 shows some examples of both cases. In the case of square lattice the Young's modulus shows a great anisotropy, it depends extremely on the regarded direction. Triangular and hexagonal structures are isotropic, but the triangular is much more stiffer for equal wall thickness and length. Considering the same relative density, stiffness of the triangular lattice is

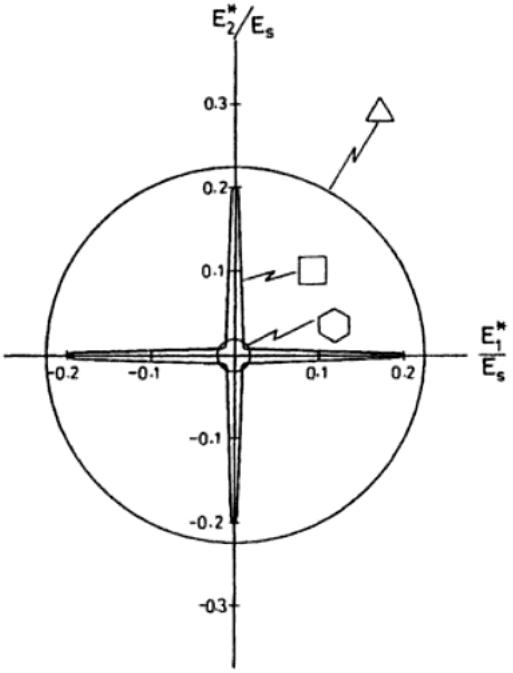

Figure 2.5: Comparison of normalized Young's modulus as function of direction for triangular, square and hexagonal cells ($t/l = 0.2$) [7].

also higher than the hexagonal.

When out-of-plane loading is applied, the cell walls extend or compress rather than bend. Therefore the Young's modulus E_3^* depends directly on the area of solid material, indeed, the relative density. The Poisson's ratios are equal to those for the solid itself:

$$\frac{E_3^*}{E_s} = \frac{\rho^*}{\rho_s}, \tag{2.4}$$

$$\nu_{31}^* = \nu_{32}^* = \nu_s. \tag{2.5}$$

Honeycombs are much stiffer and stronger when loaded along the axis, and also in case of applying out-of-plane shear. The estimations of shear modulus depend on cell topology and cannot be calculate in a simple way (further information in [7]).

2.5 Elastic deformation in open-cell foams

The mechanisms of linear elasticity depend on whether the cells are open or closed. In the present case, open-cell foams, the cells are built with struts along the cell edges, allowing space connection through their faces. The elastic behavior of open-cell foams, as with two-dimensional lattices, can be derived from analytical calculations depending on both structure type and connectivity. By connectivity is to understand the number of struts that connect at each point or node of the structure.

Independent of the deformation mechanism (tension, compression...), at low relative densities open-cell foams deform primarily by cell-wall bending. But as the relative density increases ($\rho^*/\rho_s > 0.1$) the contribution of simple extension or compression of the cell walls becomes more significant. In the case of isotropic foams two moduli are needed to characterize their linear response, chosen from the Young's modulus, E^*, the shear modulus, G^*, the bulk modulus, K^*, and the Poisson's ratio, ν^*. More are required when it is not isotropic.

The behavior is the same in tension as in compression in small strains, and its Young's modulus can be estimated with the same law of honeycombs, namely equation (2.3). Analytical calculus suggests values for this formula of $b = 2$ and $B = 1$ with great accuracy, as showed in [7]. The Poisson's ratio can have the range $-1 < \nu < 0.5$. For a material which is isotropic the shear modulus is obtained from the well known relation $G = E/2(1 + \nu)$.

2.6 Effect of defects

Estimations are made for ideal regular structures, and this project is restricted to calculations with perfect regular structures. In the reality, cellular materials posses a wide range of geometrical imperfections as well as defects in form of holes or damaged struts. Stiffness and strength depend directly on these defects, and their effects have been examined in many studies. Gibson and Ashby in [7] give a general insight about these questions, more specific damage effect quantification of defects can be found in the works of Fleck et al. [6] and Luxner et al. [12], [14], [13], among others.

Chapter 3

Failure of brittle cellular structures

Foams made up of a brittle material, like ceramic or glass, have a linear-elastic response up to a fracture stress, at which failure occurs in a brittle mode. A difference is made between fracture in tension and in compression. The explanation of these processes is again referred to the work of Ashby and Gibson [7]. In tension the foam fails by the propagation of a single crack, that can be treated as a fracture problem; in compression it crushes progressively caused by collapse and densification of struts inside the crack, as explained before (see figure 2.2). Under compression, failure can also occur because of instabilities. Buckling in the struts would cause high stresses, originating failure. Figure 3.1 shows an example for an hexagonal honeycomb, where failure is represented by a fracture surface. The fracture surface corresponds to different failure mechanisms according to the loading case.

When a cell wall reaches its ultimate fracture stress, which finds itself at the wall surface, a micro-crack grows in a brittle unstable way and causes the complete break of the beam. It defines the failure of a cell strut. Because of the catastrophic propagation of the micro-crack, failure is considered to occur at the first moment a cell wall reaches the fracture stress. Two criteria have been proposed for failure: a first one, considering the maximal local stress on the cell walls; and a second one, considering the buckling of the struts. Because of the brittle nature of the material, the dissipation in the fracture can be neglected, therefore no energy lost per dissipation needs to be considered.

Fracture mechanics approaches can be applied to calculate the strength of structures where some cell walls are missed, treating these defects as cracks. In this chapter the fracture mechanics theory is reviewed, with some remarks on some other fracture concepts. Then the failure mechanisms and predictions are showed, and how they are treated analytically and numerically in the literature.

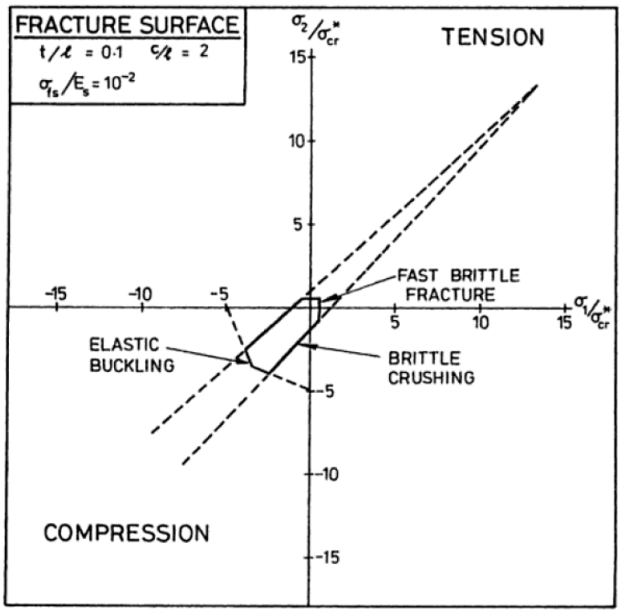

Figure 3.1: Fracture surface for a regular hexagonal honeycomb. The stresses are plotted in units of the uniaxial crushing strength σ^*_{cr}. The surface may be truncated on the compressive side by elastic buckling or axial crushing, and on the tensile side by fast brittle fracture [7].

A summary of properties approximations is recalled in a last point. In [21], [16] and [6] can be found some research studies about the topic, where this fracture mechanics approach is well conducted to cellular solids.

3.1 Fracture mechanics theory

Fracture mechanics is the continuum mechanics approach to the mechanical behavior of solids which are weakened by cracks. Within this approach, the cracks already exist and may extend under certain conditions of loading. The theory derives from the classic works by Irwin [11] and Griffith [8]. Griffith presented an energy balance approach for strictly brittle materials which Irwin extended to include material behavior controlled by small scale plasticity. The problems can be addressed from a stress intensity factor based approach or from an energy balance approach, but both give identical results. Because of the easier methodology, the stress intensity factor based scheme is preferred for engineering purpose in most problems.

For this project, even though dealing with non continuum materials, principles of fracture mechanics based on continuum assumptions can be applied. Many researchers have shown the good accuracy of the predictions, specially in the case of long cracks, when the strut length becomes small relatively to the crack-tip zone. In the present section the linear theory of fracture is reviewed, besides some

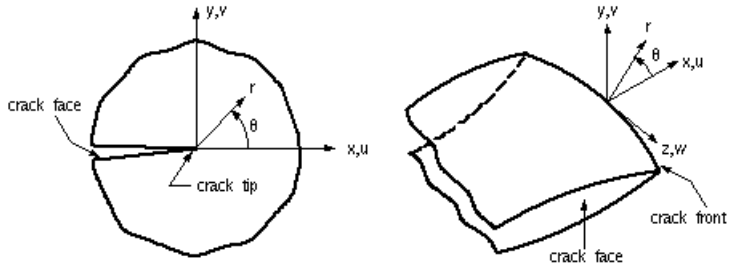

Figure 3.2: Crack tip with cylindrical coordinate system, 2-D and 3-D models [17].

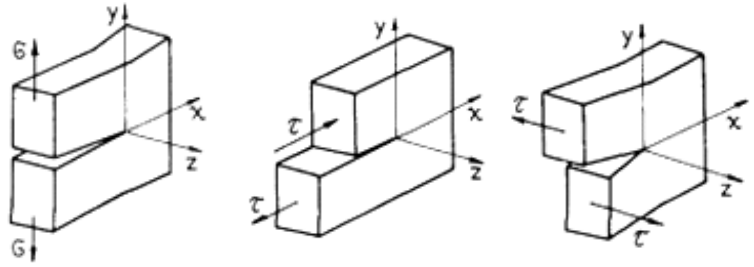

(a) Mode-I (b) Mode-II (c) Mode-II

Figure 3.3: The three fundamental modes of fracture. (a): mode-I, tensile or opening mode; (b): mode-II, in-plane shear or sliding mode; (c): mode-III, anti-plane shear or tearing mode [17].

special concepts that are used for the purposes of this project.

3.1.1 Linear Elastic Fracture Mechanics (LEFM)

Linear Elastic Fracture Mechanics (LEFM) considers the fracture problem from a continuum mechanical viewpoint, taking the behavior as linear elastic in the whole region, while the inelastic processes are restricted to a very small zone. This small zone, in which plastic deformations take place, is negligible and does not affect to the macroscopic treatment. LEFM is suitable for the description of brittle fracture, as being the case of the current work.

As shown in figure 3.2, a crack is composed by its boundaries, named crack surfaces, ending at the crack front, also called crack tip. Depending on crack tip deformation, three different modes of fracture exist (figure 3.3): mode-I, tensile or opening mode; mode-II, in-plane shear or sliding mode; and mode-III, anti-plane shear or tearing mode.

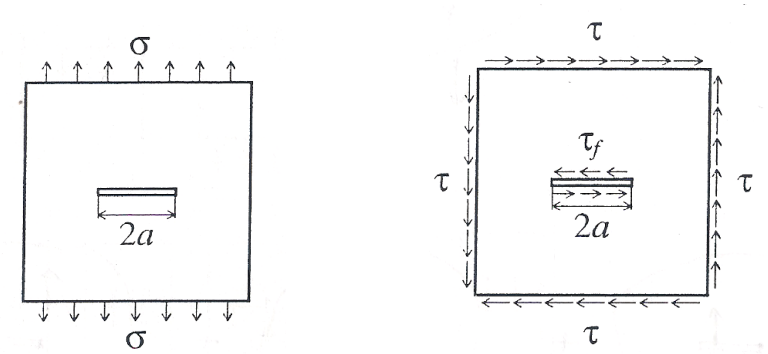

(a) Uniaxial tensile stress: $K_I = \sigma\sqrt{\pi a}$, $K_{II} = 0$, $K_{III} = 0$.

(b) Shearing stress: $K_I = 0$, $K_{II} = \tau\sqrt{\pi a}$, $K_{III} = 0$, (if friction operates: $\tau = \tau - \tau_f$.

Figure 3.4: Stress intensity factors of the two fundamental crack cases [17].

Crack tip stress field, Stress intensity factor

For the three fundamental modes of deformation, the stresses in an isotropic solid close to the crack tip are given by

$$\sigma_{ij} = \sum_{k=1}^{3} \frac{K_k}{\sqrt{2\pi r}} f_{ij}^k(\Theta) + O(1), \tag{3.1}$$

where the functions f depend on the circumferential coordinate Θ and are given according to the material directions i and j, whereas K_k denotes the stress intensity factors for mode-k. Polar coordinates are denoted by r and Θ, referring to the distance from crack tip and angle from crack plane, respectively (see figure 3.2). Stress intensity factors of the same mode are additive.

An infinite body with a single crack of length $2a$ with an remote homogeneous stress field is considered. In case of uniaxial tensile stress σ the mode-I stress intensity factor reads:

$$K_I = \sigma\sqrt{\pi a}, \tag{3.2}$$

showed in figure 3.4(a), while the other modes are zero. For a solid subjected to shear stresses τ the only non-zero factor is

$$K_{II} = \tau\sqrt{\pi a}, \tag{3.3}$$

as depicted in figure 3.4(b). These are the two fundamental cases.

Fracture toughness

After introducing the stress intensity factor a fracture criterion can be formulated. The propagation of a crack occurs when the stress intensity factor K_i reaches a

material-specific critical value K_{ic}:

$$K_i = K_{ic} \tag{3.4}$$

with i refering to the deformation mode. The quantity K_{ic} is called fracture toughness and is a material parameter which can be determined experimentally or numerically.

As example, the critical uniaxial stress causing crack growth in figure 3.4 (a) would be given by

$$\sigma_f = \frac{K_{Ic}}{\sqrt{\pi a}}, \tag{3.5}$$

where σ_f is defined as fracture stress, applied to the macroscopic cellular material. It is to understand that the stress intensity factors are parameters calculated from the problem, whereas the fracture toughness is intrinsic to the material.

Energy balance and energy release rate

The work done during creation of a new fracture surface is a characteristic fracture quantity. If dissipative processes are neglected and the material is, from the macroscopic point of view, considered as a continuum, there is a theoretical surface energy due to the release of bonds. But, on the one hand, plastic deformation in the tip vicinity takes extra energy, and possible chemical and electromagnetic energies have to be taken into account. On the other hand, due to microscopic irregularities, the macroscopic surface is smaller than the true fracture surface.

Therefore, with practical views, an effective energy that summarizes all the work made by irreversible processes for the creation of new surfaces is considered. It is the effective fracture energy Γ, defined as

$$\Gamma = 2\gamma A, \tag{3.6}$$

γ is the fracture surface energy density and A is the macroscopic fracture surface. Multiplication by two is because two new surfaces are created.

The energy balance of first law of thermodynamics states that the change of total energy (internal energy + kinetic energy) of a body is equal to the energy flow into the body. If we include the fracture energy, the energy balance has the form

$$\dot{\mathcal{E}} + \dot{\mathcal{K}} + \dot{\Gamma} = \mathcal{P} + \mathcal{Q}. \tag{3.7}$$

$\mathcal{E}$, $\mathcal{K}$, and $\mathcal{P}$ are the internal energy, the kinetic energy, and the power of

external forces, respectively. They are given by:

$$\mathcal{E} = \int_V \rho e dV, \tag{3.8}$$

$$\mathcal{K} = \frac{1}{2}\int_V \rho \dot{\mathbf{u}} \cdot \dot{\mathbf{u}} dV, \tag{3.9}$$

$$\mathcal{P} = \int_{\partial A} \mathbf{t} \cdot \dot{\mathbf{u}} dA, \tag{3.10}$$

where e is the specific internal energy, $\dot{\mathbf{u}}$ the velocity, and $\mathbf{t}$ the force density per area. The quantity $\mathcal{Q}$ describes an energy transport rate into the body which is not covered by $\mathcal{P}$, as e.g., heat flux. For an elastic material ρe can be described as the strain energy U. Due to the irreversibility of the process, $\dot{\Gamma} \geq 0$ holds.

Now, we analyze a quasi-static fracture process. The plastic zone, where inelastic processes take place, is considered small. Accordingly, the kinetic energy $\mathcal{K}$ and the non-mechanical energy transport $\mathcal{Q}$ do not play a role. The internal energy $\mathcal{E}$ can be replaced by the strain energy Π^{int}. Additionally, it is presumed that the external forces have a potential Π^{ext}. The energy balance equation (3.7) is then in differential form

$$d\Pi^{int} + d\Pi^{ext} + d\Gamma = 0, \tag{3.11}$$

with $\mathcal{P}dt = -d\Pi^{ext}$. The total potential Π can be also decomposed as

$$\Pi = \Pi^{int} + \Pi^{ext}. \tag{3.12}$$

Thus, during the fracture process when crack grows the change of the sum of the total potential, Π, and the effective fracture energy, Γ, is assumed to be zero. Related to the crack surface change it can be written as

$$\frac{d\Pi}{dA} + \frac{d\Gamma}{dA} = 0. \tag{3.13}$$

At this point the energy release rate is introduced. The released energy during an infinitesimally small crack advance is called energy release rate

$$\mathcal{G} = -\frac{d\Pi}{dA}, \tag{3.14}$$

where dA is the infinitesimally crack surface advance. Or

$$\mathcal{G} = -\frac{d\Pi}{da}, \tag{3.15}$$

related to the unit thickness for a plane problem, where da is an infinitesimally small crack extension. The energy release rate has the dimension of a force (per unit thickness). Therefore it is also denoted as the crack extension force. When a problem is given, the energy release rate can be calculated supposing a crack advance. At the moment a crack starts to grow, it equals the critical energy release rate:

$$\mathcal{G} = \mathcal{G}_c, \tag{3.16}$$

which is a material property. In the linear elastic case, the energy release rate can be expressed in terms of stress intensity factors, obtaining the same results. The equivalence for the three modes is

$$\mathcal{G} = \frac{1}{E'}(K_I^2 + K_{II}^2) + \frac{1}{2G}K_{III}^2. \tag{3.17}$$

Here, $E' = E/(1-\nu^2)$ for plane strain and for the three-dimensional case while $E' = E$ for plane stress.

The equation (3.13) is the *Griffith's fracture criterion*, first applied by A.A. Griffith. It states that at initiation and during the evolution of quasi-static crack advance, the released energy must be equal to the energy needed for the fracture process. Combining equation (3.13) with the eqns. (3.6), (3.14), and (3.16) gives $\mathcal{G}_c = 2\gamma$: the fracture energy equals the work required for the creation of the new crack surfaces.

3.1.2 Finite Fracture Mechanics approach (FFM)

The fracture mechanics of finite crack extension theory (FFM) involves a modification to the traditional Griffith energy balance from LEFM. A finite amount of crack extension, Δa, is used instead of an infinitesimal extension, da, when calculating the energy release rate [20], [15].

A straight, through-crack of length $2a$ in a flat plate is considered, whose width and length are large enough to be considered infinite. The plate is subjected to a remote tensile stress σ applied normal to the crack. The strain energy per unit thickness associated with the half-length a of the crack can be defined as

$$W = \frac{\sigma^2 a^2 \pi}{2E}, \tag{3.18}$$

as shown in [17] and referenced in [20]. It is derived from the energy balance of a crack during crack growth (refer to [17] for further information).

Normally, the energy changes are considered by an infinitesimal amount of crack length, da. But in FFM the crack extension is considered a finite value, Δa.

The associated change in strain energy is then integrated as

$$\Delta W = \int_a^{a+\Delta a} \frac{\sigma^2 \pi}{E} a da = \frac{\sigma^2 \pi}{2E}(2a\Delta a + \Delta a^2). \tag{3.19}$$

Equating it to $G_c \Delta a$ gives a new form for the fracture stress:

$$\sigma_f = \sqrt{\frac{G_c E}{\pi(a + \Delta a/2)}} = \frac{K_c}{\sqrt{\pi(a + \Delta a/2)}} \tag{3.20}$$

This finite amount of crack extension Δa is assumed to be a material constant. When a is large compared to Δa, this equation returns to the normal LEFM prediction for long cracks, equation 3.5. But as a decreases, the fracture stress becomes lower than predicted by LEFM, tending to a constant value as a approaches zero (see figure 3.5). This constant value is called "inherent strength" of the material, σ_{in}:

$$\sigma_{in} = \frac{K_c}{\sqrt{\pi(\Delta a/2)}}, \tag{3.21}$$

that may or may not be equal to the strength of uncracked specimens. If it refers to the ultimate stress, a constant L can be defined, which is equal to $(\Delta a/2)$. The constant L depends on the material's strength and toughness:

$$L = \frac{1}{\pi}\left(\frac{K_c}{\sigma^*_{ult}}\right)^2 = \frac{1}{\pi}\frac{G_c E^*}{(\sigma^*_{ult})^2} \tag{3.22}$$

where σ^*_{ult} is the ultimate strength of the cellular material. This definition allows to predict the propagation of a crack using material strength and toughness characteristics, which can be obtained from independent tests. More information is to be found in [20].

The situations where this theory can be applied is when LEFM is normally invalid because the continuum assumption is not longer adequate. For instance in the case of short cracks and notches.

3.1.3 Anti-crack deformation mode

When dealing with cracks in cellular materials, another extra deformation mode can appear. In the case of solid continuous materials, if a compressive stress perpendicular to the crack faces is applied, contact between opposite surfaces (assuming a practically zero-thickness crack) is immediately generated. The deformation of the crack is not allowed and hence, neither stress concentration near the tip occurs nor crack growth is possible in this way.

In contrast, there exist some special cases that allow the deformation although

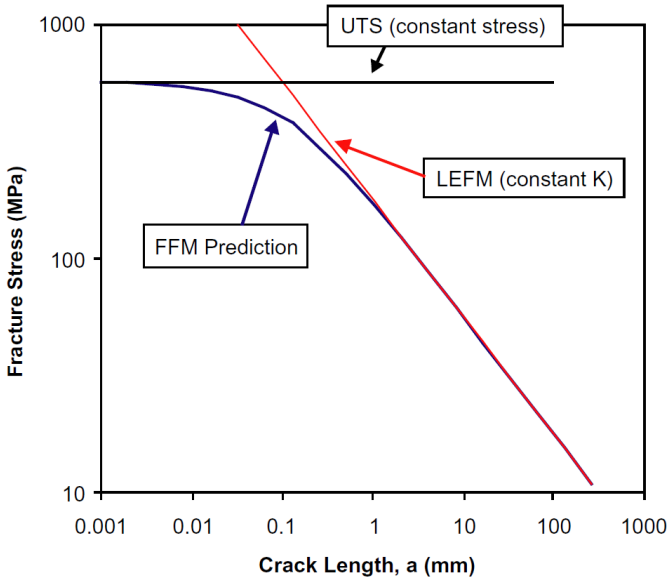

Figure 3.5: Example of prediction of fracture stress σ_f using finite fracture mechanics (FFM). Extracted from [20].

the presence of perpendicular compressive stress, where a void allows the inwards displacements (figure 3.6). A first example of this case is given by compaction bands in sandstone. Compactation bands can collapse because of their porosity and are treated as anti-cracks [19]. Other example appears with snow. Snow slab avalanches can be triggered when a big pressure under snow blocks compress weak snow layers. The volumetric collapse of snow behaves as an anti-crack, and when the crack is large enough, the gravity load because of the slope leads to an mode-II fracture, causing the avalanche of the snow block.

Cellular structures, object of this project, are also a possible case of this anti-crack behavior. The crack faces are not continuous and the contact between crack faces is only established at some points, before further deformation leads to densification. Therefore, an anti-crack deformation mode should be considered here for brittle foams. A crack evolution can occur with compressive forces, corresponding to a displacement field equal in magnitude but opposite in sign to that of a classical mode I, are applied (figure 3.6). This mode would correspond to cell displacement and deformation with a contrary sign as in mode-I, but not necessarily satisfying the same fracture criteria. Specific fracture properties have to be considered and calculated to this mode.

3.1.4 Statistics of failure

In practice, the assumption of constant fracture properties of brittle cellular materials is unrealistic. Brittle fracture is a stochastic process, dependent on the

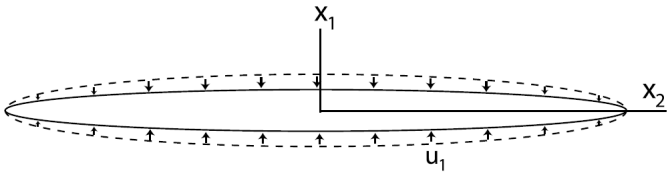

Figure 3.6: Anti-crack displacement schema of an anti-crack mode I [19].

presence and distribution of defects in the struts [16]. The Weibull statistical distribution can describe adequately these events.

Depending on the width of this distribution, modulus m in the Weibull formulation, the failure of the first strut may or may not trigger the failure of the whole. The tensile and compressive strengths are significantly influenced by the flaw distribution in the bodies, giving a variability in the strength of brittle cellular materials. It is important to consider this variability when estimations are being made assuming constant properties.

3.2 Failure by brittle fracture or crushing

In honeycombs and foams, the cells suffer progressive crushing when compression forces are applied. In tension, the cells fail by brittle failure. The failure takes place when the stress in a cell wall exceeds the solid material ultimate strength, σ_{fs}.

A recent review about the two-dimensional lattices is made by I. Quintana-Alonso and Norman A. Fleck in [16]. They present the most important methods, theories and experiments to determine the fracture properties of cellular solids, giving a very good summary of the relevant literature. For three-dimensional foams less research has been made and few literature is available. A well defined study is found in [21], that gives a good understandable analysis for tetrakaidecahedral structures.

3.2.1 Strength approximation

From linear analysis an approximation can be made for the stress at which failure of the cellular solid would occur, considering a complete grid without lack of any cell strut. The critical macroscopic uniaxial strength σ_c is approximated by the law

$$\overline{\sigma_c} = \frac{\sigma_c}{\sigma_{fs}} = C\overline{\rho}^c, \tag{3.23}$$

scaled with the ultimate strength of the cell wall material, σ_{fs}. It shows the direct relationship with the solid density. C and c are constants that depend on the

sort of structure. Some example coefficients are summarized in section 3.5 for triangular, hexagonal and tetrakaidecahedral structures.

3.2.2 Fracture toughness

A variety of theoretical predictions have been made to determine the fracture toughness of cellular solids. The expressions are functions of relative density again and of topology. Some numerical approaches have been developed too.

In an ideal case, triangular lattices deform by stretching mechanisms, independent of the loading mode, and K_{IC} scales linearly with $\overline{\rho}$. It means that the local deformation of cell walls is almost completely in a tensile or compressive way. On the other hand, the hexagonal honeycomb deform by cell wall bending, such that K_{IC} scales with $\overline{\rho}^2$ [6]. The third structure is the Kagome lattice (figure 2.1d), which shows a mixture of flexural and stretching deformation. It gives a a high fracture toughness with a high damage tolerance.

LEFM assumes a constant fracture toughness. Direct analytical solutions can be proposed. For instance for regular, uniform hexagonal honeycombs, approximations are made in [7]. But in order to put into question this assumption for cellular materials, finite element analysis is a decisive method to do it.

3.2.3 Finite element studies

The finite element method has been used to determine the failure behavior as well as some of the material constants, mainly the fracture toughness. Many studies have been made for a wide range of 2D lattice structures and some for 3D foams.

A micromechanics finite element approach has been used by several authors to obtain the toughness of a cellular solid. It was first used by Schmidt and Fleck in [18]. The approach consists in modeling a small region around the crack tip using beam elements. Along the boundary displacement boundary conditions are applied according to a K-field for a given Mode I, Mode II or a mixed mode. Some more studies with the same approach are made by Choi and Sankar in [3], or by Sankar et al. in [21]. An actual good review can be found in [16], comparing different finite element studies with analytical laws, mainly for two-dimensional structures.

In these studies is concluded that the fracture toughness, as a fracture mechanic characteristic parameter, is independent of the crack length in cellular materials up to a crack length magnitude of a few wall cells length. There are some discrepancies in that limit, from a single cell length to eight or ten cells crack length. For example in [6] is said that LEFM predictions are acceptable for cracks longer than about one cell dimension.

3.3 Failure by elastic buckling

When compressive forces appear in the cell walls or cell edges, specially in the case of cellular solids with low relative densities, they first bend and compress. But then buckling instabilities can take place before another failure mechanism. Buckling is more considered as a phenomenon in the case of elastoplastic bulk material. But in a brittle material instabilities can also cause high local stresses and originate the strut fracture. Consequently, the elastic buckling can be seen as a failure criterion for brittle cellular materials.

3.3.1 Buckling stress estimations

Gibson and Ashby [7] developed an approximation for ideal hexagonal structures, analytically extracting the axial force in the cell wall and using classical beam stability criteria from Euler. A key adjustment is which factor is taken for the buckling load in Euler formula for the end constraints: cell wall ends are neither in a condition of free rotation nor of complete constraint. Taking a compromise between them both, the approximation results as

$$\frac{\sigma^*_{el}}{E_s} = 0.22 \left(\frac{t}{l}\right)^3, \tag{3.24}$$

where σ^*_{el} is the uni-axial stress at which buckling occurs, E_s the stiffness of the solid material, and t and l the thickness and length of the walls, respectively. Ideal regular hexagonal structures have been considered for this law, assuming isotropic behavior. For more details about buckling estimations refer to [7].

3.3.2 Finite element studies

Some studies can be found in the literature for ideal structures, but more interesting for the present case is to mentioned the few that treat cellular structures with cell voids or lacking of some cell walls in them.

An important and interesting study was made by Guo and Gibson in [9]. In it finite element calculations were performed for honeycomb structures with some walls or cells missing. The paramers considered were the size of the defects and in the case of several defects, the relative distance between them. Of interest is the fact that they ended up with similar scaling walls as with strength criteria.

On the other hand no literature has been found where the defects have been treated as cracks, applying fracture mechanics theories. In [9] scaling laws where derived for flawed lattices, thus, it seems an appropriate approach to treat missing cells as cracks an try if LEFM can be used with buckling failure.

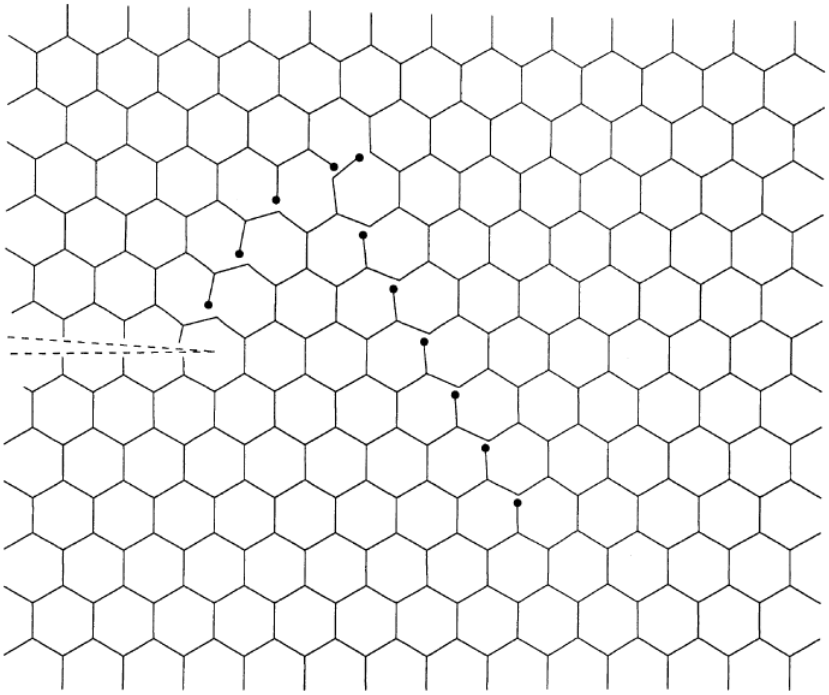

Figure 3.7: Predicted path in a regular honeycomb for mode I [18].

3.4 Growth and propagation of cracks

Independent of the structure, cracks in cellular solids do not develop as expected from fracture mechanics theory. For example in Mode I the crack would be expected to advance in a straight line. But observing in detail which struts continue to break, it does not happen. Figure 3.7 from [18] shows an explicative example in a regular honeycomb subjected to mode I loading. Figure 3.8 from [6] depicts how unexpected the path can be, in this case for combined mode I and II in several honeycomb structures.

Therefore it is important to take into account that not always the expected strut will be the next that breaks. For evaluating the fracture toughness with energy methods, where the internal energy is measured before and after the crack grows, this can be a cause of error.

3.5 Summary of scaling laws

This is a summary of parameters for some isotropic cellular structures for the before presented approximations/laws (table similar as in [6]), all dependent on geometrical and solid material parameters. The expressions for relative density, stiffness and strength are equations

$$\overline{\rho} = \frac{\rho^*}{\rho_s} = A\left(\frac{t}{l}\right)^a, \tag{3.25}$$

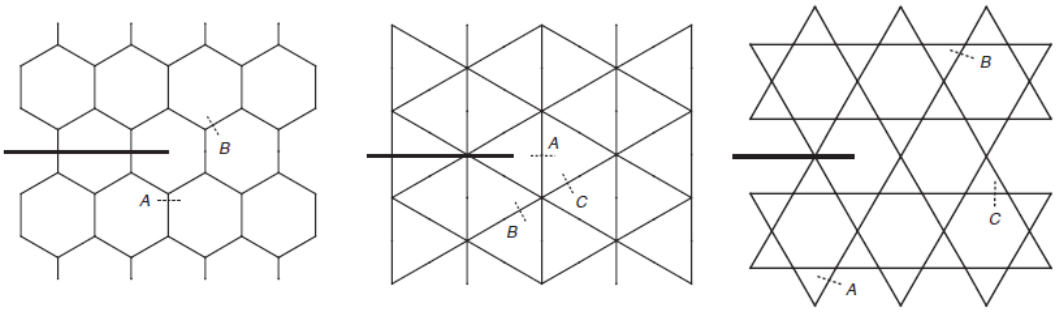

Figure 3.8: Predicted site of failure in hexagonal, triangular and Kagome structures for combined mode I and mode II [6].

Topology	A	a	B	b	ν	C	c
Triangular	$2\sqrt{3}$	1	1/3	1	1/3	1/3	1
Hexagonal	$2/\sqrt{3}$	1	3/2	3	1	1/3	2
Tetrakaidecahedral	$3/(2\sqrt{2})$	2	1	2	0.5	0.3	3/2

Table 3.1: Summary of parameters in isotropic cellular structures.

$$\overline{E} = \frac{E^*}{E_s} = B\overline{\rho}^b, \tag{3.26}$$

and

$$\overline{\sigma_c} = \frac{\sigma_c}{\sigma_{fs}} = C\overline{\rho}^c, \tag{3.27}$$

respectively, being the parameters shown in table 3.1. In it also appears the Poisson's ratio, ν. All approximations are analytical derived, mostly extracted from [7].

Chapter 4

Finite element modeling

In order to analyze the effects of cracks in cellular structures, a model based on the finite element method is built. The model predicts an homogeneous stress field around the crack, simulating the necessary conditions to apply fracture mechanics methods. For this, an embedded cell model is used.

There are some simplifications and idealizations of the model to note:

- Perfect regular structures with constant wall thickness/diameter.
- The struts connect in a single point at nodes, neglecting that the cell walls collide around the joints.
- A deterministic process is presumed; imperfections and statistical methods are not considered.
- The length of the crack is always considered between cell centers.
- Only structures with isotropic elastic properties are considered.

Two types of analysis are performed with the model: a static analysis according the strength failure criterion and a buckling analysis for the stability failure criterion. In both cases the analyses are linear, with neither material nor geometrical non-linearity.

The software used is Abaqus in its version 6.13, from the company Dassault Systemes. The numerous analysis are built with Python scripts, automatizing the parameter studies with the different characteristics of the model: structure topology, orientation, material properties, analysis type, loading modes, etc.

4.1 Cellular topologies

For the modeling, honeycombs with triangular and hexagonal cells in two-dimension (see figures 4.1a and 4.1b) are the covered structures. In three-dimension, a open-

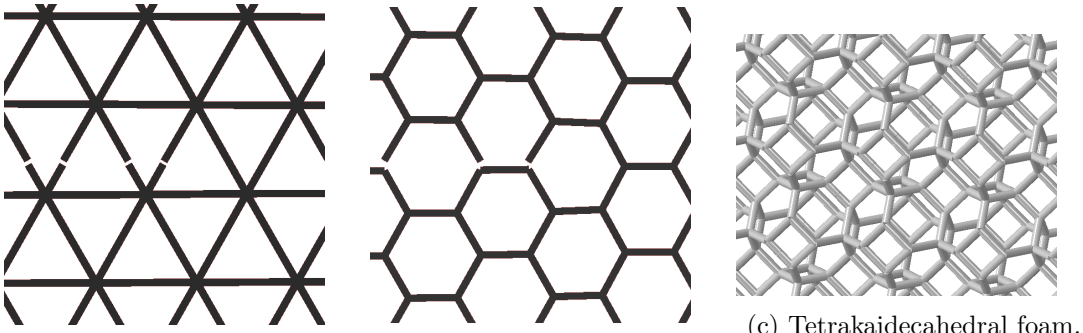

(a) Triangular honeycomb. (b) Hexagonal honeycomb. (c) Tetrakaidecahedral foam.

Figure 4.1: Simulated isotropic cellular structures.

cell foam with a tetrakaidecahedral cell unit is selected (figure 4.1c). All these topologies share a similar characteristic: their mechanical properties are considered isotropic. This is because of the lattice orientation is not significant to the cells stiffness. An exception is the tetrakaidecahedral structure, in which a slightly anisotropy can derived depending on the orientation, as shown in [14]. As explained above, only regular structures are considered in this study.

4.2 Embedded cell model

In the literature, FEM micromechanical models are used to calculate fracture toughnesses. In these models the boundary conditions are based on the near-tip displacement fields from K-factors. Giving the K-field displacements for the boundary conditions is not valid for our purpose since short cracks are considered, the near-tip region size is not longer small in comparison with the crack length. An alternative that implies multi-scale modeling, coupling the macroscopic with the microscopic behavior of the material is presented.

This corresponds to the Embedded Cell Approaches from micromechanics. A type of embedded cell approach is used to create the model, allowing the application of a homogeneous stress field in the crack proximity with an reasonable and economic number degrees of freedom.

4.2.1 Embedded cell approach

As explained in [2], Embedded Cell Approaches (ECAs) aim at predicting the micro-fields in inhomogeneous materials at high spatial resolution. These models consist of a core containing a discrete phase arrangement that is embedded within some outer region that serves mainly for introducing loads into the core. A suitable description of the outer region must be chosen, so that errors in the accommodation of stresses and strains are avoided.

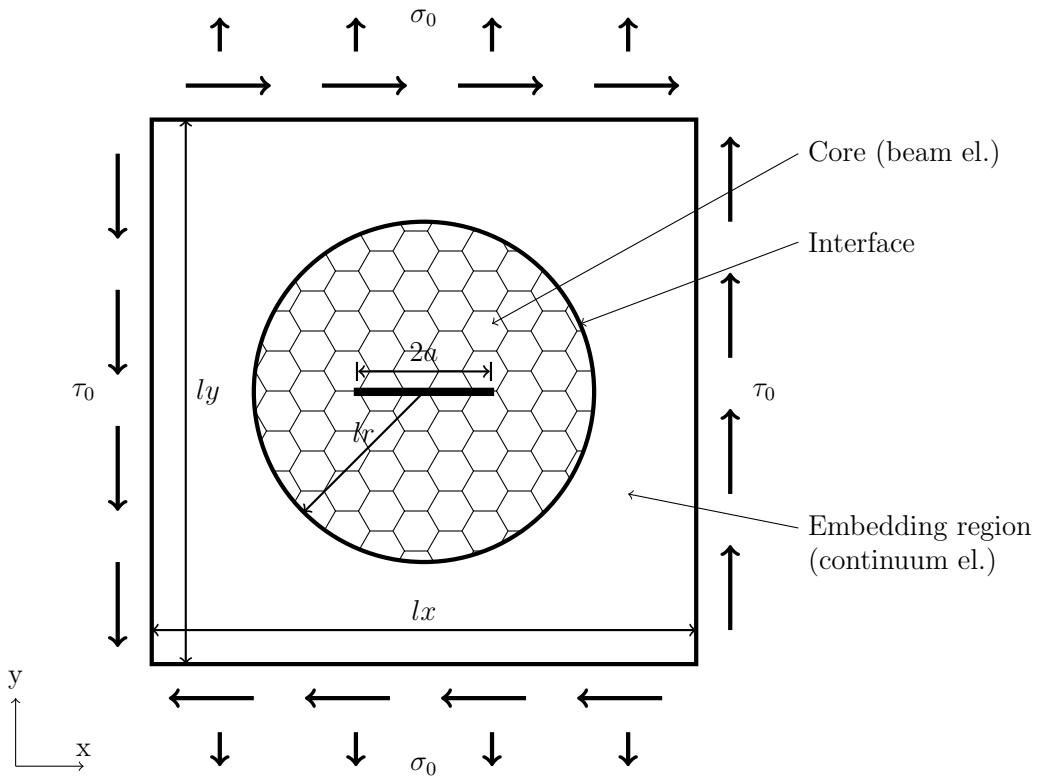

Figure 4.2: Sketch of the finite element model, embedded cell approach.

There are several types of embedding approaches. They are grouped in three basic types in [2]. In this case an embedding approach is chosen, in which the behavior of outer regions is described via appropriate constitutive models. These constitutive models correspond to semiempirical or simplified constitutive laws that correspond closely to the overall behavior of the core. In this way simple models can be built for studying local phenomena such as the stress and strain distributions in the vicinity of crack tips or the growth of cracks in inhomogeneous materials, which is the case.

The figure 4.2 shows a sketch of the model. In it the embedded core of beam elements can be loaded by homogeneous stresses or strains applied to the outer boundaries, made of continuum elements.

4.2.2 Finite elements used

According to the zones pictured in figure 4.2, the used elements from the Abaqus library have been:

Core region

- Two-dimensional foam: 3-node quadratic beam, B22
- Three-dimensional foam: 3-node quadratic beam, B32

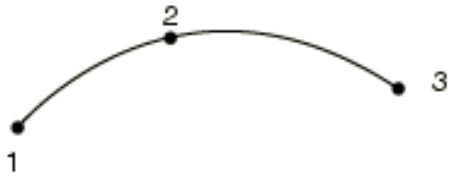

(a) Element B22 (2D), B32 (3D).

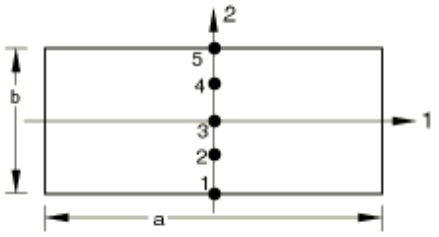

(b) Integration points for beam elements in plane.

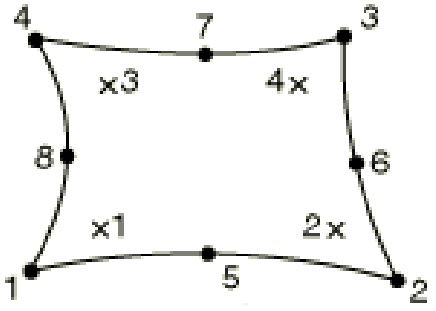

(c) Continuum element in plane strain CPE8.

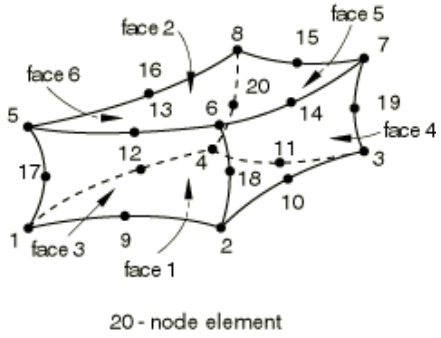

(d) Continuum element in space C3D20.

Figure 4.3: Finite elements available in Abaqus and used in the model [4].

Embedding region

- Two-dimensional foam: 8-node biquadratic plain strain element with full integration, CPE8
- Three-dimensional foam: 20-node quadratic brick with full integration, C3D20

The chosen beam elements posses a quadratic interpolation with a middle node in the beams (see figure 4.3a). Their interpolation follows a Simpson scheme: the distribution of the section integration points includes positions at the beam elements boundaries, so that stresses can be evaluated at them. At these thickness boundaries appear usually the highest stresses. Figure 4.3b shows the in-plane case for a rectangular section with five points, which is the standard value. Since linear material behavior is assumed, three points would be sufficient.

Figures 4.3c and 4.3d show the 2D and 3D continuum elements, respectively. They also posses quadratic integration. Node numbering and integration points numbering can be see seen in the pictures.

4.2.3 Interface constraint

The model needs to transfer the degrees of freedom between the core and embedding regions along the interface. A difficulty arouses about it: continuum elements have displacement d.o.f. (two in plane, three in space), whereas beam elements

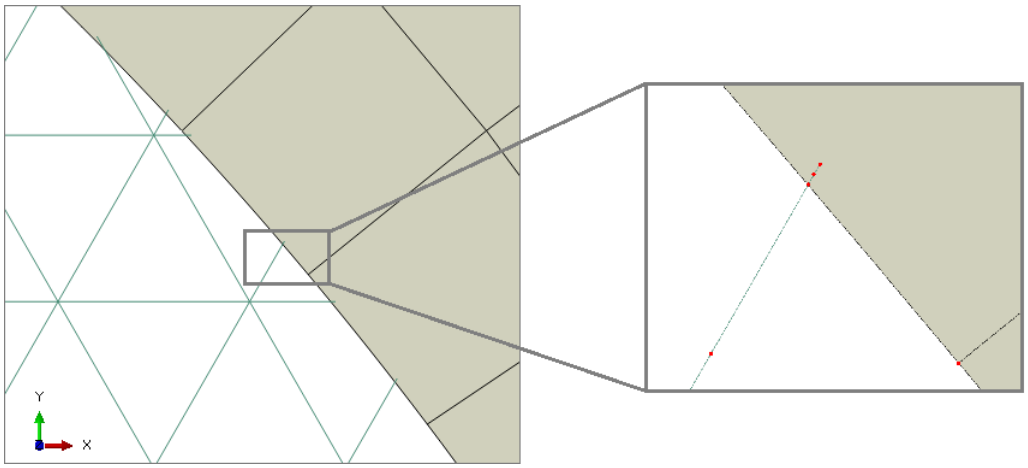

Figure 4.4: Detail of interface constraint between core and embedding region.

also posses rotational degrees of freedom (two more in plane, three more in space). The rotation of the beam nodes need to be coupled in some way through the interface to accomplish a better homogeneous behavior.

The solution to the interface was using the embedding region technique of Abaqus ("*EMBEDDED ELEMENT" constraint). This is a kinematic constraint that constraints the translational degrees of freedom of "embedded elements" into a group of "host elements". The embedded nodes must lie in the host elements (see details in Abaqus Documentation [4]).

To overcome the difficulty of transferring the rotation of beams, not only one node per strut is constraint to the embedding region but a small part of the beam elements penetrates in the continuum elements, as seen in figure 4.4. This penetration establishes an error, the stiffness is too high. But as the thickness of the penetration is very small (about a thousandth of the core radius), so that the error can be neglected. The displacement contours of the solutions verify its accuracy. For accomplishing the automatic model building by the scripts, an overlapping of the two regions was programmed. After that, a cut over the continuum region boundary was made to the beam elements, giving a "ring" of cell segments with the desired small thickness. This overlapped core region was then meshed with one beam element per segment, whose nodes were subjected to the embedded constraint. So it was assured that three nodes of each beam transfer displacement and rotation between regions (see figure 4.4).

4.2.4 Boundary conditions

For both types of analysis, static and buckling, displacement boundary conditions were applied according to the deformation modes. The displacements correspond to a tensile/compressive stress σ_0 or to a shear τ_0 (see figure 4.2), and have been ap-

plied to the complete border of the model. For the calculation of the displacements, a continuous field is assumed: the crack effect is considered local and negligible at the boundaries, since the crack size is very small compared with the embedding region. In this way a direct strain is calculated proportional to the desired trial stress, using a continuum Young's modulus as obtained in the next subsection.

4.3 Evaluation of macroscopic stiffness

A step in the modeling, according to the embedded cell approach, is to give an accurate constitutive behavior to the embedding region as well accurate material constants, as in the region continuum elements must behave as the cellular structure. Thus, it is important to define reliable elastic properties for this region. Because of the isotropy, only two parameters are important: E^* and ν^*. An important consideration is that the Young's modulus scales with the stiffness of solid material: E^*/E_s. In this study, parametric calculations are made for four relative densities (0.01, 0.05, 0.1 and 0.2) and four different orientations (cell angle regarding load direction). They are compared with analytical estimations as well.

4.3.1 Triangular cells honeycomb

Table 4.1 shows the relative stiffness for regular triangular cells as function of relative density. It can be seen the good agreement with the analytical values (from [7]), even for the different angles. Those stiffness will be later used for the embedding region.

The four relative densities, 0.01, 0.05, 0.1 and 0.2, correspond to the following thickness-length ratios: $t/l = 0.0577, 0.0289, 0.0144, 0.00289$. Other model parameters are a considered model size of $32l$x$32l$, beeing l a strut length of unity. Orientation is defined being at 0 degrees one cell wall parallel with the load direction.

A trial displacement has been imposed to an upper boundary, constraining the lower in the load direction. Then, from the reaction force a Young's modulus is calculated, scaling it with the trial solid elastic stiffness. According to brittle deformations, no geometrical linearities have been considered. It is to note that the Poisson's ratio has been manually adjusted: definition of the displacements in the load perpendicular direction is directly given according to the Poisson's ratio. Manual adjusting was made until the rectangular region showed uniform displacements, resulting in $\nu^* = 0.33$ for all relative densities.

Results shown in table 4.1 determines a small anisotropy of the structure, even if in theory it is isotropic. This is caused by the finite length of the model, but

	ρ^*/ρ_s			
	0.01	0.05	0.1	0.2
FEM (0 dg.):	3.32E-3	1.66E-2	3.32E-2	6.65E-2
FEM (10 dg.):	3.27E-3	1.64E-2	3.28E-2	6.56E-2
FEM (20 dg.):	3.29E-3	1.65E-2	3.30E-2	6.60E-2
FEM (30 dg.):	3.37E-3	1.68E-2	3.37E-2	6.75E-2
FEM - averaged:	**3.31E-3**	**1.66E-2**	**3.32E-2**	**6.64E-2**
Analytical value:	3.32E-3	1.66E-2	3.32E-2	6.64E-2
Difference with analytical value:	∼0%	∼0%	∼0%	∼0%

Table 4.1: E^*/E_s as function of relative density for triangular cells.

	ρ^*/ρ_s			
	0.01	0.05	0.1	0.2
FEM (0 dg.):	1.48E-6	1.83E-4	1.42E-3	1.01E-2
FEM (10 dg.):	1.47E-6	1.82E-4	1.41E-3	1.00E-2
FEM (20 dg.):	1.46E-6	1.81E-4	1.40E-3	0.99E-2
FEM (30 dg.):	1.47E-6	1.82E-4	1.41E-3	1.00E-2
FEM - averaged:	**1.47E-6**	**1.82E-4**	**1.41E-3**	**1.00E-2**
Analytical value:	1.49E-6	1.87E-4	1.49E-3	1.19E-2
Difference with analytical value:	1%	3%	6%	19%

Table 4.2: E^*/E_s as function of relative density for hexagonal cells.

since the differences between angles are very small, it is valid for the present study and more complex boundary conditions, as periodic unit cells, are not needed.

4.3.2 Hexagonal cells honeycomb

The results are showed in table 4.2 showing worse agreement with the analytical predictions as the density goes up. That is understandable as the analytical approximation only takes into account the bending of cell walls. When the density is higher, a considerable amount of deformation is caused by stretching, which is indeed in the FEM results captured. Here the Poisson's ratio changes with the relative density as well, beeing $\nu^*(\frac{\rho^*}{\rho_s} = 0.20) = 0.88$, $\nu^*(\frac{\rho^*}{\rho_s} = 0.10) = 0.96$, $\nu^*(\frac{\rho^*}{\rho_s} = 0.05) = 0.98$ and $\nu^*(\frac{\rho^*}{\rho_s} = 0.01) = 1.00$. The value of the lowest density is in accordance with the Poisson's ratio predicted analytically in [7], namely $\nu^* = 1$. The obtained FEM solutions are used for the posterior analysis.

Calculations have been made exactly in the same way as for triangular honeycomb, with the only difference being the size of the model of $64l$x$64l$ bigger. In this case the corresponding thickness-length ratios are $t/l = 0.173, 0.0866, 0.0433, 0.00866$ for relative densities of 0.2, 0.1, 0.05 and 0.01, respectively.

	ρ^*/ρ_s		
	0.01	0.05	0.1
FEM (0 dg.):	5.51E-5	1.22E-3	4.19E-3
FEM (15 dg.):	5.30E-5	1.16E-3	4.07E-3
FEM (30 dg.):	5.04E-5	1.10E-3	3.91E-3
FEM (45 dg.):	5.58E-5	1.17E-3	4.14E-3
FEM - averaged:	**5.36E-5**	**1.16E-3**	**4.08E-3**
Analytical value:	1.00E-4	2.50E-3	1.00E-2
Difference with analytical value:	46%	54%	59%

Table 4.3: E^*/E_s as function of relative density for tetrakaidecahedral cells.

4.3.3 Tetrakaidecahedral open-cell foam

For the three dimensional tetrakaidecahedral structure three relative densities are analysed, namely $\overline{\rho} = 0.01, 0.05, 0.1$, using a circular beam section. The correspondent diameter-length relations for these are $d/l = 0.1096, 0.2450, 0.3465$. A cube model size of $16l$x$16l$x$16l$ has been used for the analyse.

Results are gathered in table 4.3, showing great differences with the only rough approximation from [7]. The obtained Poisson's ratio from simulations, dependent on density, are $\nu^*(\frac{\rho^*}{\rho_s} = 0.10) = 0.49$, $\nu^*(\frac{\rho^*}{\rho_s} = 0.05) = 0.45$ and $\nu^*(\frac{\rho^*}{\rho_s} = 0.01) = 0.45$.

Given the three-dimensionality of the structure, orientation is more complex to define. Here in this study, 0 degrees orientation is defined when all square faces of a tetracaidecahedral unit cell are either parallel or normal to the load direction. From there, rotation around an only one axis is made, remaining all cells in a plane for all considered cell orientations which is parallel to the load direction.

4.3.4 Comparison with analytical values

Triangular results show good agreement with its analytical approximation. On the other hand, hexagonal and tetrakaidecahedral structures diverge with the predictions, showing a more complex deformation behavior, especially as the density is higher. The same occurs with the Poisson's ratio. Figure 4.5 depicts the differences.

This point is crucial in order to obtain a reliable continuum region in the embedded model, and as posterior analyses prove, good uniform isotropic regions are simulated.

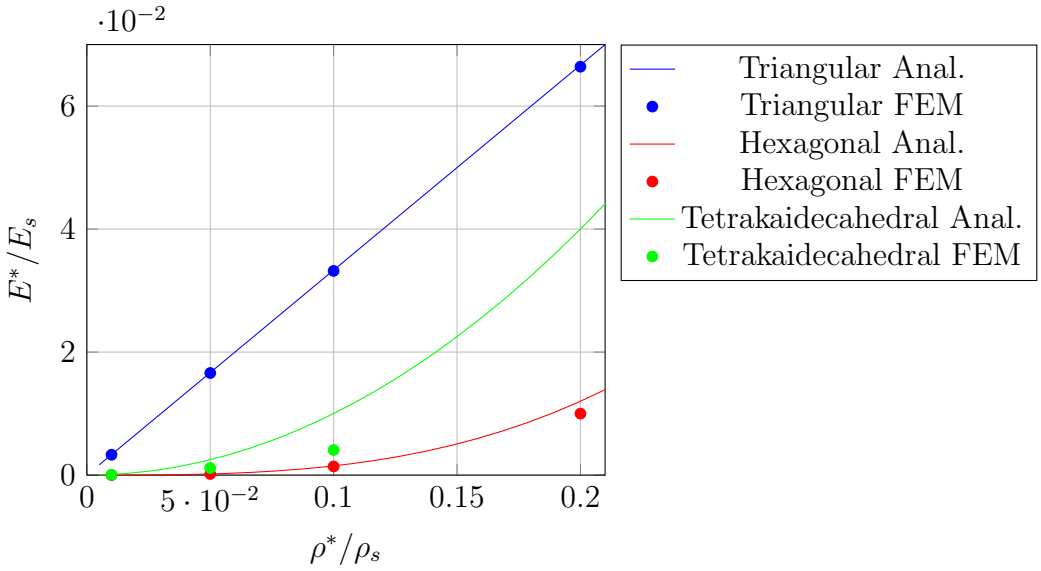

Figure 4.5: comparison of relative stiffness between different structures.

4.4 Failure criteria

An hypothesis must be taken in order to evaluate the failure in the foam struts and consequently crack growth. Here, two possible criteria are presented and used in the model: a strength and a stability failure criterion.

4.4.1 Strength: Maximum local tensile stress

It describes appropiately brittle failure of materials. The local principal stress in a solid wall reaches a critical value, a microcrack is formed there, and the wall breaks in a fragile way without stress increase. The critical ultimate tensile stress is indicated as σ_{fs}, meaning the subscript s that it is a solid material property.

To evaluate is the local stress in the beam in the axial direction, calculated at the integration points. As explained above, Simpson integration includes points at the wall surfaces, where the maximum stresses rise. Top and bottom points are used in the evaluation.

For the analyses, a test value $\sigma_{fs} = 1000$ has been taken as maximum tensile stress. It does not have any units, since the significance is to allow a numerical treatment of the data. As all the results are presented in a general way as normalized values, they do not depend on material constants.

It must be pointed out that in reality the materials have a failure compressive strength as well, but in the present study only the tensile limit is considered under the consideration that compressive strength is higher than tensile in most brittle materials and does not suppose the critical failure cause.

4.4.2 Stability: Elastic buckling

In case of buckling failure of some struts a different criterion must be adopted. When failure occurs is at the moment that a part of the structure becomes instable or buckles. In order to analyze that with FEM a buckling analysis is to be performed.

The FEM buckling analysis considers an applied load and looks for magnitudes of that load that produce instabilities. Several loads can cause buckling in different zones, but the first is of interest, corresponding to the lowest load.

For the present work an innovative approach is used, obtaining a stress toughness with buckling failure criteria. An applied stress intensity factor K is calculated with the crack length and load for an infinite uni-axial loaded structure, as usual. Then the finite element analysis gives the load at which the structure buckles. This buckling is to be expected at the crack tips or close to them. After that, with the buckling load the fracture toughness K_c is obtained.

4.5 Determining model size by convergence study

A convergence study was performed in order to determine an accurate enough and efficient model size. The maximum local stress on the lattices is selected to be the parameter to compare (BEAM STRESS, S11, from Abaqus). This value will be later a critical value to calculate the fracture toughness. The model dimensions to determine are the radius of the microstructural zone and the continuum zone size. The values are given as strut length function. On the other hand an appropiate number of beam elements per strut is desired to be known. It means how many beams are the minimum to discretize each wall.

A strut length of unit is used, with a relative density of 0.1 (t=0.0866), for a hexagonal honeycomb. A crack length of 50 cell lattices is in the model. The elastic properties for the continuum elements are taken from the simulations discussed above ($E^* = 141$, $\nu^* = 0.96$), with a Young's modulus of 100000 units for the beams solid material. A tensile strain of 0.01 in vertical direcction is imposed to the model, implying a Mode I fracture. The resulting maximum local stress has only comparison value.

In a first step, a microstructural region with radius $90l$ and a external continuum box of $10000l$ x $10000l$ are taken. Three discretizations of the struts are made, with 4, 2 and 1 beam elements per strut. A maximum local tension of $1956N/mm^2$ was obtained for the case of four elements per strut, and practically no difference was found for the other calculations, meaning that a single beam element discretizes the lattice deformation with enough accuracy.

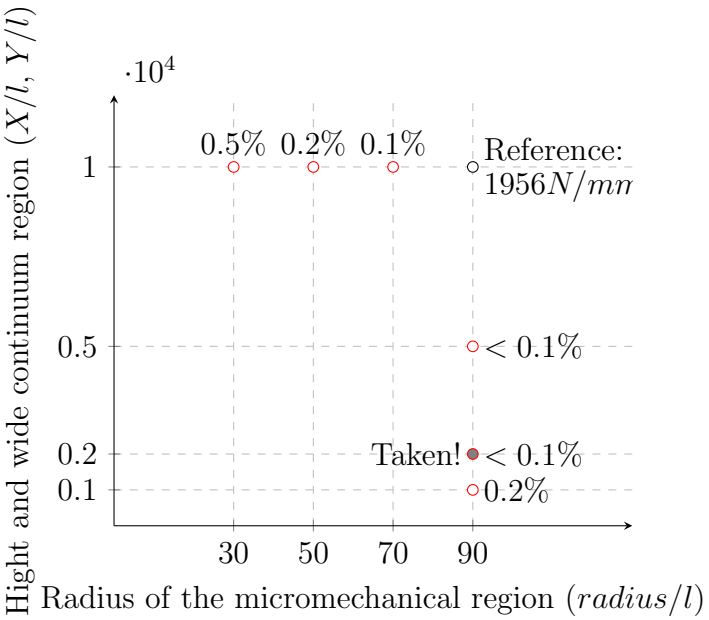

Figure 4.6: Comparison of maximum local stress according to the core and embedding region. Percentage difference with reference value.

In the next step the geometrical measures of the model were tested, considering the single beam discretization to be good. The figure 4.6 shows the accuracy for different internal and outer regions. A outer model size of 2000x2000 units was chosen as suitable, as the difference with the biggest reference size is smaller than 0.1%.

For the section integration the standard number of five points along the beam thickness is given, which is the default value. Less points can also be valid, since elastic material behavior is considered.

Chapter 5

Fracture analysis under LEFM approach

Based on the linear elastic fracture mechanics theory (LEFM), the stress intensity factor is represented by K_i, dependent on the far field loading mode i. The critical value of a stress intensity factor at which a crack advances is defined as the fracture toughness, K_{ci}, which is also dependent on the mode i. For this reason it is important to know the fracture toughnesses of a material in order to be able to determine when a crack is going to grow.

In this section the fracture toughness is determined for triangular, hexagonal, and tetrakaidecahedral foams using the finite element model. Since the crack length of the calculations is sufficiently long in comparison with the cell size, as described in chapter 4, a constant fracture toughness characteristic of the cellular material can be assumed. This fracture toughness is constant and independent of the crack length, according to the continuum approach of LEFM. The special case of shorts cracks, in which the assumptions of LEFM are to be questioned, is analyzed in chapter 6.

5.1 Analysis method

The FEM model as described in chapter 4 is used to perform the present analysis. For each of the structures a trial stress is applied to the model, according to subsection 3.1.1, which gives the intensity factors

$$K_I = \sigma\sqrt{\pi a},\ K_{II} = \tau\sqrt{\pi a},\ K_{-I} = -\sigma\sqrt{\pi a}, \tag{5.1}$$

with K_{-I} referring to an anti-mode I intensity factor. Stress σ is applied to the model in form of displacement boundary conditions. The displacements are determined using the elastic properties of the cellular material, which are independent

of the cell orientation in the considered structures. In addition of Mode I and mode II an anti-mode I has been analyzed, for the spaces inside the cells allow the displacements under compression.

The next step depend on the failure criterion. Two failure criteria are considered as trigger for the crack advance: a local strength criterion and a stability criterion, as discussed in section 4.4. Therefore, once the trial intensity factor is applied, fracture toughness is derived according to the failure criterion. The details of this calculation are given in the following sections.

Results are obtained as a function of the relative density and of the properties of the solid material, as made in the literature (e.g. in [7]). Different scaling exists for the local strength criterion, dependent on the modulus of rupture σ_{fs}, and for the stability criterion, dependent on the Young's modulus.

These calculated fracture toughnesses can be used as reference for practical applications, considering the fact that they are calculated for ideal structures. However, real cellular materials are not perfect and include flaws and irregularities, as well as there are some assumptions made in the finite element model, that would give certain deviations.

Some explanation about the FEM model are then necessary. Regarding the model dimensions, a crack length about 50 lattice lengths is used for plane structures and 20 for three-dimensional structures, being the length of a lattice the length of a cell wall. It is not easy to give an exact definition of crack length for cellular structures, for they are not continuous anymore, so the location of the "crack tip" is ambiguous. Here the the crack length is assumed to be between cell centers between the most separated broken cells. It is also to consider that the length is not always a whole number as the orientation of the cells changes and the cell wall are not longer parallel to the crack orientation.

The definition of the structure orientation is as follows: for two-dimensional structures by the zero degree orientation a cell wall is parallel to crack direction, being the rotation direction trivial. The tetrakaidecahedral foam is three-dimensional and only one orientation variation is applied, similar to the 2D structures. The rotation is normal to the plane of analysis, being the orientations in the other axes unchanged.

Each cell wall is discretized using a single quadratic beam element for economy of computing resources. Some deformations of higher order are not possible with a single element, but after comparing some results with a more refined meshing no changes were observed. Thus, those higher order effects can be neglected and a single element quadratic element per cell wall was taken as valid.

5.2 Fracture toughness for local strength criterion

A linear static analysis is performed for the model applying the above explained trial stress for a given intensity factor. After running the calculation, the maximum local stress is evaluated, which is used to obtain the fracture toughness of each mode. The fracture toughness is obtained as the scaling of the applied intensity factor

$$K_C = K\frac{\sigma_{fs}}{\sigma_{s0max}}. \tag{5.2}$$

where σ_{fs} is the ultimate strength of the cell walls. It represents the maximum tensile stress at which the wall breaks. On the denominator, σ_{s0max} is the resulting maximum tensile stress at the section points.

The results are presented in tables 5.1, 5.2 and 5.3. Plots 5.1, 5.2 and 5.3 for triangular structures, 5.4, 5.5 and 5.6 for hexagonal, and 5.7, 5.8 and 5.9 for tetrakaidecahedral, depict the data.

Results are scaled with the ultimate strength, σ_{fs}, inversely proportional to the fracture toughness. Another scaling is made with l, the strut length. The fracture toughness is inversely proportional to the square root of the strut length, as the results show. Together with the results some approximations from other authors are shown, which are defined as density dependent laws. From the present calculations similar laws have been derived, with different coefficients, and are summarized in section 5.4.

The current FEM-based results show a good matching with those found in the literature [6]. Comparisons with [7] show some variability since they are based on analytical calculations. Low variability regarding the structure orientation is shown for plane structures, whereas for tetrakaidecahedral foam more variation is observed. Nevertheless, no more than ten percent deviation from the approximation law exists. Therefore, the assumption of a characteristic fracture toughness as per LEFM is validated, being the approximation laws and scaling method confirmed.

		$\frac{K_{IC}}{\sigma_{fs}\sqrt{l}}$			
		0 °	10 °	20 °	30 °
Triangular	$\overline{\rho} = 0.01$	5.81E-3	5.38E-3	5.06E-3	4.98E-3
	$\overline{\rho} = 0.05$	2.79E-2	2.61E-2	2.48E-2	2.47E-2
	$\overline{\rho} = 0.1$	5.32E-2	5.03E-2	4.84E-2	4.88E-2
	$\overline{\rho} = 0.2$	9.71E-2	9.38E-2	9.22E-2	9.53E-2
Hexagonal	$\overline{\rho} = 0.01$	6.58E-5	6.99E-5	7.50E-5	7.47E-5
	$\overline{\rho} = 0.05$	1.63E-3	1.72E-3	1.84E-3	1.85E-3
	$\overline{\rho} = 0.1$	6.39E-3	6.74E-3	7.15E-3	7.21E-3
	$\overline{\rho} = 0.2$	2.44E-2	2.56E-2	2.67E-2	2.73E-2
		0 °	15 °	30 °	45 °
Tetrakaidecahedral	$\overline{\rho} = 0.01$	2.88E-4	2.93E-4	2.90E-4	3.31E-4
	$\overline{\rho} = 0.05$	3.08E-3	3.25E-3	3.23E-3	3.49E-3
	$\overline{\rho} = 0.1$	8.63E-3	9.22E-3	9.27E-3	9.44E-3

Table 5.1: Fracture toughness results for mode I with tensile strength failure criterion.

		$\frac{K_{IIC}}{\sigma_{fs}\sqrt{l}}$			
		0 °	10 °	20 °	30 °
Triangular	$\overline{\rho} = 0.01$	4.55E-3	4.37E-3	4.27E-3	4.03E-3
	$\overline{\rho} = 0.05$	2.20E-2	2.14E-2	2.11E-2	1.99E-2
	$\overline{\rho} = 0.1$	4.22E-2	4.16E-2	4.12E-2	3.93E-2
	$\overline{\rho} = 0.2$	7.80E-2	7.90E-2	7.87E-2	7.64E-2
Hexagonal	$\overline{\rho} = 0.01$	3.33E-5	3.78E-5	3.71E-5	3.97E-5
	$\overline{\rho} = 0.05$	8.24E-4	8.24E-4	9.21E-4	9.88E-4
	$\overline{\rho} = 0.1$	3.29E-3	3.35E-3	3.68E-3	3.94E-3
	$\overline{\rho} = 0.2$	1.21E-2	1.33E-2	1.46E-2	1.55E-2
		0 °	15 °	30 °	45 °
Tetrakaidecahedral	$\overline{\rho} = 0.01$	1.06E-4	1.09E-4	1.20E-4	6.78E-5
	$\overline{\rho} = 0.05$	1.15E-3	1.11E-3	1.28E-3	7.37E-4
	$\overline{\rho} = 0.1$	3.18E-3	2.93E-3	3.65E-3	2.06E-3

Table 5.2: Fracture toughness results for mode II with tensile strength failure criterion.

		$\frac{K_{-IC}}{\sigma_{fs}\sqrt{l}}$			
		0 °	10 °	20 °	30 °
Triangular	$\overline{\rho} = 0.01$	1.89E-2	1.72E-2	1.77E-2	1.76E-2
	$\overline{\rho} = 0.05$	9.30E-2	8.44E-2	8.70E-2	8.69E-2
	$\overline{\rho} = 0.1$	1.79E-1	1.68E-1	1.71E-1	1.70E-1
	$\overline{\rho} = 0.2$	3.35E-1	3.20E-1	3.33E-1	3.29E-1
Hexagonal	$\overline{\rho} = 0.01$	6.63E-5	7.05E-5	7.57E-5	7.52E-5
	$\overline{\rho} = 0.05$	1.69E-3	1.80E-3	1.94E-3	1.91E-3
	$\overline{\rho} = 0.1$	6.88E-3	7.33E-3	7.90E-3	7.78E-3
	$\overline{\rho} = 0.2$	2.83E-2	3.03E-2	3.25E-2	3.16E-2
		0 °	15 °	30 °	45 °
Tetrakaidecahedral	$\overline{\rho} = 0.01$	2.92E-4	3.00E-4	2.93E-4	3.41E-4
	$\overline{\rho} = 0.05$	3.29E-3	3.42E-3	3.32E-3	3.71E-3
	$\overline{\rho} = 0.1$	9.48E-3	9.97E-3	9.62E-3	1.02E-2

Table 5.3: Fracture toughness results for anti-mode I with tensile strength failure criterion.

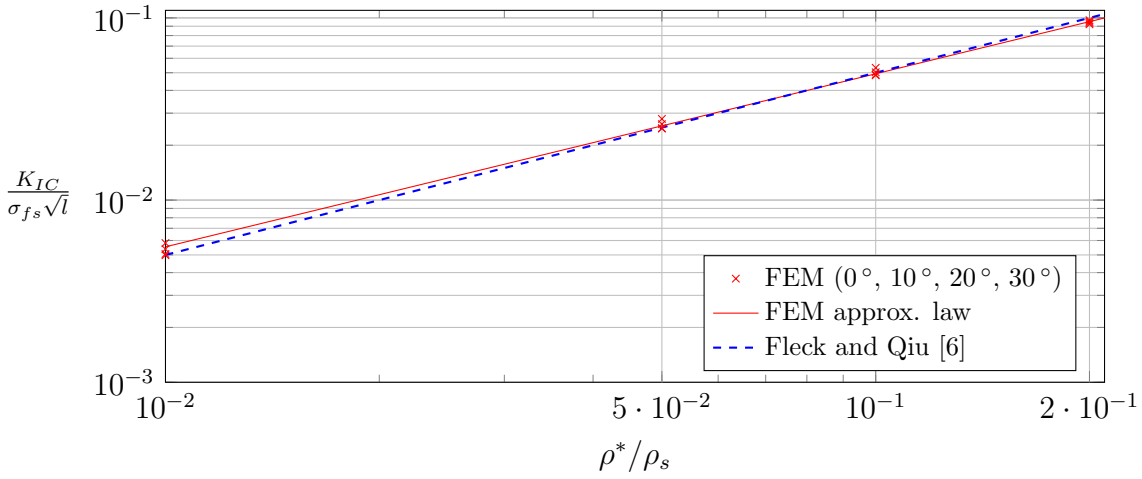

Figure 5.1: Mode I fracture toughness (triangular honeycombs, strength criterion).

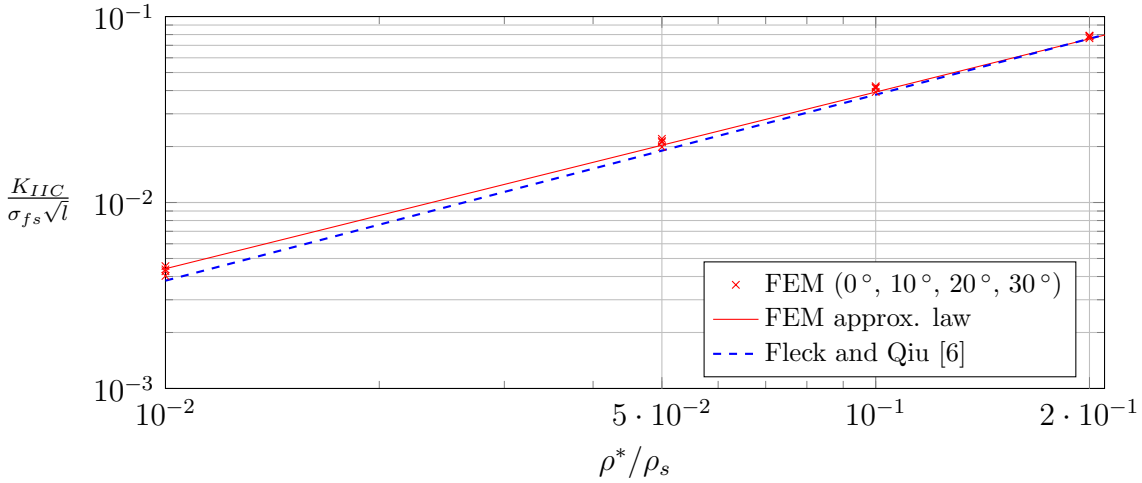

Figure 5.2: Mode II fracture toughness (triangular honeycombs, strength criterion).

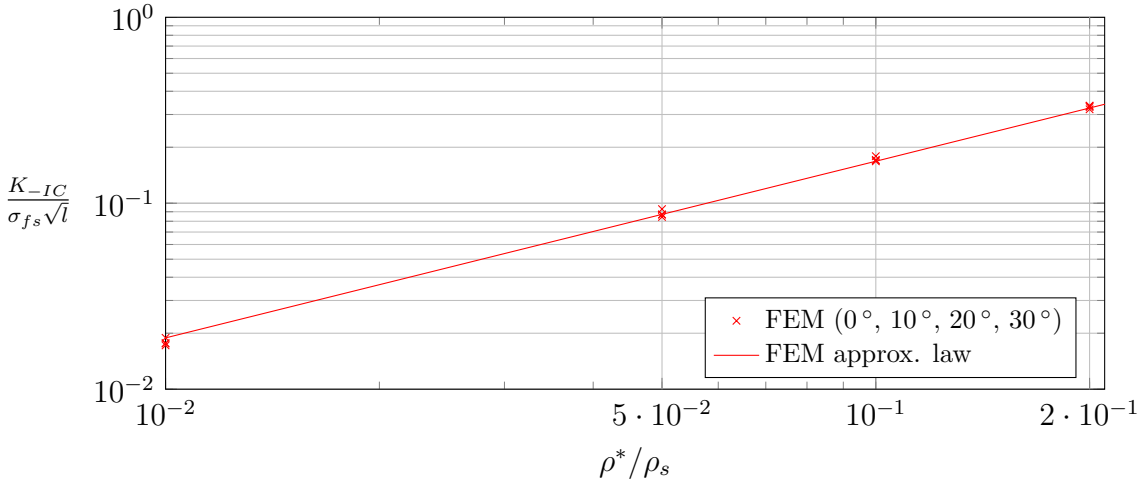

Figure 5.3: Anti-mode I fracture toughness (triangular honeycombs, strength criterion).

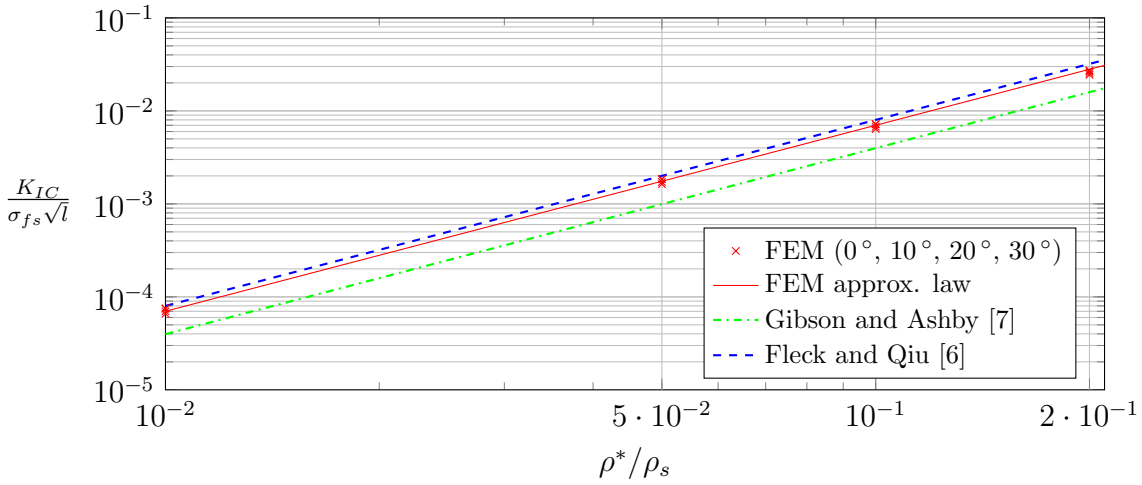

Figure 5.4: Mode I fracture toughness (hexagonal honeycombs, strength criterion).

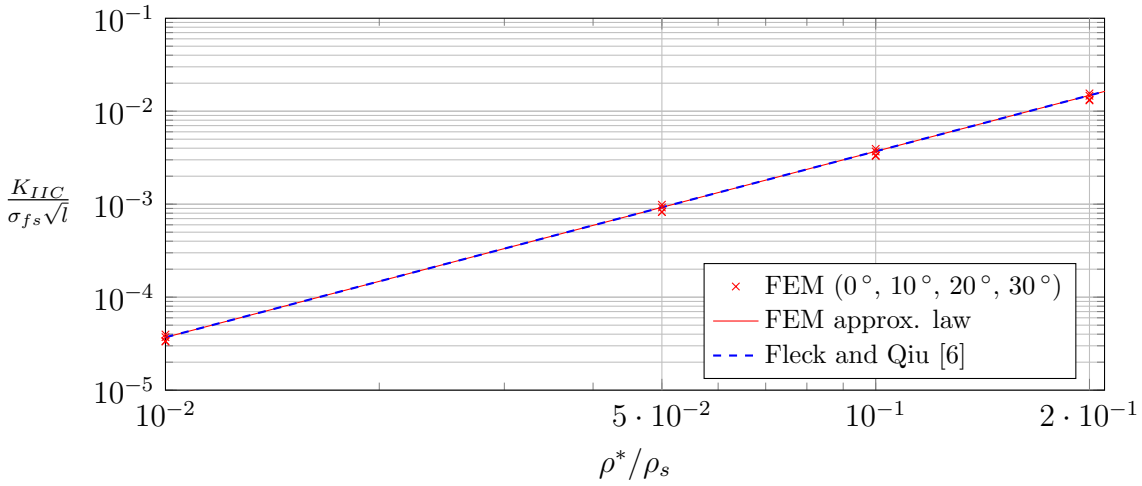

Figure 5.5: Mode II fracture toughness (hexagonal honeycombs, strength criterion).

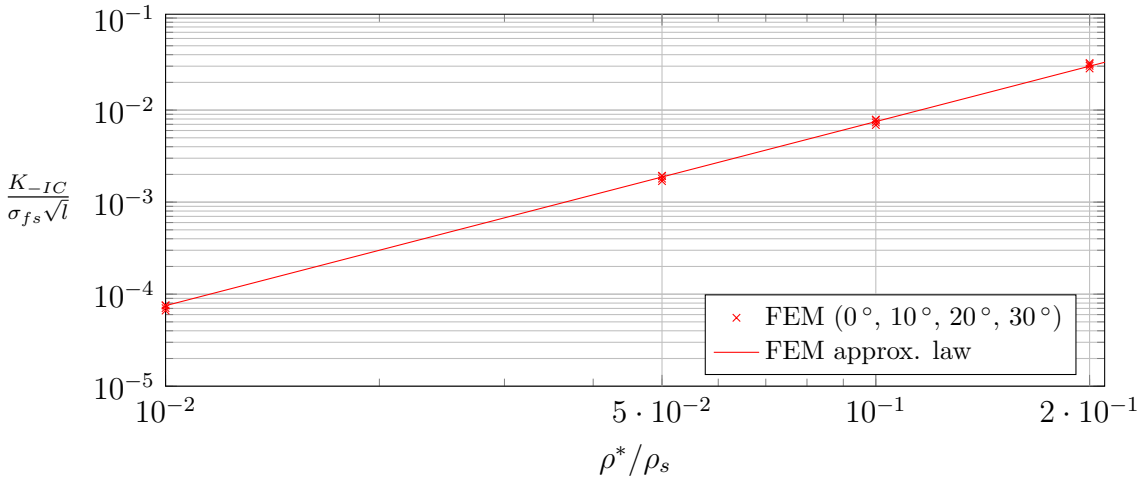

Figure 5.6: Anti-mode I fracture toughness (hexagonal honeycombs, strength criterion).

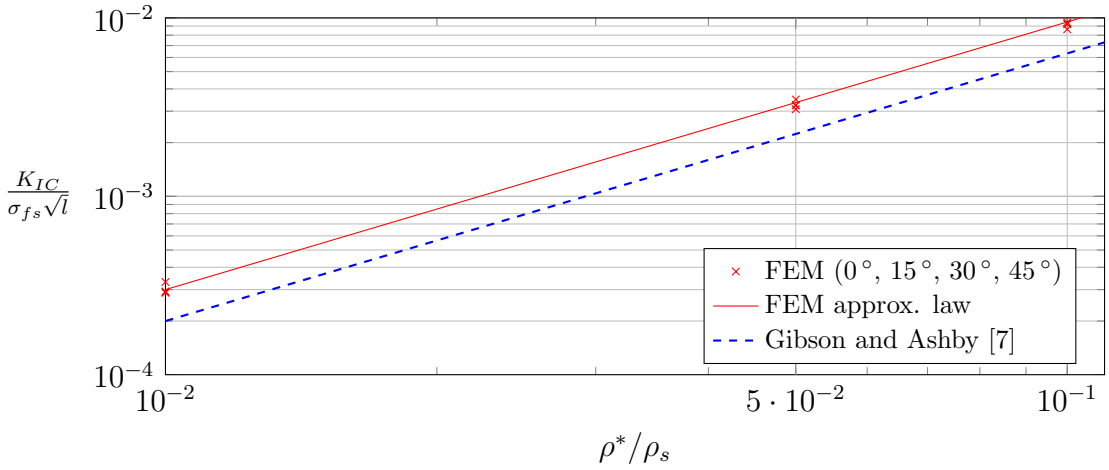

Figure 5.7: Mode I fracture toughness for tetrakaidecahedral foam (strength criterion).

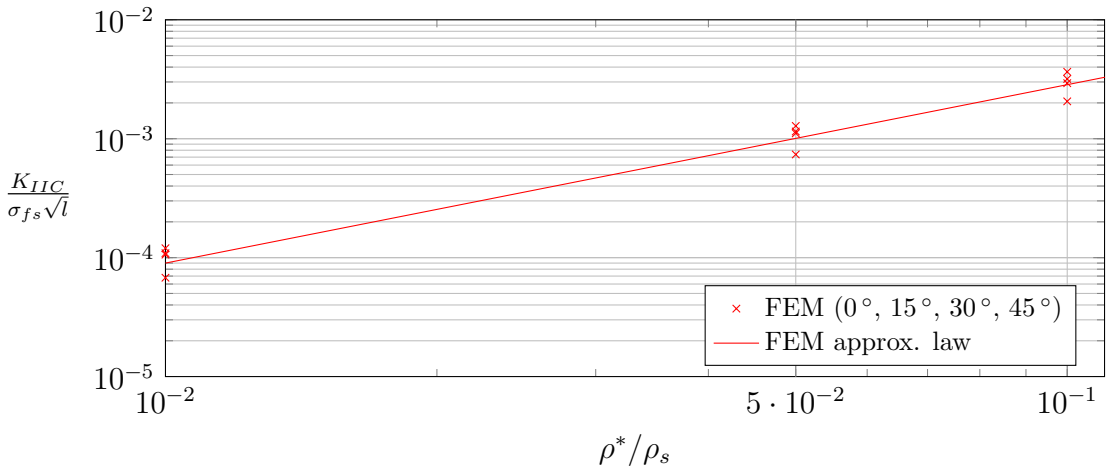

Figure 5.8: Mode II fracture toughness for tetrakaidecahedral foam (strength criterion).

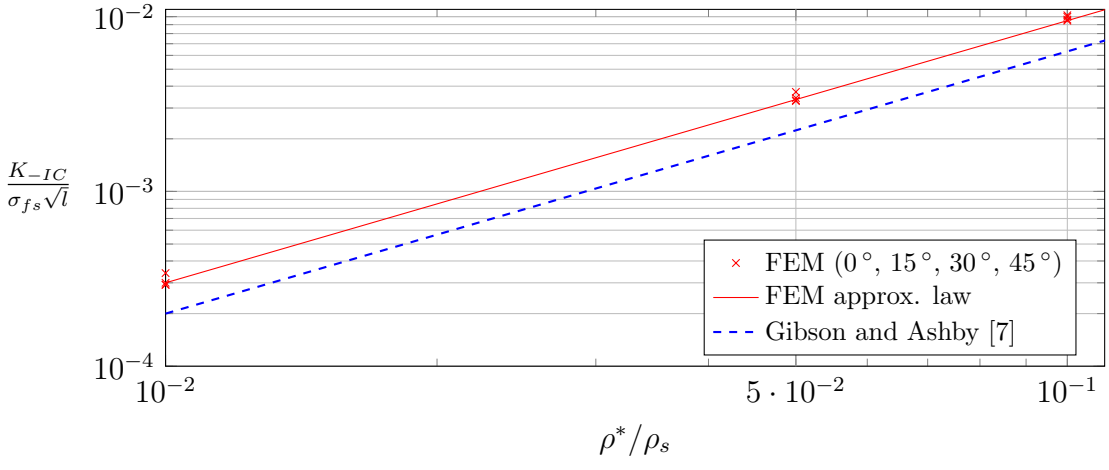

Figure 5.9: Anti-mode I fracture toughness for tetrakaidecahedral foam (strength criterion).

5.3 Fracture toughness for stability failure criterion

The stability failure criterion is based on the assumption that some strut breaks when buckling appears in the structure. In order to obtain the fracture toughness, a trial stress has been applied to the model as in the previous section, putting the structure under the same intensity factor conditions as described in equation (5.1).

Under these load conditions a buckling analysis is then run for the model, evaluating the lowest eigenvalue of interest. The scaling for the fracture toughness is in this case made directly with that lowest eigenvalue:

$$K_{Ci}^{B} = \lambda_1 K_i. \tag{5.3}$$

where λ_1 indicates the lowest eigenvalue. The superscript ^{B} makes reference to the stability criterion approach, in order to differentiate it from the toughness for the strength criterion.

It is to note that the fracture toughness inversely scales with the Young's modulus of the cell wall material. In addition, scaling is also made with the cell length l. It is shown in the results, which are depicted in tables 5.4 and 5.5. The assumption of a fracture toughness under stability failure can be in this way accepted, as approximation laws and scalings can be defined as made with the local strength criterion.

		$\frac{K^B_{-IC}}{E_s\sqrt{l}}$			
		0 °	10 °	20 °	30 °
Triangular	$\overline{\rho} = 0.01$	1.94E-7	1.90E-7	1.85E-7	1.90E-7
	$\overline{\rho} = 0.05$	2.43E-5	2.38E-5	2.32E-5	2.37E-5
	$\overline{\rho} = 0.1$	1.93E-4	1.89E-4	1.84E-4	1.88E-4
	$\overline{\rho} = 0.2$	1.49E-3	1.47E-3	1.43E-3	1.46E-3
Hexagonal	$\overline{\rho} = 0.01$	4.93E-7	5.01E-7	5.37E-7	4.76E-7
	$\overline{\rho} = 0.05$	7.12E-5	6.49E-5	6.68E-5	7.14E-5
	$\overline{\rho} = 0.1$	5.63E-4	5.13E-4	5.28E-4	5.64E-4
	$\overline{\rho} = 0.2$	4.27E-3	3.90E-3	4.00E-3	4.27E-3
		0 °	15 °	30 °	45 °
Tetrakaidecahedral	$\overline{\rho} = 0.01$	3.66E-5	3.75E-5	3.78E-5	3.72E-5
	$\overline{\rho} = 0.05$	8.39E-4	8.91E-4	8.97E-4	8.78E-4
	$\overline{\rho} = 0.1$	3.11E-3	3.32E-3	3.34E-3	3.22E-3

Table 5.4: Fracture toughness results for anti-mode I with stability failure criterion.

		$\frac{K^B_{IIC}}{E_s\sqrt{l}}$			
		0 °	10 °	20 °	30 °
Triangular	$\overline{\rho} = 0.01$	1.47E-7	1.53E-7	1.60E-7	1.64E-7
	$\overline{\rho} = 0.05$	1.78E-5	1.91E-5	2.00E-5	2.05E-5
	$\overline{\rho} = 0.1$	1.42E-4	1.51E-4	1.59E-4	1.63E-4
	$\overline{\rho} = 0.2$	1.10E-3	1.17E-3	1.23E-3	1.26E-3
Hexagonal	$\overline{\rho} = 0.01$	5.06E-7	4.61E-7	4.60E-7	4.55E-7
	$\overline{\rho} = 0.05$	6.22E-5	5.62E-5	5.67E-5	5.62E-5
	$\overline{\rho} = 0.1$	4.90E-4	4.44E-4	4.48E-4	4.46E-4
	$\overline{\rho} = 0.2$	3.72E-3	3.38E-3	3.42E-3	3.39E-3
		0 °	15 °	30 °	45 °
Tetrakaidecahedral	$\overline{\rho} = 0.01$	1.46E-5	1.74E-5	1.51E-5	1.57E-5
	$\overline{\rho} = 0.05$	3.38E-4	3.82E-4	3.40E-4	3.01E-4
	$\overline{\rho} = 0.1$	1.26E-3	1.30E-3	1.27E-3	1.14E-3

Table 5.5: Fracture toughness results for mode II with stability failure criterion.

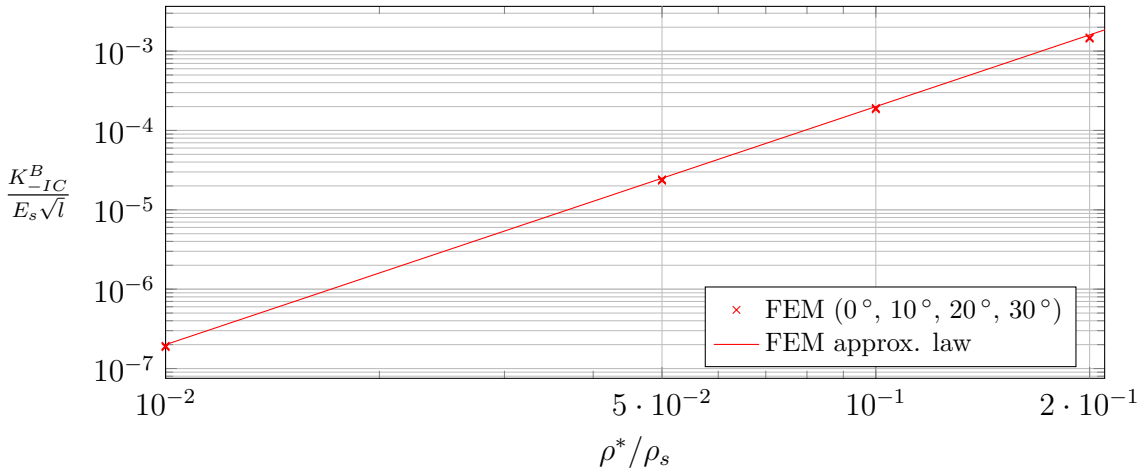

Figure 5.10: Buckling-Anti-Mode I fracture toughness for triangular honeycombs.

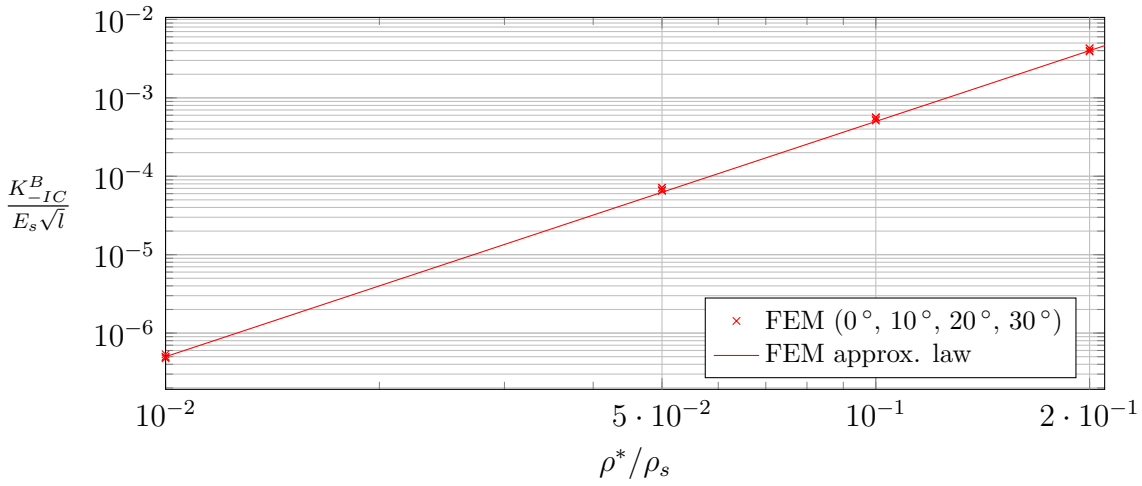

Figure 5.11: Buckling-Anti-Mode I fracture toughness for hexagonal honeycombs.

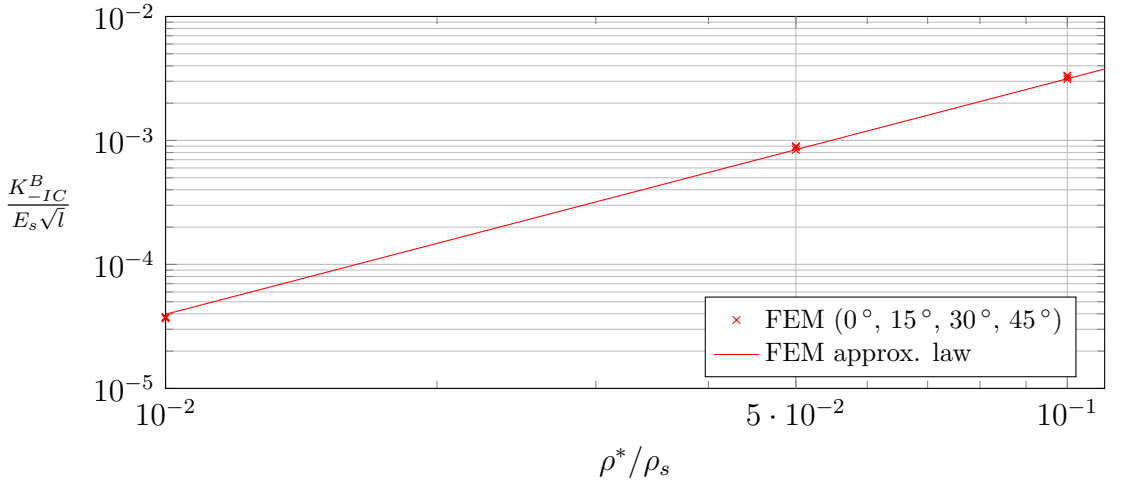

Figure 5.12: Buckling-Anti-Mode I fracture toughness for tetrakaidecahedral foams.

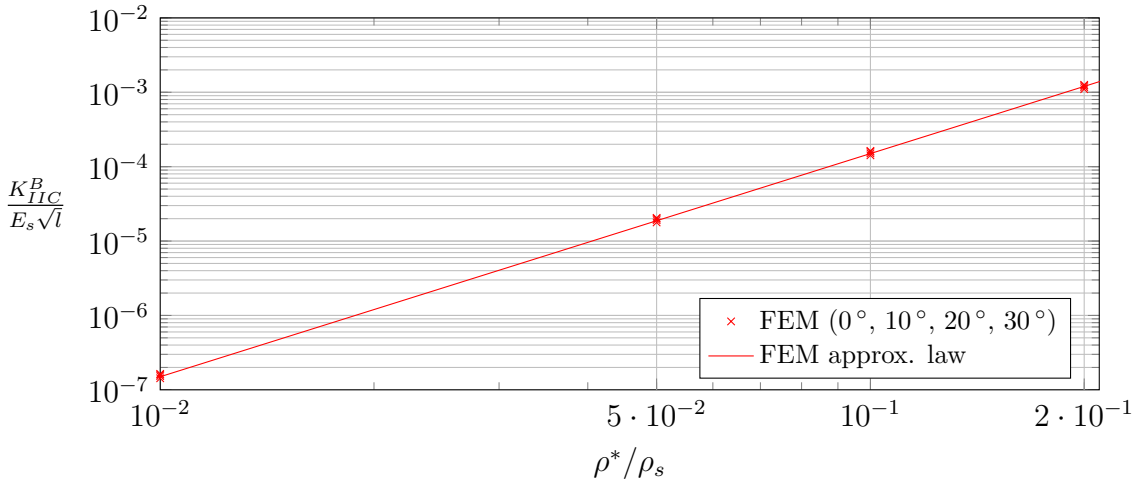

Figure 5.13: Buckling-Mode II fracture toughness for triangular honeycombs.

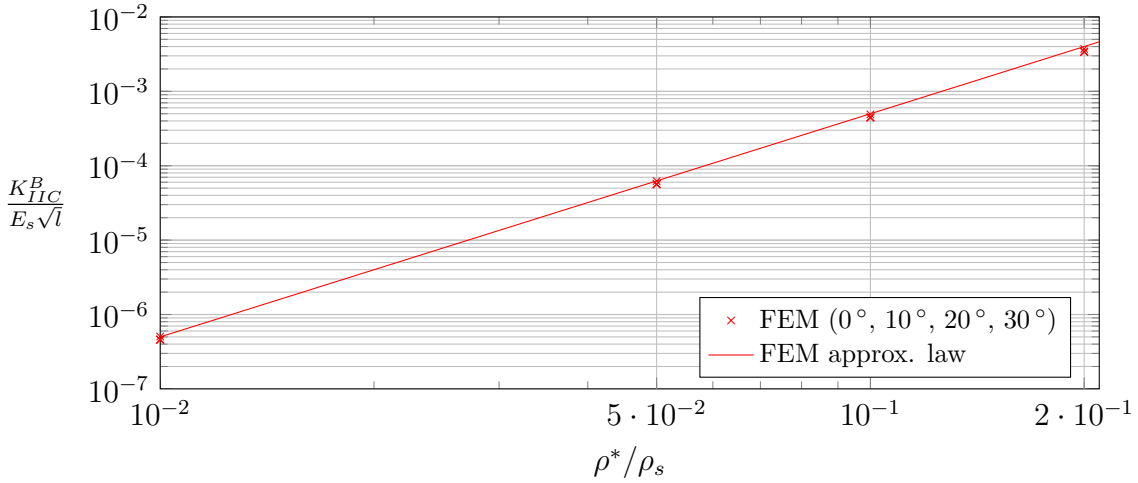

Figure 5.14: Buckling-Mode II fracture toughness for hexagonal honeycombs.

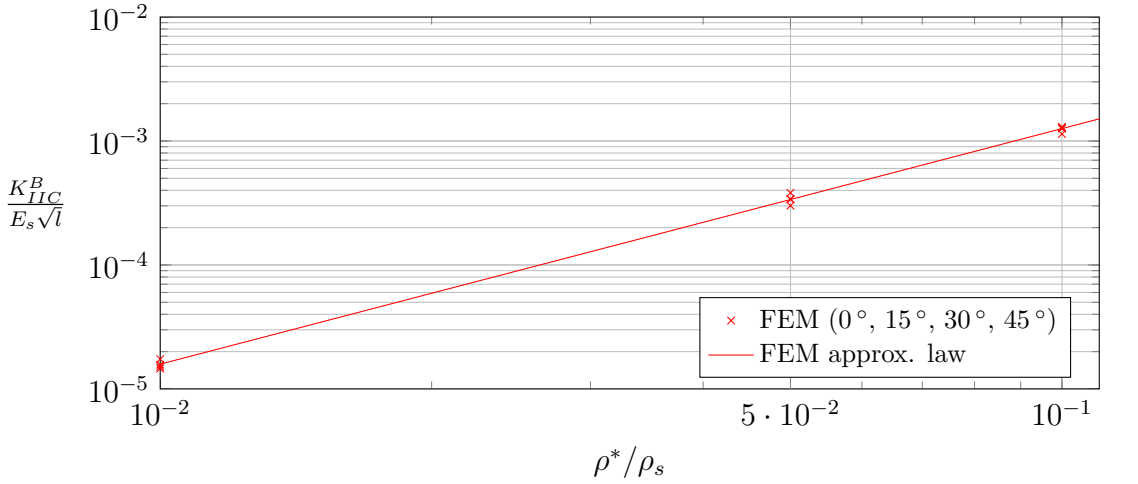

Figure 5.15: Buckling-Mode II fracture toughness for tetrakaidecahedral foams.

		Mode I	Mode II	Anti-mode I
Triangular	D	0.44	0.40	1.5
	d	0.95	0.95	0.95
Hexagonal	D	0.7	0.37	0.75
	d	2	2	2
Tetrakaidecahedral	D	0.3	0.09	0.3
	d	1.5	1.5	1.5

Table 5.6: Coefficients for fracture toughness law of equation (5.4) for strength failure criterion.

5.4 Summary of fracture toughness laws

The resulting fracture toughness can be described as dependent of the relative density with the form of the expressions here. Numerous authors have verified this dependence either analytically and numerically. The present coefficients show accordance with other studies such as in [7], [6], or [21], among others.

It is of interest to see how the exponent coefficients change regarding the structure and the failure criterion. The reason is given by the deformation mechanism and how it scales with the relative density, as explained in section 2.3.

5.4.1 For strength failure criterion

The fracture toughness is determined by the following expression:

$$\frac{K_C}{\sigma_{fs}\sqrt{l}} = D\overline{\rho}^d. \tag{5.4}$$

The coefficients D and d for the different topologies and modes are gathered in table 5.6, and represented in figure 5.16.

5.4.2 For stability failure criterion

In this case the fracture toughness is scaled with the Young's modulus of the cellular material:

$$\frac{K_C^B}{E_s\sqrt{l}} = D\overline{\rho}^d. \tag{5.5}$$

Table 5.7 and figure 5.17 ilustrate the laws.

5.5 Application example

As the two considered failure ways are not scaled in the same way, it is not possible to see which one would be critical if no material is defined. But once in an engi-

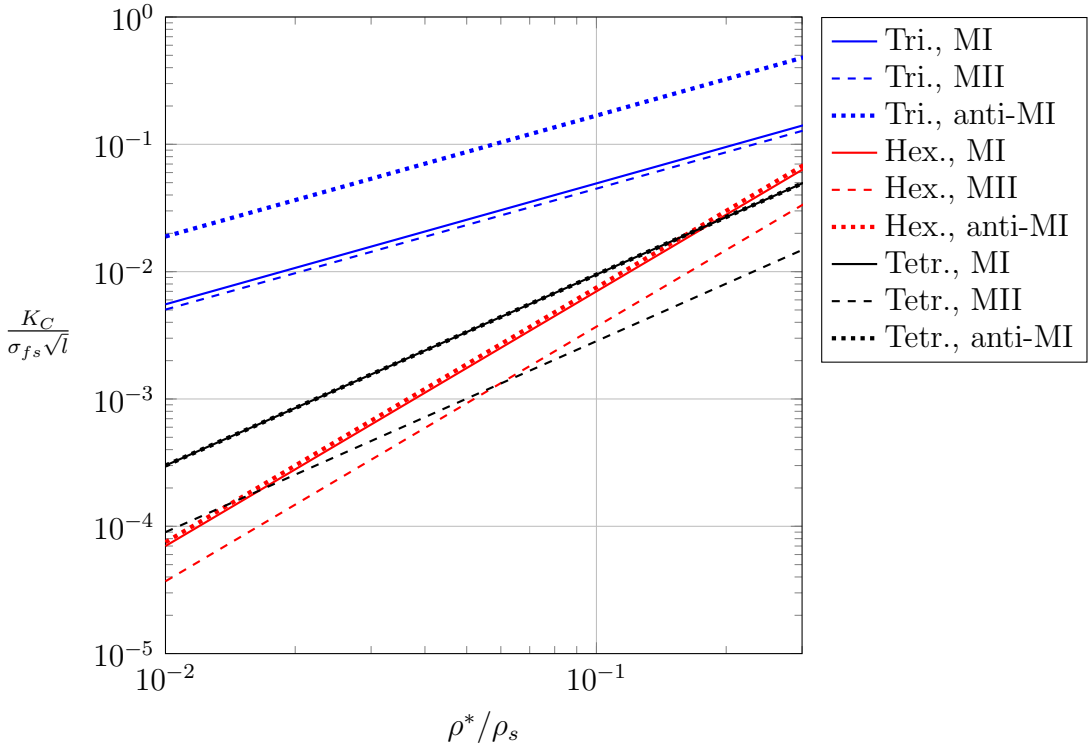

Figure 5.16: Fracture toughness approximations with strength failure criterion based on FEM results for several structures, dependent on relative density.

		Mode II	Anti-mode I
Triangular	D	0.15	0.2
	d	3	3
Hexagonal	D	0.5	0.5
	d	3	3
Tetrakaidecahedral	D	0.1	0.25
	d	1.9	1.9

Table 5.7: Coefficients for fracture toughness law of equation (5.5) for stability failure criterion.

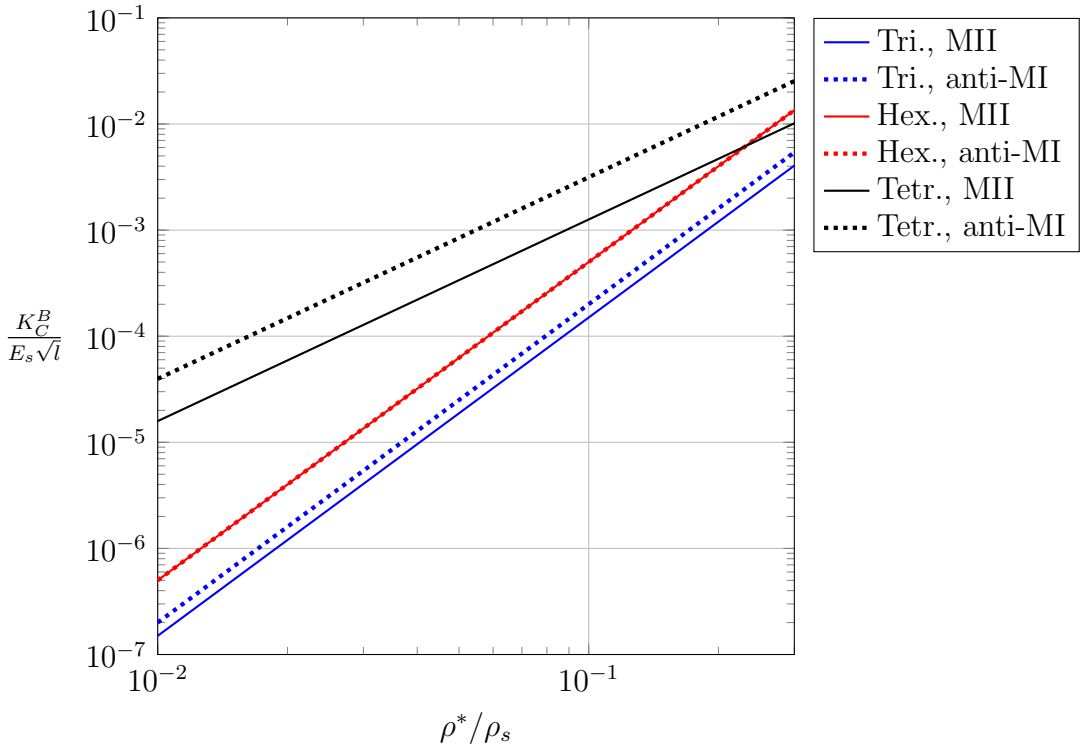

Figure 5.17: Fracture toughness approximations with stability failure criterion based on FEM results for several structures, dependent on relative density.

neering problem, when the material characteristics are known, the comparison is possible. It is easier to view it with an example: a solid material for the cell walls is considered which has a relationship between Young's modulus and modulus of rupture as:

$$\sigma_{fs} = \frac{E_s}{1000}, \tag{5.6}$$

Figure 5.18 shows the solution for an hexagonal structure, indicating that in all possible densities the critical fracture toughness would by the strength failure criterion. This is the same case for the tetrakaidecahedral foam (see figure 5.19).

Otherwise, for the triangular structure, which solution is depicted in figure 5.20, by low densities the crack would advance by buckling on the struts, and by higher densities by locally reaching the ultimate stress. That is easily understandable as by low density cell wall are much more slender, provoking an easy buckling failure. In addition, cell walls of triangular honeycombs are mainly loaded axially, which is the cause for becoming unstable.

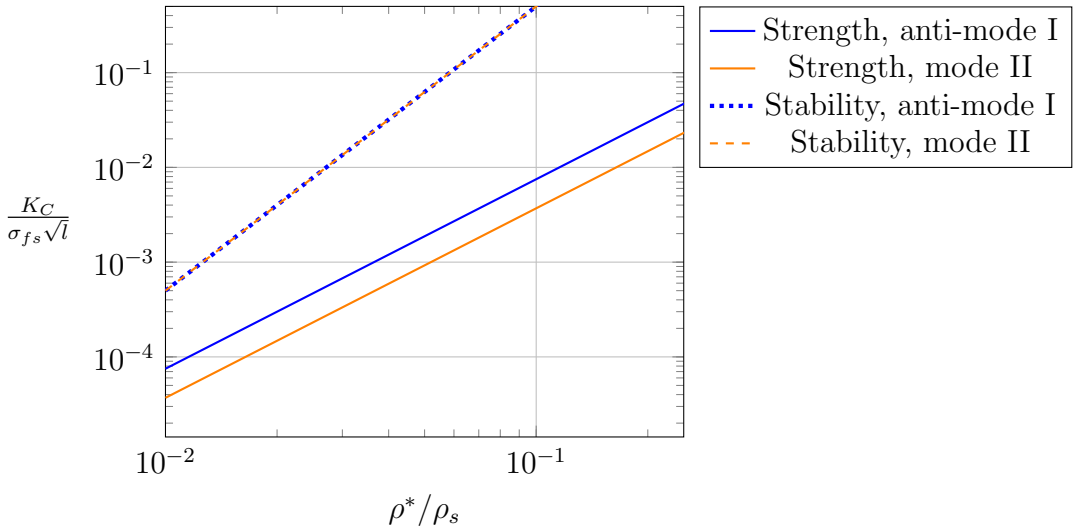

Figure 5.18: Comparison of fracture toughnesses depending on criterion for an hexagonal structure with $\sigma_{fs} = E_s/1000$.

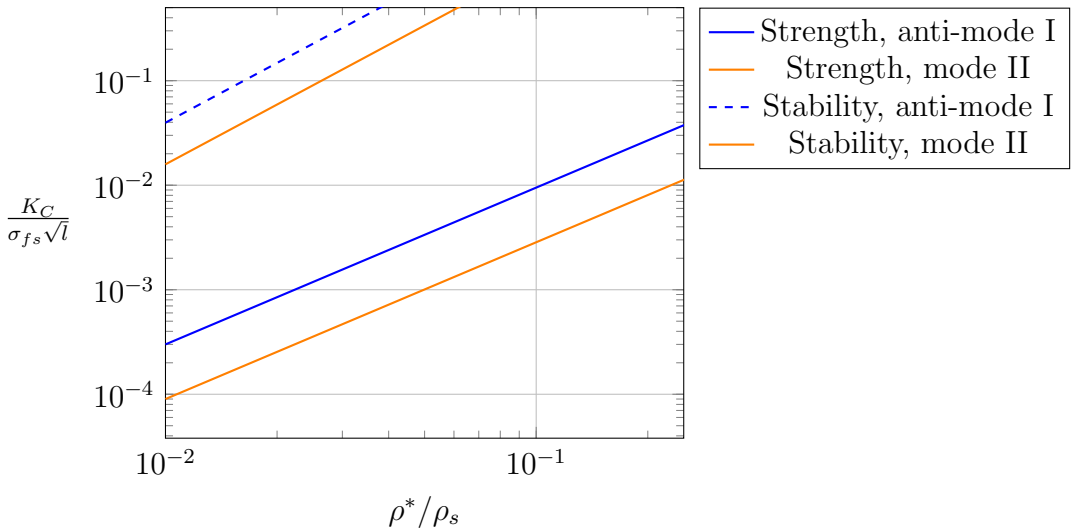

Figure 5.19: Comparison of fracture toughnesses depending on criterion for a tetrakaidecahedral structure with $\sigma_{fs} = E_s/1000$.

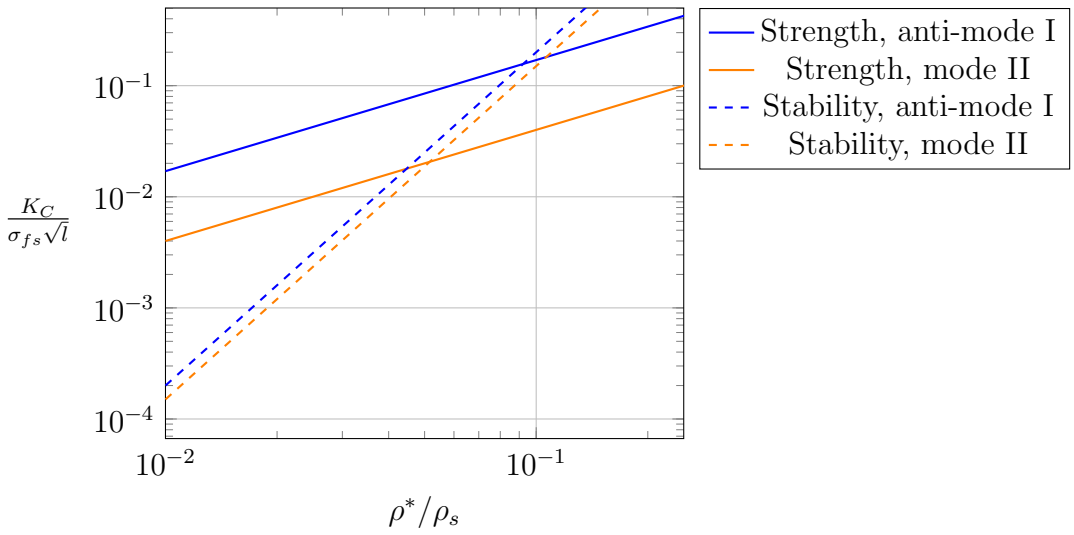

Figure 5.20: Comparison of fracture toughnesses depending on criterion for a triangular structure with $\sigma_{fs} = E_s/1000$.

Chapter 6

Fracture analysis of short cracks

As long as the crack size is large in comparison with cell size, which determines the minimum finite amount of crack growth, principles of LEFM apply correctly. But as the crack length goes shorter, the assumptions need to be questioned. In terms of fracture mechanics, the concrete questions from a practical view would be if the fracture toughness or its equivalent fracture energy remain constant in the case of short cracks. The answer to that matter is the objective of this chapter, and the main issue of this thesis. It is assumed that the critical energy release rate, also called fracture energy, is directly related to the fracture toughness with the elastic constants of the material as in continuous materials.

Two approaches are followed in order to characterize the critical fracture properties. In the first one, the fracture energy for crack growth is directly derived from the decrease in total potential when a cell wall breaks. For that, the strain energy is measured before and after disconnecting a cell wall.

In a second approach the fracture toughness is measured as it was made in the previous chapter for relative long cracks. The difference with the previous section is that for short cracks principles of Finite Fracture Mechanics (FFM) are considered. More details are explained in the following sections.

6.1 Fracture energy for finite crack growth

The critical energy release rate or fracture energy, $\mathcal{G}_c$, defines the released energy during the crack growth, as explained in section 3.1.1. In order to obtain it numerically, the energy balance is solved using the Finite Element model at the moment of fracture, when the crack grows. Crack growing is supposed to occur when the local strength failure criterion according section 4.4.1 is accomplished. The stability failure criterion has not been used in this analysis.

The used method starts from the energy balance as defined by equation (3.7). From this balance the terms kinetic energy, $\mathcal{K}$, power of external forces, $\mathcal{P}$, and

non-mechanical energy transport rate, $\mathcal{Q}$, are assumed to be zero. The remaining terms define the energy release rate for an infinitesimally crack surface advance as shown in equations (3.13) and (3.15), and then the critical energy release rate is defined when crack growth exists per equation (3.16).

If a finite crack advance occurs as in the case of cellular structures, the critical energy release rate can be defined as

$$\mathcal{G}_c = -\frac{\Delta\Pi}{\Delta a}. \tag{6.1}$$

Therefore, the critical energy release rate can be obtained by measuring the total potential before and after a finite crack growth, which means that a cell wall breaks. For this purpose the followed method assures that

$$\Pi^{ext} = 0, \tag{6.2}$$

so that according equation (3.12) it becomes

$$\mathcal{G}_c = -\frac{\Delta\Pi_{int}}{\Delta a}, \tag{6.3}$$

that can be directly evaluated from the Finite Element results, as Π^{int} corresponds to the strain energy.

6.1.1 Analysis approach

In the analysis a very large model in size is simulated in comparison with the crack length, in which an uniform far field stress σ_0 is applied. Since the problem is linear and results are scaled, the amount of the trial stress σ_0 is not important. Under this far field stress state a intensity factor for a certain fracture mode (MI, MII, or anti-MI) is applied, according section 3.1.1.

The far field stress is applied to the model using using displacement boundary conditions at the boundaries of the outside area, as shown in figure 6.1. For that purpose, the corresponding strain is calculated using continuum properties obtained in chapter 4, under the assumption that the crack effect is negligible against the whole model size. Displacements are then derived from ε_0 as

$$\varepsilon_0 = \frac{\varepsilon_0}{E^*}. \tag{6.4}$$

A linear static analysis is performed with the loads, from which the total internal energy and the maximum tensile stress at the section points are extracted as output. Figure 6.2 shows an example of the stress results. The section points

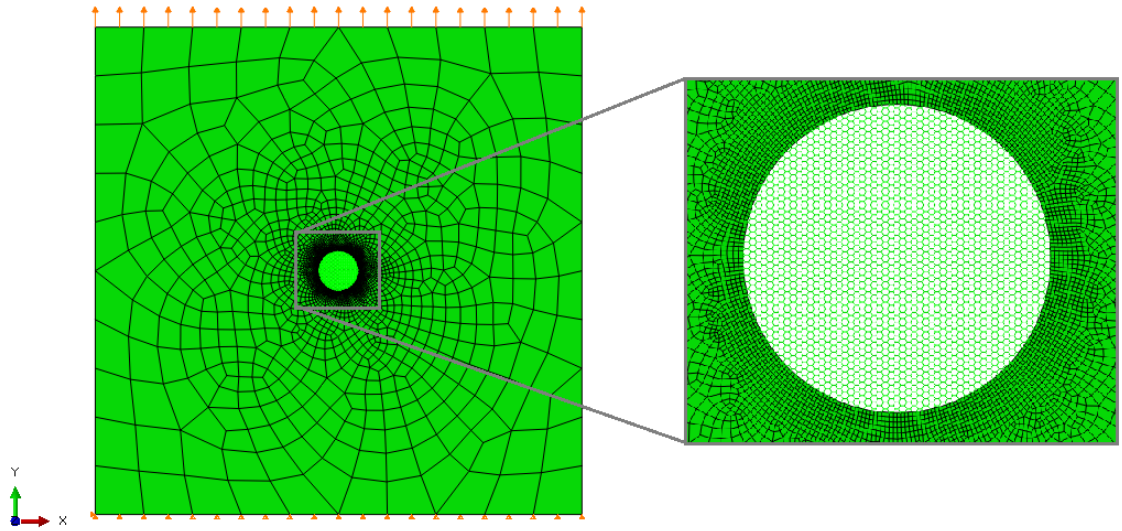

Figure 6.1: Example of model for an hexagonal structure under MI.

are those according to the Simpson interpolation, reaching the beam border. The total strain energy, defined as $U_0(a, \sigma_0)$, is evaluated from the whole model, being a the half crack length. The maximum local tensile stress from the beam elements, $\sigma_{max0s}(a, \sigma_0)$, must be also be extracted. The analysis needs to be repeated for each crack length a considered in the analysis.

Once the outputs $U_0(a, \sigma_0)$ and $\sigma_{max0s}(a, \sigma_0)$ are obtained for each crack length a, the critical far field stress that would cause failure can be determined as

$$\sigma_f(a) = \frac{\sigma_{fs}}{\sigma_{max0s}(a, \sigma_0)} \tag{6.5}$$

for a given crack length a, being σ_{fs} the ultimate strength of the solid material. The next step is to calculate the total strain energy when that local strength criterion is accomplished, given by

$$U_f(a, \sigma_f(c)) = U_0(a, \sigma_0) \left(\frac{\sigma_f(a)}{\sigma_f(a, \sigma_0)} \right)^2 . \tag{6.6}$$

This is done applying LEFM principles by combination of equation (3.1) and (3.17) for a certain failure mode. The same can be done with a finite crack growth, but still at the same macroscopic stress, scaled as

$$U_f(a + \Delta a, \sigma_f(c)) = U_0(a + \ \sigma_0) \left(\frac{\sigma_f(a)}{\sigma_f(a, \sigma_0)} \right)^2 . \tag{6.7}$$

In this step it was assumed that the same far field stress to the whole model is not affected by the finite crack growth, given the relative small size of the crack against the model. In this way no work is done by the boundary conditions and

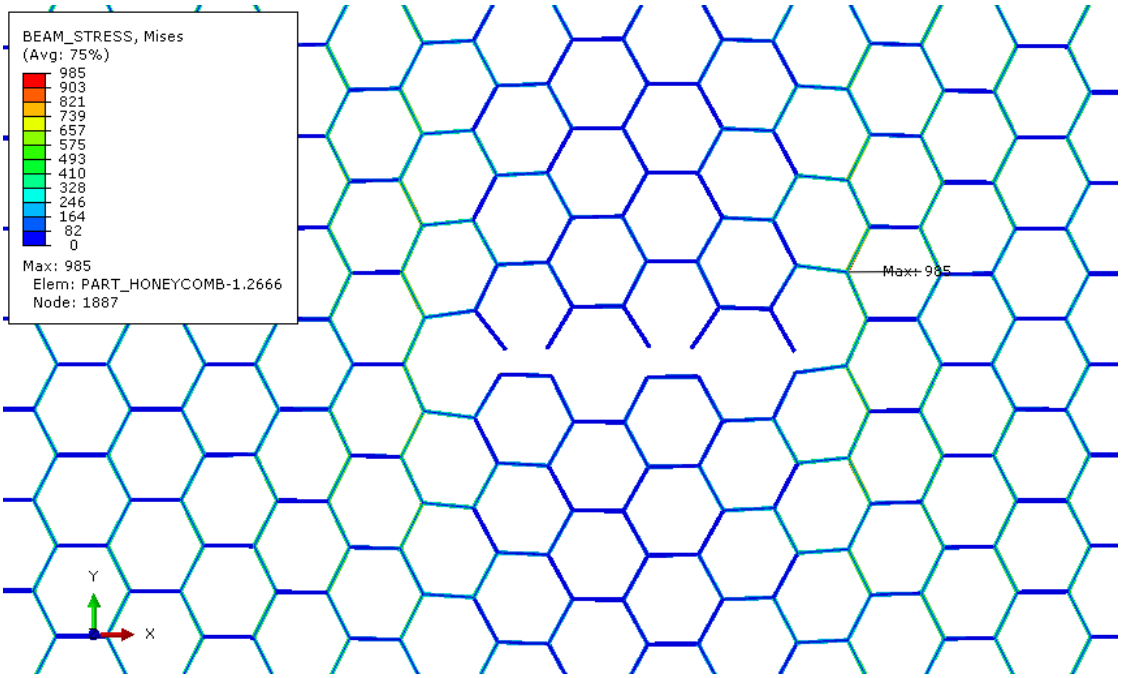

Figure 6.2: Example of stress results for an hexagonal structure under mode I. Maximum local tensile stress S11 is depicted.

the power of external forces can be neglected in the balance equation. Finally, the critical energy release rate is determined for each crack length by

$$\mathcal{G}_c = -\frac{\Delta U}{\Delta a} = \frac{U_f(a, \sigma_f(a)) - U_f(a + \Delta a, \sigma_f(a))}{\Delta a} \tag{6.8}$$

This methodology assumes brittle behavior with linear elastic properties. This is evaluated before and after disconnecting the cell wall beam. In this way the external work does not need to be considered, as long as the assumption is valid. It is verified that the amount of energy reduction because of the crack growth is negligible against the whole model internal energy.

6.1.2 Triangular cells honeycomb

The following values have been used for the simulation:

- Orientation of crack plane: 0° (cell wall is parallel to crack)
- $\rho^*/\rho_s = 0.1$
- $l = 1$
- $t = 0.02887$ (see equation 3.25)
- $E^* = 3320$ (see table 4.1)

- $\nu^* = 0.33$ (see section 4.3.1)
- $E_s = 100000$
- $\nu_s = 0.3$
- Applied strain: $\varepsilon_0 = 0.01$,
- Load stress: $\sigma_0 = E^*\varepsilon_0 = 33.2$
- Core region radius = 20
- Model width = 1000
- Model height = 1000

According to FEM theory the values are given in the analysis without specifying the units. They must correspond to a consistent unit system, which usually and in this work is based on Millimeter, Newton, and Tonne. The rest of needed units in this report are directly derived from those, as for example Megapascal (N/mm^2).

Figure 6.3 shows the results for the different modes, and the comparison with the derived fracture energy from the previous chapter values, which are obtained for long cracks. a corresponds to the half crack length and l to the wall cell length, considering crack length always between cell centers distance. Results on the plots are scaled with l and σ_{fs} with LEFM principles, being dimensionless.

For mode I and II results, depicted in detail in figure 6.4, the fracture energy remains quite constant for all crack lengths. Especially it is constant for mode I, practically independent even for very short cracks. For mode II a small increase exists, but no more than 15% for 2-3 cell wall length. The calculated values from LEFM in section 5, calculated according equation 3.17, match with the energy release approach.

As remark, results are only obtained for 0° orientation, for the method is complex to performed for more orientations by the fact of determining the crack length is not straightforward. Depending on how the cells are at the crack tip the length changes, as well as the finite crack growth. For this reason the process cannot be easily automated and is tedious to follow.

Solution for anti-mode I depicts a strange behavior that can be easily explained: the calculated decrease of strain energy is of no interest as the next excluded cell wall is not the critical one, as shown in figure 6.5. In this deformation mode the next strut breaking is not geometrically the next in the crack according the failure criterion, therefore results of anti-mode I are of no account. This problem did not appear in the previous chapter since there was no crack extension prescribed.

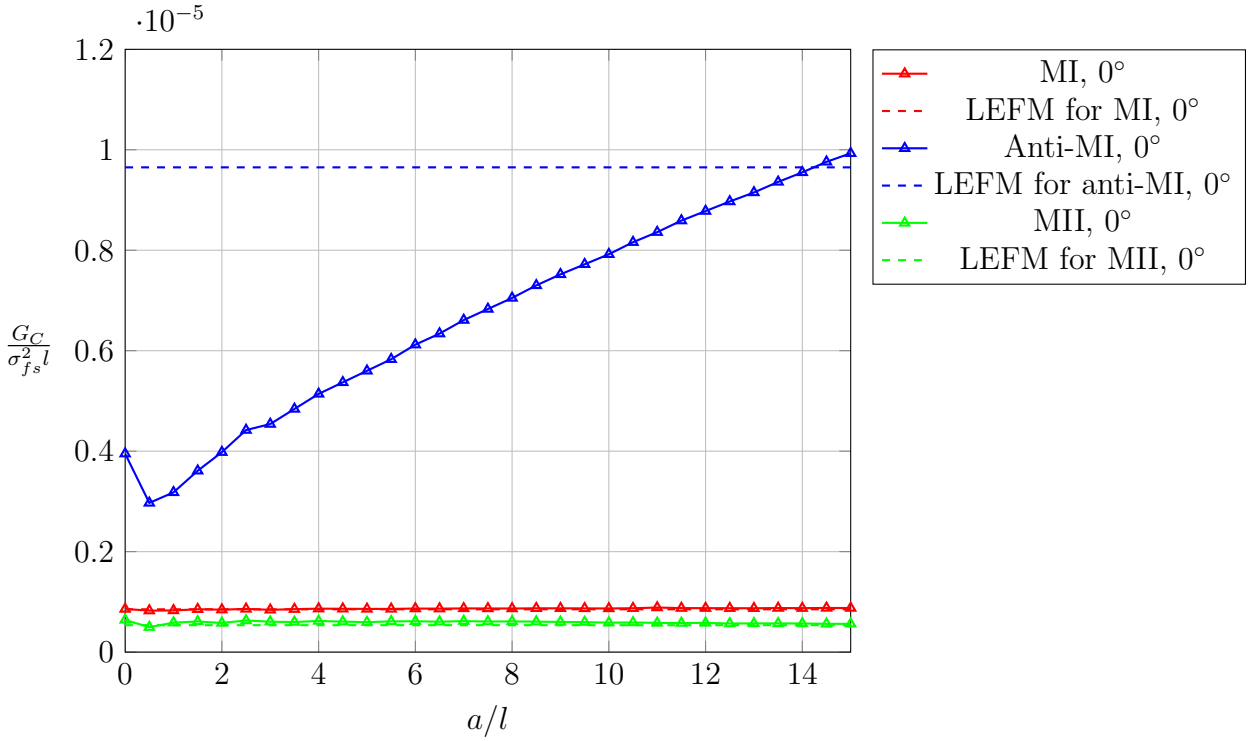

Figure 6.3: Fracture energy of triangular honeycombs with dependence on crack length.

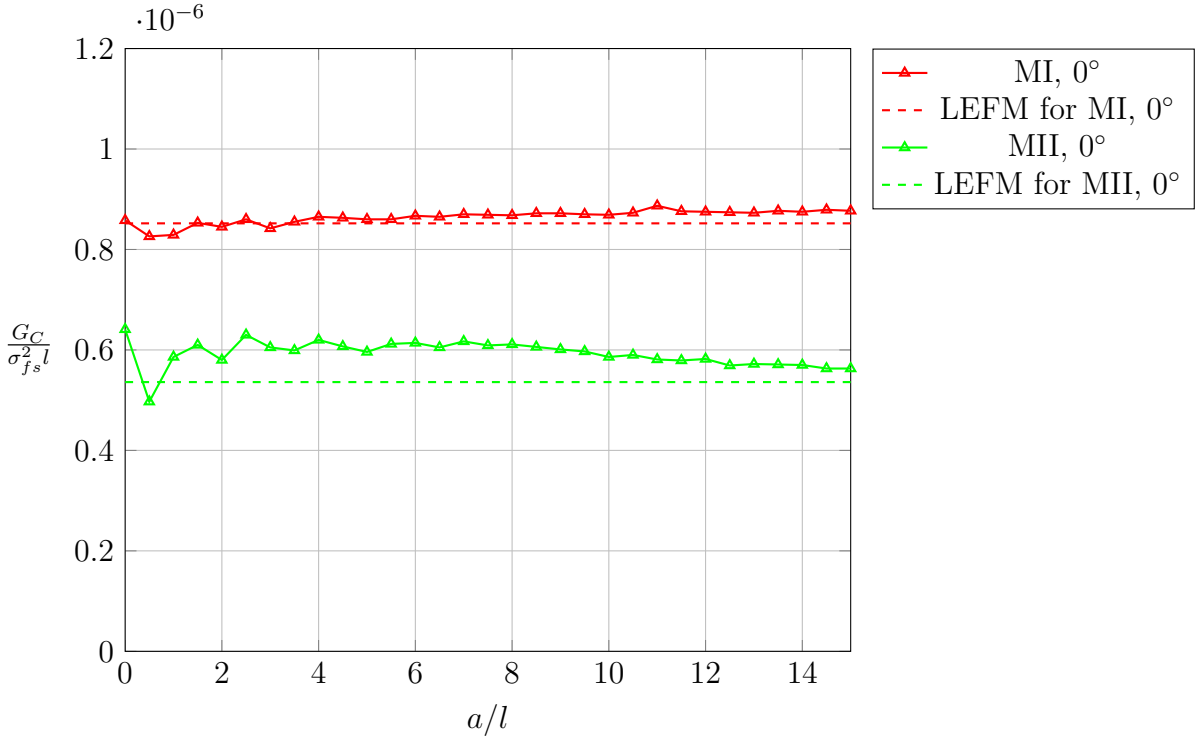

Figure 6.4: Fracture energy of triangular honeycombs with dependence on crack length (detailed plot for Mode I and Mode II).

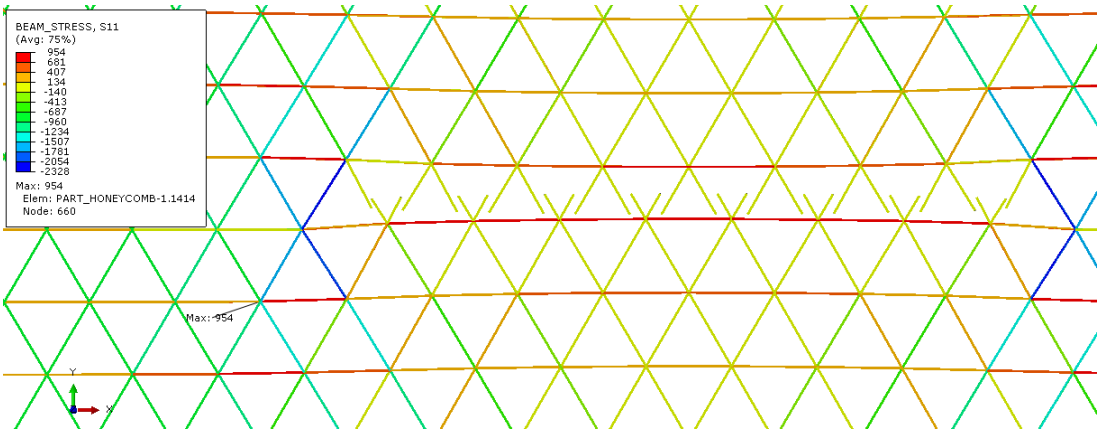

Figure 6.5: Example of stress results for a triangular structure under anti-MI stress field. Maximum local tensile stress S11 is depicted.

It has to be taken into account that the failure criterion only considers the maximum (positive) tensile stress, neglecting compressive stresses, which for many materials would be wrong. For example figure 6.5 shows a much critical compressive stress than tensile. One strategy for using the results with tensile/compressive strength criteria is to combine mode I/anti-mode I results. As the calculations are linear, fracture variables for anti-mode I can be determined using the values from mode I with the compression strength instead of the ultimate tensile strength.

6.1.3 Hexagonal cells honeycomb

For the case of hexagonal honeycomb the following values are used in the simulation:

- Orientation of crack plane: 0°, 30° (at 0° a cell wall is parallel to the crack)
- $\rho^*/\rho_s = 0.1$
- $l = 1$
- $t = 0.0866$ (see equation 3.25)
- $E^* = 141$ (see table 4.1)
- $\nu^* = 0.96$ (see section 4.3.1)
- $E_s = 100000$
- $\nu_s = 0.3$
- Applied strain: $\varepsilon_0 = 0.01$,
- Load stress: $\sigma_0 = E^*\varepsilon_0 = 1.41$

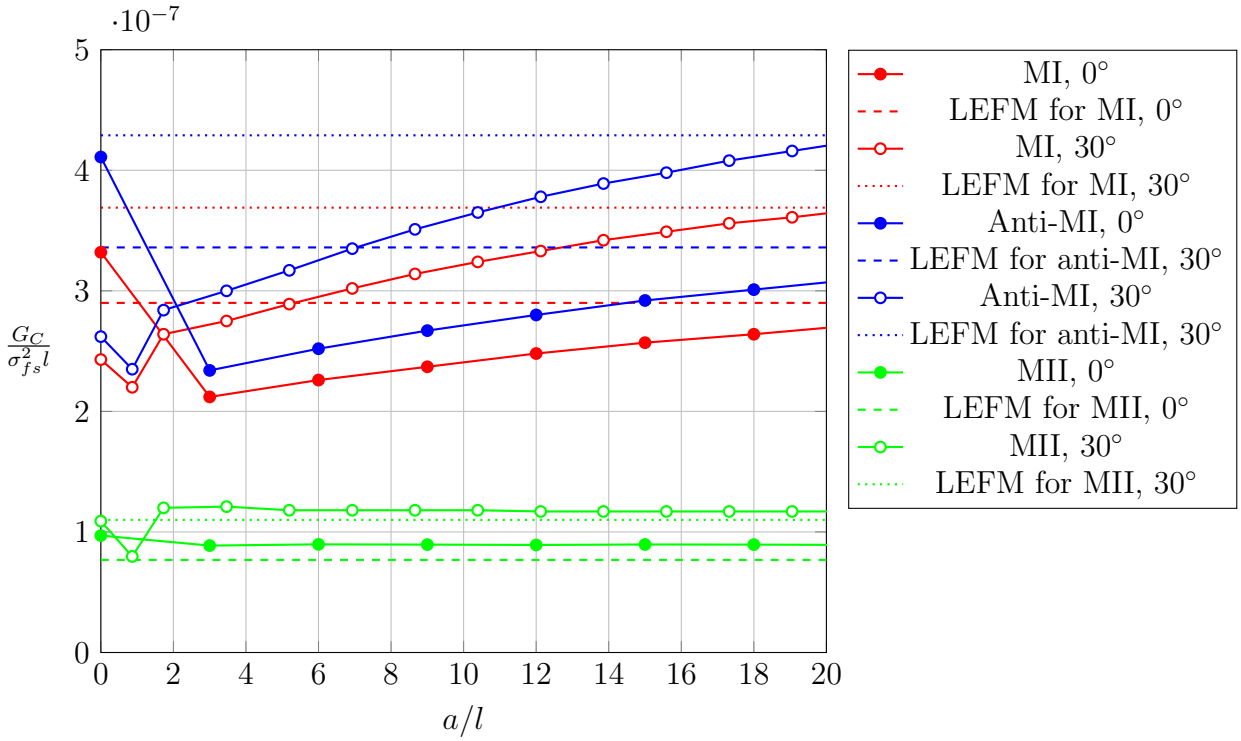

Figure 6.6: Fracture energy of hexagonal honeycombs with dependence on crack length.

- Core region radius = 45
- Model width = 2000
- Model height = 2000

As in the triangular structures, only two orientations are calculated because of the complex process of given the right crack length and finite crack growth for each case, so no direct results can be obtained using scripts.

In contrast with the triangular structure, hexagonal structures shows a clear dependence of crack length is observed in the results from figure 6.6. For mode I and anti-mode I a decrease can be observed as the crack length diminish, with a jump below two cell wall units. For mode II a uniform behavior is shown, again with a characteristic behavior below a crack length of two cell wall units. Besides, a uniform difference between 0° and 30° angle is observed, matching with LEFM results of section 5 for different orientations.

However, the reliability of results must be taken with caution. Even though the asymptotic development to the LEFM solutions at the right of figure 6.6 seems to be right, no length dependence is expected above 8-10 cell walls half crack length according to literature (see section 3.2.3). It is possible that the assumption made in the method is not correct, namely that the small size of the crack does not affect the relative larger size of the model and the far field stress remain constant

when the next cell wall is disconnected (finite crack growth). It only happens to the hexagonal structure, which has a Young's modulus much lower than the triangular, being possible that a larger model would be necessary.

6.2 Failure stress of short cracks

This second approach is based also in LEFM principles, being this method considerably easier to adopt. The idea is to apply a stress intensity factor according to a failure mode and obtain the macroscopic stress at which the failure would occur. This is done for each structure and for each failure criterion, using parametric studies for crack length, orientation, and deformation mode.

In order to obtain far field failure stress, first a stress intensity factor must be applied. This is done giving as load a far field stress according LEFM principles (section 3.1.1) as done in the previous approach. Figure 6.1 shows an example of the applied boundary conditions. Loads are given as displacements for the strength failure criterion, whereas for the stability criterion stresses are applied to the outer limit elements.

Critical stress values are obtained for a range of crack lengths in the structures of interest. Crack length is always normalized with cell strut length in order to give dimensionless results. The solution when no crack exists are also presented in the results for comparing purposes, so that the strength solution for ideal structures without flaws can be contrasted with the failure stresses for very short cracks.

The Finite Element results are compared on one side with the fracture stresses that would be obtained using LEFM. A theoretical fracture toughness calculated in chapter 5 is used, assumed constant for all crack orientations. It results for example in

$$\sigma_f(LEFM) = \frac{K_{IC}}{\sqrt{\pi a}} \tag{6.9}$$

for mode I with a crack of length $2a$. Two different σ_f are obtained for the two different failure criteria. A second comparison is made using FFM (Finite Fracture Mechanics) methods to calculate fracture stresses. For this a characteristic length Δa is defined as explained in section 3.1.2, ending up with the formula

$$\sigma_f(FFM) = \frac{K_{IC}}{\sqrt{\pi(a + \Delta a/2)}} \tag{6.10}$$

for mode I. Similar equations are used for the other modes. More information is to be found in chapter 3. It is to note that results are given dimensionless, scaled with geometric and material variables as relative density, $\overline{\rho}$, solid material strength, σ_{fs}, and Young's modulus of the solid material, E_s.

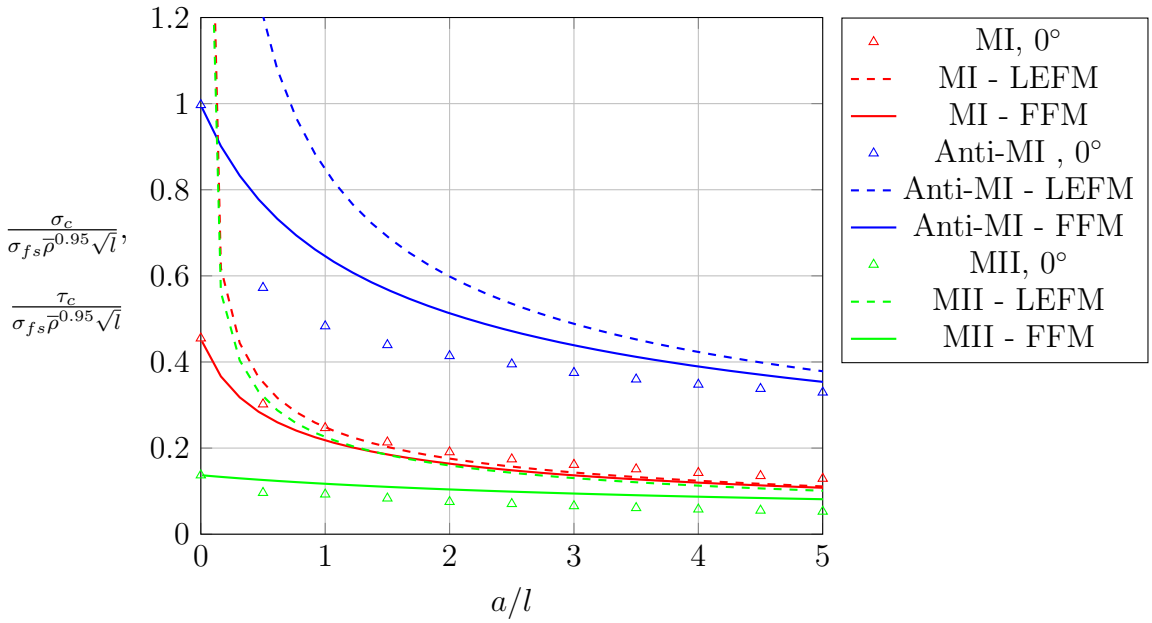

Figure 6.7: Fracture stress of triangular honeycombs with dependence on crack length, strength failure criterion. FEM: Finite Element Method, LEFM: Linear Elastic Fracture Mechanics, FFM: Finite Fracture Mechanics.

6.2.1 Local strength failure criterion

For using the strength failure criterion a linear static analysis is performed with the Finite Element Model as explained in section 4.4.1, applying a far field stress for a certain known fracture toughness according equation (3.1). From the results the maximum local tensile stress is scaled using the ultimate strength of the solid material. An example of the results can be seen in figure 6.5 for better understanding. It can be seen how the maximum local tensile stress "S11" is depicted in the inside beam structure in a triangular structure. The method is repeated for each configuration depending on structure, angle, and crack length.

Results for triangular structure are to be found in figure 6.7. The fracture stresses are scaled with the ultimate strength of the solid material in order to have comparable values. The ratio a/l refers to the crack length between cell centers to the cell wall length. That is a problem with rotated configurations, but because of the cellular structure no better way of measuring the crack length can be found. In the next figures the same scaling is used.

It can be seen in figure 6.7 how the fracture stress becomes higher as the crack is shorter. Logically, longer cracks need lower stresses to grow. Observing the left side, where the crack is approaching zero length, fracture theories show different behaviors: the classical fracture mechanics (FM) rises asymptotically towards infinite as the length becomes zero. On the other hand, finite fracture mechanics (FFM) approaches the material strength as the crack length is zero,

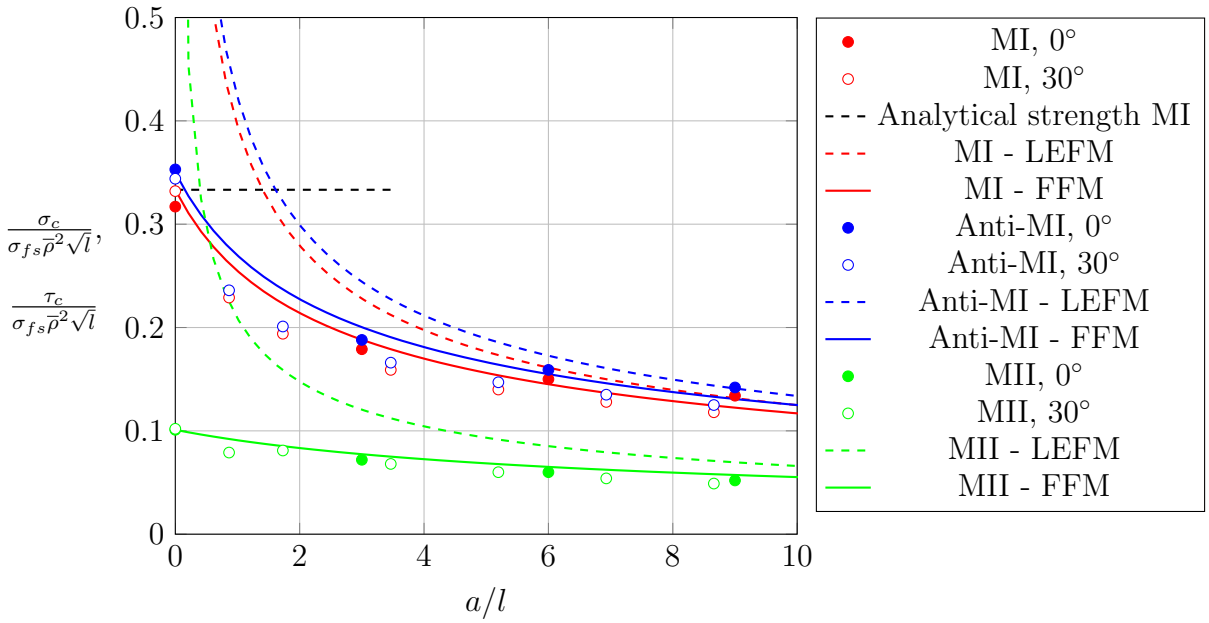

Figure 6.8: Fracture stress of hexagonal honeycombs with dependence on crack length, strength failure criterion. FEM: Finite Element Method, LEFM: Linear Elastic Fracture Mechanics, FFM: Finite Fracture Mechanics.

maintaining a similar level as FM for long cracks. FFM can be understood as a theory that unifies the tensile strength of unnotched structures with the predictions of LEFM.

The Finite Element results show a very good matching for mode I deformation even with very short cracks, as shown in figure 6.8 for hexagonal structure. Value at crack length zero is obtained from the model without any flaw. In the case of mode II FEM values are about 30% below the approximations , remaining similar for very short cracks. Anti-mode I values are also below fracture theories, coinciding with FFM when no crack exists.

It is to note that some difference exists with the predicted stresses at the right side of the plots, when the cracks are relatively large. The reason is that LEFM and FFM curves have been created using the averaged result from all orientations, as derived in chapter 5. There is up to 10-15% difference, as in the fracture toughness results from section 5.2.

6.2.2 Stability failure criterion

Using the stability failure criterion a linear buckling analysis is performed with the model, as explained in section 4.4.2. Fracture stress is then obtained using the first eigenvalue of the solution and directly multiplying it with the applied far field stress. Figure 6.9 serves as example for an hexagonal structure under mode II.

Figure 6.10 shows for triangular 2D structures with only 0° orientation. As

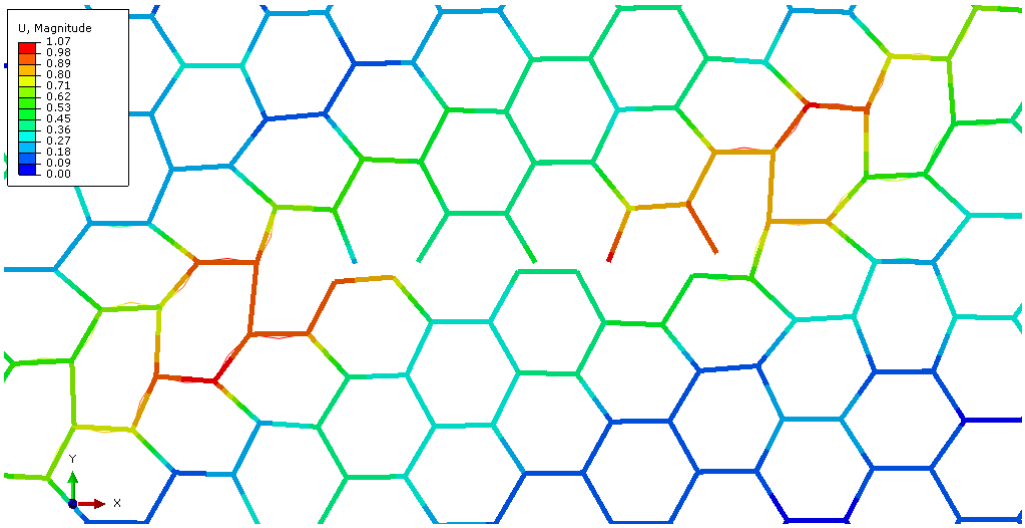

Figure 6.9: Example of buckling results for an hexagonal structure under mode II. First eigenmode is shown.

before said, a good matching can be seen for both Anti-Mode I and Mode II with the Finite Fracture Mechanics predictions. Obviously, FFM law matches with the results without crack since the length unit used for the predictions is obtained from this FEM value. Other methods or approaches could be used to define that fracture constant from FFM (see section 3.1.2 for details), as for example the own cell dimension of the structure.

In the case of hexagonal lattices two directions have been analyzed, with 0° and 30° orientation, as shown in figure 6.11. Here there is more scattering of results in both modes and in the two orientations, nevertheless a good agreement is to be found, specially with FFM theories at very short cracks. It has to taken into account that predictions of fracture stresses are difficult to make with precision, thus to be able to know the behavior in case of short cracks could help in determined problems.

Similar observations can be made for the results with the buckling criterion. A relatively good agreement between FEM results and LEFM/FFM predictions is accomplished, being the FFM slightly better with small cracks. Nevertheless, predicted fracture stresses with classical Fracture Mechanics theory results can be acceptable up to short cracks of a few cell walls. According to the results, this limit can be approximately two cells for half crack length in triangular lattices (figure 6.10), and 4-5 cell walls for half crack length in hexagonal ones (figure 6.11).

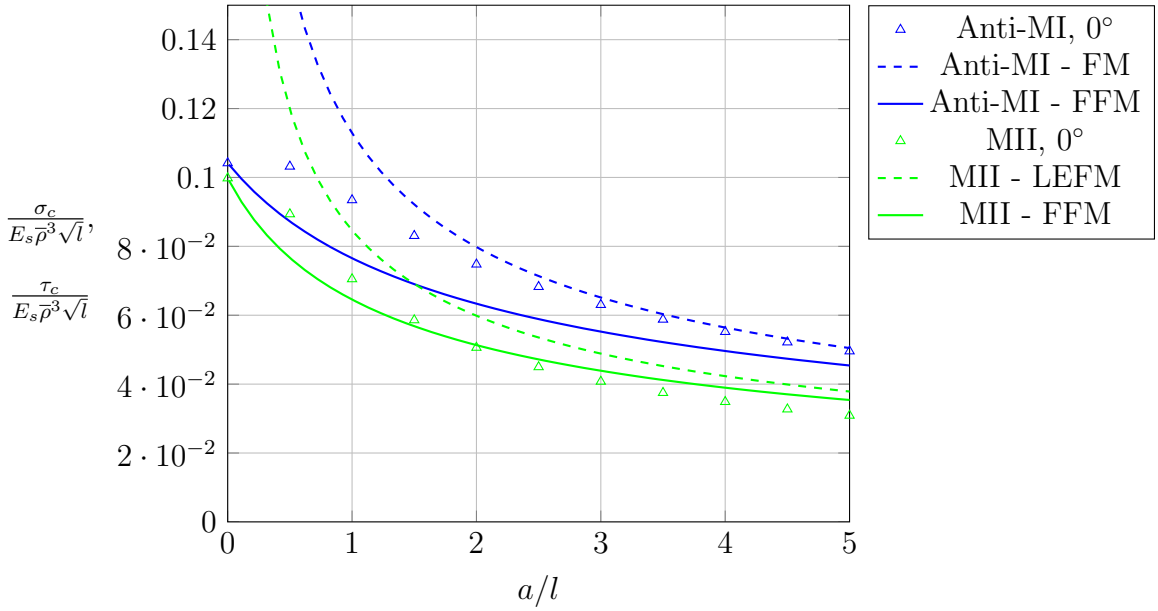

Figure 6.10: Fracture stress of triangular honeycombs with dependence on crack length, stability failure criterion. FEM: Finite Element Method, LEFM: Linear Elastic Fracture Mechanics, FFM: Finite Fracture Mechanics.

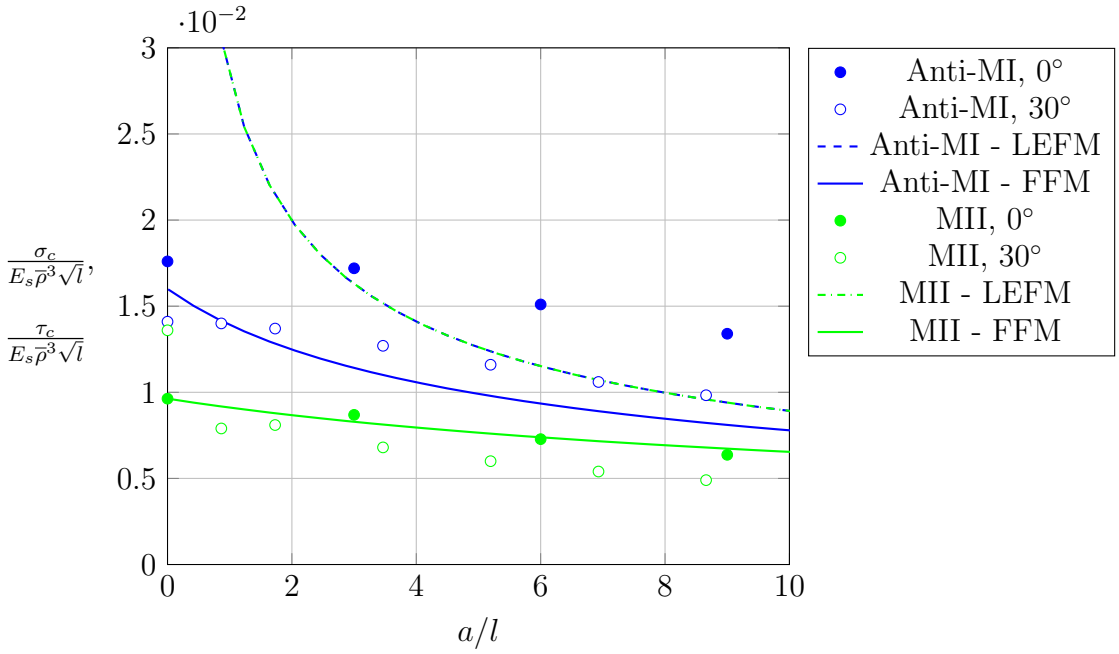

Figure 6.11: Fracture stress of hexagonal honeycombs with dependence on crack length, stability failure criterion. FEM: Finite Element Method, LEFM: Linear Elastic Fracture Mechanics, FFM: Finite Fracture Mechanics.

Chapter 7

Growth direction of cracks

As long as the assumption of an isotropic continuum material is true, the theory of Linear Elastic Fracture Mechanics predicts properly the way a crack grows, referring to in which direction it develops. But in case of cellular materials, where a discrete structure exists, it is not so accurate. When dealing with cellular materials, if the crack length is very large in comparison with the cell length, continuum assumptions are still correct. The small deviations in the crack direction are local and negligible for a major scale consideration, causing that LEFM principles apply. This is also the case of solid materials, as metals or ceramics, where at molecular scale very irregular failure may occur. But when the crack faces are observed at larger scales no such irregularities are to be of significance.

Focusing on cellular materials when the characteristic cell length is not negligible in front of the crack size, different conclusions in the way the crack grows need to be made.

7.1 Crack growth test in an hexagonal structure

In figure 7.1 an example is illustrated to see how a crack grows. A hexagonal structure is used applying the strength criterion with an initial crack length between cell centers of about 20 cell walls. Mode I load is applied.

The opening of the crack or break of the cell walls is made manually. Elements that are critical in each step are disconnected, which means that they do not longer exist in the analysis. So the procedure is running the calculation with an initial crack and after that disconnecting the element with the maximum tensile stress. Then the static calculation is made again in the same way. The process is repeated 30 times, considering that 30 struts break.

Images in figure 7.1 show that the next strut in the tip crack is not the critical one, but a zone close to the crack tip. Besides, the developing of the crack is not

in the usual direction of Mode I. Growing direction is at about 30^{o} of the crack plane, clearly affected by cell structure.

It was only a qualitative example but it can be seen that local failure of cellular structures differ a lot from continuum assumptions, being affected by the structure itself. A crack growth mode more similar to mode II could be appreciated. Explanation for that could be derived from results in previous section, since fracture toughness for mode II is smaller than for mode I and therefore the difference in direction.

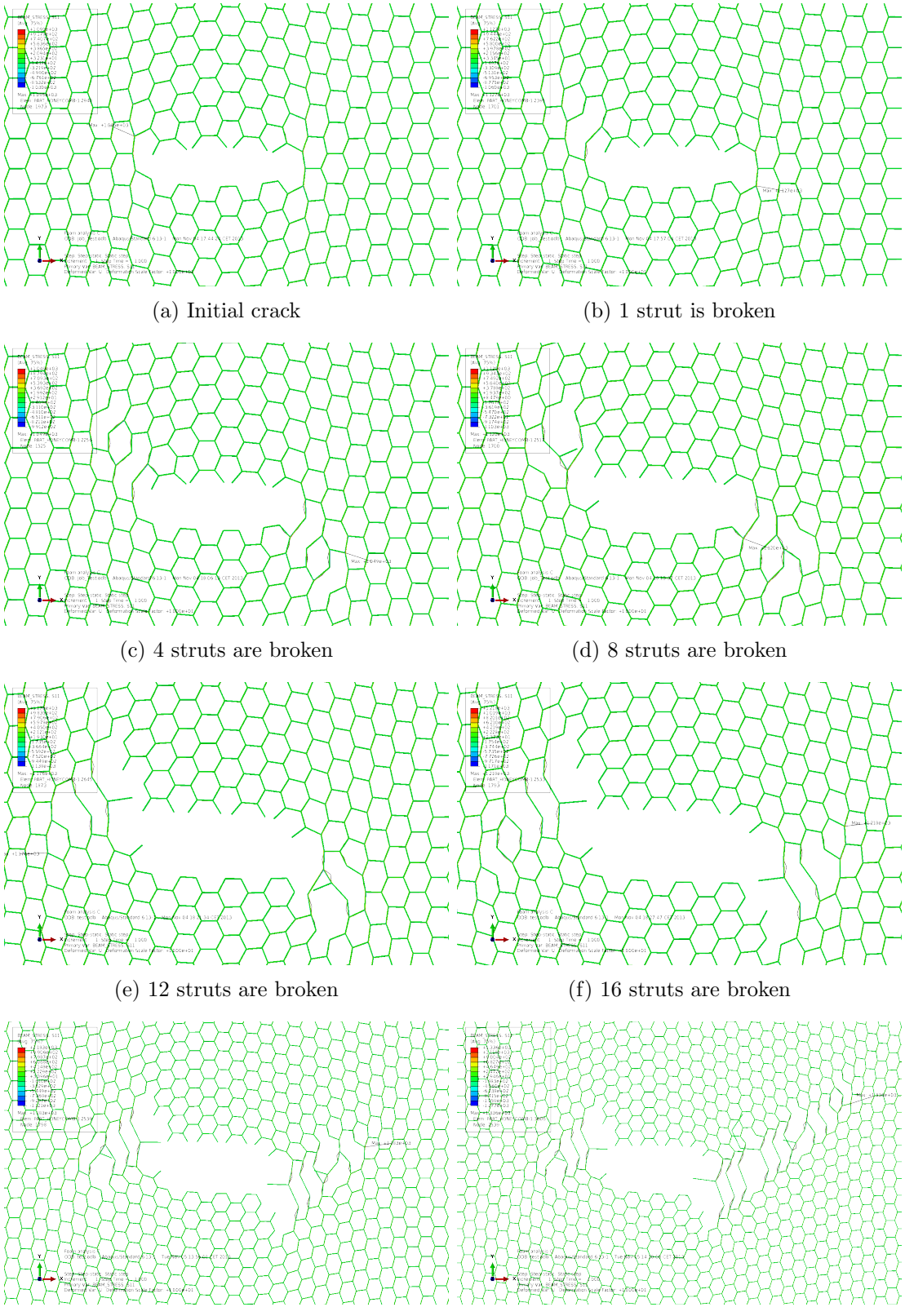

(a) Initial crack

(b) 1 strut is broken

(c) 4 struts are broken

(d) 8 struts are broken

(e) 12 struts are broken

(f) 16 struts are broken

(g) 22 struts are broken

(h) 30 struts are broken

Figure 7.1: Crack growth analysis of hexagonal structure exposed to tensile stress (Mode I). After each static analysis the beam with the maximal local tensile stress is "disconnected" from the corresponding node, corresponding to the crack growth by strength failure criterion.

Chapter 8

Conclusions

Cellular materials are widely used in the industry because of their good qualities, and an increasing implementation is expected in the near future. Therefore, a good knowledge of their mechanics is desired for design and application purposes. However, their mechanical behavior is not yet totally understood, specially in the case of structures containing flaws or cracks.

Some important conclusions about the fracture behavior of cellular structures can be gathered based on the numerical simulations performed in this thesis. These findings can help for better understanding in cellular materials applications. This is relevant not only because of the actual use of these materials, but in view of a growing usage in the industry for a close future, since new additive manufacturing techniques allow their production. It is to note that cellular structures show very attractive strength characteristics to low density ratios.

With the restriction of regular structures with quasi isotropic behavior, properties like the Young's modulus can be defined analytically using equations. These equations relate the density, solid material properties and geometric parameters for each cellular lattice. The same approach can be made in Fracture Mechanics problems, where fracture toughness can be defined with similar laws, remaining under the assumption of a continuous material and considering long cracks in relation with the cell wall length. All these expressions have been investigated previously in the literature, and for the case of triangular, hexagonal and tetracaidecahedral structures they are verified in the this work using Finite Element Methods with similar results.

A step further has been made in the analysis of short cracks. In the literature the application of Linear Elastic Fracture Mechanics principles is said to be limited by a minimum crack of a few cell walls length. Here it is numerically determined which these limits are, being the length of only a few lattice cell walls. It is to be remarked that certain scattering of the data was obtained but acceptable for fracture mechanics results. That can be attributed to the anisotropy in the crack

tip area.

An attractive approach that was satisfactorily used in the analysis of short cracks is the application of Finite Fracture Mechanics. It is based on the utilization of a length parameter dependent on the cellular structure in order to determine the fracture stress. In this way the typical behavior at very short cracks changes to an approximation up to the strength of the material. Results showed the validity of the method, so that the simplification helps working with short cracks problems. Some variability was found again in the values, though they kept relatively small. In this thesis the length parameter used in FFM, which is an important consideration, is determined from the material strength. The use of cell wall lenght directly as parameter remains a topic for further study.

Furthermore, the new proposition of using a stability fracture criterion together with fracture principles was validated. Fracture toughnesses and stresses could be determined in this way. It can be important for low density cellular materials, where the ratio of cell wall length to strut section dimension is very high.

Results and conclusions from these ideal cases, in which two approaches are applied, could also be extrapolated to more complex problems, as irregular or anisotropic structures, or plastic material behavior, although that question is beyond the scope of the present thesis.

Appendix A: Abaqus model script

The FEM analyses are done using a python script in Abaqus/CAE. In this appendix a short explanation of the parts is presented: In a first part, after the heading, the functions are to be found, which create the model in different steps. After that the variables of the analysis are to be found, which were changed depending on the particular analysis. At the end, functions are called, using the parameters defined before. Those functions can be repeated using buckles when necessary for the parametric simulations.

Heading

The necessary modules from Abaqus are loaded so that their functions and objects can be used.

```
######################################################
# Calculate Foam: Script for analyse open cells foam #
######################################################

####################
# Importing modules #
####################

from abaqus import *
from abaqusConstants import *
backwardCompatibility.setValues(includeDeprecated=True, reportDeprecated=False)
import math
import part
import assembly
import material
import section
import step
import load
import mesh
import job
import visualization
import odbAccess
import displayGroupOdbToolset as dgo
...
```

Functions

The model is created following several steps, with each one in a separated function for clear understanding. For example, the function *createModel0 2D* creates a two dimensional model of the desired structure and properties. The creation of the crack is made in other functions.

```
####################
# Defining functions #
####################

# Model0 creates a pattern of the desired type of cell
# Model1 cuts according to a figure the assembly of Model0 and creates sets
# ModelA uses Model1 with circle figure to create an analysis with boundary conditions at beams
# ModelB uses Model1 with rectangle cut to create an analysis to obtain the continuum properties of a structure
# ModelC uses Model1 with circle figure to create an analysis with beam and continuum elements

def createModel0_2D(model0Name, cell, oriAngle, lstrut, imax):

# Calculated variables
#======================
orientation_2D = (math.cos(oriAngle*math.pi/180.0),
      math.sin(oriAngle*math.pi/180.0))

# Create a model
#================
model0 = mdb.Model(name=model0Name)

# Create basic cell geometry
#============================
mySketch = model0.ConstrainedSketch(name='Sketch_cell', sheetSize=250.)

if cell=='TRI':
ltriangle = lstrut/(2*math.cos(math.pi/6))
p1 = (ltriangle*math.cos((oriAngle+210)*math.pi/180),
  ltriangle*math.sin((oriAngle+210)*math.pi/180))
p2 = (ltriangle*math.cos((oriAngle+330)*math.pi/180),
  ltriangle*math.sin((oriAngle+330)*math.pi/180))
p3 = (ltriangle*math.cos((oriAngle+ 90)*math.pi/180),
  ltriangle*math.sin((oriAngle+ 90)*math.pi/180))

l1 = mySketch.Line(point1=p1, point2=p2)
l2 = mySketch.Line(point1=p2, point2=p3)
l3 = mySketch.Line(point1=p3, point2=p1)

elif cell=='HEX':
p1 = ( lstrut*math.cos((oriAngle+240)*math.pi/180), lstrut*math.sin((oriAngle+240)*math.pi/180))
p2 = ( lstrut*math.cos((oriAngle+300)*math.pi/180), lstrut*math.sin((oriAngle+300)*math.pi/180))
p3 = ( lstrut*math.cos((oriAngle+360)*math.pi/180), lstrut*math.sin((oriAngle+360)*math.pi/180))
p4 = ( lstrut*math.cos((oriAngle+180)*math.pi/180), lstrut*math.sin((oriAngle+180)*math.pi/180))

l1 = mySketch.Line(point1=p1, point2=p2)
l2 = mySketch.Line(point1=p2, point2=p3)
l3 = mySketch.Line(point1=p4, point2=p1)

else:
print 'Error: the selected cell type is not correct.'
raise ValueError

Part_cell = model0.Part(name='Part_cell', dimensionality=TWO_D_PLANAR, type=DEFORMABLE_BODY)
Part_cell.BaseWire(sketch=mySketch)

# Create cell pattern in the assembly
#=====================================

model0.rootAssembly.Instance(name='Instance_cell', part=Part_cell, dependent=OFF)

if cell=='TRI':
dir1 = ( math.cos(oriAngle*math.pi/180.0), math.sin(oriAngle*math.pi/180.0), 0)
dir2 = ( math.cos((oriAngle+120)*math.pi/180.0), math.sin((oriAngle+120)*math.pi/180.0), 0)
Spacing1=lstrut
Spacing2=lstrut

elif cell=='HEX':
dir1 = ( math.cos((oriAngle+30)*math.pi/180.0), math.sin((oriAngle+30)*math.pi/180.0), 0)
dir2 = ( math.cos((oriAngle+90)*math.pi/180.0), math.sin((oriAngle+90)*math.pi/180.0), 0)
Spacing1=2*lstrut*math.cos(30*math.pi/180.0)
Spacing2=2*lstrut*math.cos(30*math.pi/180.0)

model0.rootAssembly.translate(instanceList=('Instance_cell', ),
  vector=(-2**imax/2*Spacing1*dir1[0],
  -2**imax/2*Spacing1*dir1[1], 0.0))
model0.rootAssembly.translate(instanceList=('Instance_cell', ),
  vector=(-2**imax/2*Spacing2*dir2[0],
  -2**imax/2*Spacing2*dir2[1], 0.0))

listInstances1 = model0.rootAssembly.LinearInstancePattern(instanceList=('Instance_cell', ),
```

```
   direction1=dir1, direction2=dir2,
   number1=2, number2=2,
   spacing1=Spacing1, spacing2=Spacing2)

...
```

Variables definition

According to the desired analysis to perform variables, structure, dimensions and other parameters are defined. They will be afterwards used in the correspondent functions.

```
#############
# Variables #
#############
MODELONAME = 'Model_0'
MODEL1NAME = 'Model_1'
MODELANAME = 'Model_A'
MODELBNAME = 'Model_B'
MODELCNAME = 'Model_C'
JOBNAME = 'Job_Test'

CELL = 'TRI' #'TRI', 'HEX' for 2D, 'KV' for 3D
LSTRUT = 1.0
THICKNESS = 0.002887 #or radius (KV: 0.1096/2, 0.2450/2, 0.3465/2)
ORIANGLE = 0.0
ROTANGLE = 0.0
ROTANGLEALPHA = 0.0
ROTANGLEBETA = 0.0
IMAX = 6 #Number of iterations creating the cell structure pattern (6, 7, 4)
CUTFORM ='Circle' #'Circle', 'Rectangle'

NCRACK = 20.0 #0.0 gives an error, for analysis without crack, take a small value
NRREGION = 20.0 #For circle (25, 40, )
NXREGION = 16.0 #For rectangle
NYREGION = 16.0 #For rectangle
XCENTERBOX = 0.0
YCENTERBOX = 0.0
NXBOX = 1000.0 #Continuous region
NYBOX = 1000.0 #Continuous region
NZBOX = 16.0 #Continuous region

ANALYSIS = 'Buckling' #Static, Buckling
ECONT = 331.0 #(KV: 5.36, 116, 408)
NUCONT = 0.33
NSEGMENTS = 1
NLGEOM = 0 # 0->no, 1->yes
LOAD = 'Strain' #'Strain', 'Stress', 'Shear', 'ShearStrain'
STRAINYY = -0.01
DY = STRAINYY*LSTRUT*NYREGION
PRESS = 1.00 #Pressure up and down (+: Compression, -: Tension)
SHEAR = 1.00 #Shear according to mode II (four boundaries)
```

Running functions

Functions are called depending on the simulations. Earlier functions must be executed in order to first create the model. After that, evaluation of the results is made also by their respective functions, as for example with the *valueMaxS11* function for obtaining automatically maximum local stress.

Combining these functions with the variables definitions gives the possibility to create parametric studies using loops.

```
##############
# Running analyses #
##############
```

```
createModel0_2D(model0Name=MODEL0NAME, cell=CELL, oriAngle=ORIANGLE, lstrut=LSTRUT, imax=IMAX)
#createModel0_3D(model0Name=MODEL0NAME, cell=CELL, oriAngle=ORIANGLE, lstrut=LSTRUT, imax=IMAX)
createModel1_2D(model0Name=MODEL0NAME, model1Name=MODEL1NAME, rotAngle=ROTANGLE, lstrut=LSTRUT, nrregion=NRREGION,
nxregion=NXREGION, nyregion=NYREGION, xCenterBox=XCENTERBOX, yCenterBox=YCENTERBOX, cutForm=CUTFORM)
#createModel1_3D(model0Name=MODEL0NAME, model1Name=MODEL1NAME, rotAngleAlpha=ROTANGLEALPHA, rotAngleBeta=ROTANGLEBETA, lstrut=LSTRUT,
 nrregion=NRREGION, nzBox=NZBOX, nxregion=NXREGION, nyregion=NYREGION, xCenterBox=XCENTERBOX, yCenterBox=YCENTERBOX, cutForm=CUTFORM)
#createModelA_2D(model1Name=MODEL1NAME, modelAName = MODELANAME, jobName = JOBNAME, lstrut = LSTRUT, thickness=THICKNESS,
rotAngle = ROTANGLE, ncrack = NCRACK, nsegments=NSEGMENTS, dy=DY, NLgeom=NLGEOM)
#createModelB_2D(model1Name=MODEL1NAME, modelAName = MODELBNAME, jobName = JOBNAME, lstrut = LSTRUT, nyregion=NYREGION,
thickness=THICKNESS, ncrack = NCRACK, nsegments=NSEGMENTS, dy=DY, NLgeom=NLGEOM, nuCont=NUCONT)
#createModelB_3D(model1Name=MODEL1NAME, modelAName = MODELBNAME, jobName = JOBNAME, lstrut = LSTRUT, nxregion=NXREGION,
nyregion=NYREGION, nzBox=NZBOX, thickness=THICKNESS, ncrack = NCRACK, nsegments=NSEGMENTS, dy=DY, NLgeom=NLGEOM, nuCont=NUCONT)
#createModelC_2D(model1Name=MODEL1NAME, modelCName = MODELCNAME, jobName = JOBNAME, lstrut = LSTRUT, NLgeom=NLGEOM,
nrregion=NRREGION, thickness=THICKNESS, rotAngle = ROTANGLE, ncrack = NCRACK, nxBox=NXBOX, nyBox=NYBOX,nsegments=NSEGMENTS,
load=LOAD, strainYY=STRAINYY, press=PRESS, shear=SHEAR, ECont=ECONT, nuCont=NUCONT, analysis=ANALYSIS)
#createModelC_3D(model1Name=MODEL1NAME, modelCName = MODELCNAME, jobName = JOBNAME, lstrut = LSTRUT, NLgeom=NLGEOM,
nrregion=NRREGION, thickness=THICKNESS, ncrack = NCRACK, nxBox=NXBOX, nyBox=NYBOX, nzBox=NZBOX, nsegments=NSEGMENTS, dy=DY,
press=PRESS, strainYY=STRAINYY,  shear=SHEAR, ECont=ECONT, nuCont=NUCONT, load=LOAD, analysis=ANALYSIS)
#runJobA(jobName = JOBNAME)

############################
# Visualization and output #
############################
#RF1_up = calculateRF1(jobName = JOBNAME, setName='n_up')
#print 'RF1 = ' + str(RF1_up)
#RF2_up = calculateRF2(jobName = JOBNAME, setName='F_UP')
#print 'RF2 = ' + str(RF2_up)
#Erel = RF2_up * NYREGION / NXREGION / DY /100000
#print 'Erel = ' + str(Erel)
#ErelFoam = RF2_up * NYREGION / NXREGION / NZBOX / DY /100000
#print 'ErelFoam = ' + str(ErelFoam)

#valueALLIe = calculateALLIE(jobName = JOBNAME)
#print 'ALLIe = ' + str(valueALLIe)
#valueMaxS11 = calculateMaxS11(jobName = JOBNAME)
#print 'MaxS11 = ' + str(valueMaxS11)
#Eigenvalue1 = calculateEigenvalue(jobName = JOBNAME)
#print 'Eigenvalue1 = ' + str(Eigenvalue1)

######################
# Parametric studies #
######################
# KV - MII
ANALYSIS = 'Static'
LOAD = 'ShearStrain'
CELL = 'KV'
NCRACK = 20.0
NRREGION = 20.0
for ROTANGLEALPHA in [ 0, 15, 30, 45]:
createModel0_3D(model0Name=MODEL0NAME, cell=CELL, oriAngle=ORIANGLE, lstrut=LSTRUT, imax=IMAX)
createModel1_3D(model0Name=MODEL0NAME, model1Name=MODEL1NAME, rotAngleAlpha=ROTANGLEALPHA, rotAngleBeta=ROTANGLEBETA, lstrut=LSTRUT,
 nrregion=NRREGION, nzBox=NZBOX, nxregion=NXREGION, nyregion=NYREGION, xCenterBox=XCENTERBOX, yCenterBox=YCENTERBOX, cutForm=CUTFORM)
i=1
for THICKNESS in [ 0.1096/2, 0.2450/2, 0.3465/2]:
if i==1:
ECONT = 5.36
NUCONT = 0.45
if i==2:
ECONT = 116.0
NUCONT = 0.45
if i==3:
ECONT = 408.0
NUCONT = 0.45
JOBNAME = CELL + '_MII_angle-' + str(ROTANGLEALPHA) + '_t-' + str(i)
createModelC_3D(model1Name=MODEL1NAME, modelCName = MODELCNAME, jobName = JOBNAME, lstrut = LSTRUT, NLgeom=NLGEOM, nrregion=NRREGION,
 thickness=THICKNESS, ncrack = NCRACK, nxBox=NXBOX, nyBox=NYBOX, nzBox=NZBOX, nsegments=NSEGMENTS, dy=DY, press=PRESS,
 strainYY=STRAINYY, shear=SHEAR, ECont=ECONT, nuCont=NUCONT, load=LOAD, analysis=ANALYSIS)
runJobA(jobName = JOBNAME)
valueMaxS11 = calculateMaxS11(jobName = JOBNAME)
i = i + 1
...
```

Bibliography

[1] Ableidinger, A., Some aspects of the fracture behavior of metal foams, Master Thesis. Institute of Lightweight Design and Structural Biomechanics (ILSB) Vienna University of Technology, 2000.

[2] Bohm, H.J., A short introduction to basic aspects of continuum mechanics. Institute of Lightweight Design and Structural Biomechanics (ILSB) Vienna University of Technology, 1998.

[3] Choi, S., Sankar, B.V., A micromechanical method to predict the fracture toughness of cellular materials. Int. J. Solids Struct. 42 (5-6), 1797–1817, 2005.

[4] Dassault Systemes, Abaqus 6.13 Documentation. Simulia, 2013.

[5] Deshpande, V.S., Ashby, M.F., Fleck, N.A., Foam topology bending versus stretching dominated architectures. Acta Mater. 49 (6), 1035-1040, 2001.

[6] Fleck, N.A., Qiu, X., The damage tolerance of elastic-brittle, two-dimensional isotropic lattices. J. Mechan. Phys. Solids 55 (3), 562–588, 2007.

[7] Gibson, L.J., Ashby, M.F., Cellular solids, Structure and properties, second ed. Cambridge University Press, 1999.

[8] Griffith, A. A., The phenomena of rupture and flow in solids, Philos. Trans. R. Soc. London Ser. A 221, 163–198, 1921.

[9] Guo, X.E., Gibson, L.J., Behavior of intact and damaged honeycombs: a finite element study. Int. J. Mech. Sci. 41 (1), 85–105, 1999.

[10] Heierli, J., Gumbsch, P., Zaiser, M., Anticrack nucleation as triggering mechanism for snow slab avalanches. Science 321 (5886), 240-243, 2008

[11] Irwin, G., Analysis of stresses and strains near the end of a crack traversing a plate. J. Appl. Mech. 24, 361–364, 1957.

[12] Luxner, M.H., Modeling and simulation of highly porous open cell structures - Elasto-plasticity and localization versus disorder and defects, Dissertation. Institute of Lightweight Design and Structural Biomechanics (ILSB) Vienna University of Technology, 2006.

[13] Luxner, M.H., Woesz, A., Stampfl, J., Fratzl, P., Pettermann, H.E., A finite element study on the effects of disorder in cellular structures. Acta Biomater. 5 (1), 381-90, 2009.

[14] Luxner, M.H., Pettermann, H.E., Stampfl, J., Numerical simulations of 3D open cell structures – influence of structural irregularities on elasto-plasticity and deformation localization. Int. J. Solids Struct. 44 (9), 2990–3003, 2007.

[15] Pugno, N.M., Ruoff, R.S., Quantized fracture mechanics. Philos. Mag. 84 (27), 2829–2845, 2004.

[16] Quintana-Alonso, I., Fleck, N.A., Fracture of Brittle Lattice Materials: A Review, in: Daniel, I.M., Gdoutos, E.E., Rajapakse, Y.D.S. (Eds.), Major Accomplishments in Composite Materials and Sandwich Structures: An Anthology of ONR Sponsored Research. Springer Science+Business Media B.V., pp. 799-816, 2010.

[17] Rossmanith, H.P., Fracture mechanics course notes. Viena University of Technology, 2013.

[18] Schmidt, I., Fleck, N.A., Ductile fracture of two-dimensional cellular structures. Int. J. Fract. 111 (4), 327-342, 2001.

[19] Sternlof, K.R., Rudnicki, J.W., Pollard, D.D., Anticrack inclusion model for compaction bands in sandstone. J. Geoph. Res. 110 (B11), 1-16, 2005.

[20] Taylor, D., Cornetti, P., Pugno, N., The fracture mechanics of finite crack extension. Eng. Frac. Mech 72, 1021-1038, 2005.

[21] Thiyagasundaram, P., Wang, J., Sankar, B.V. Arakere, N. K., Fracture toughness of foams with tetrakaidecahedral unit cells using finite element based micromechanics. Eng. Frac. Mech. 78, 1277–1288, 2011.